

Metabolic regulation of dendritic cell function and activation

by

Hannah Guak

Department of Physiology

McGill University, Montreal

April 2021

A thesis submitted to McGill University in partial fulfillment of the
requirements of the degree of Doctor of Philosophy (Ph.D)

© Hannah Guak, 2021

Table of Contents

| | |
|---|-----------|
| Abstract..... | 5 |
| Résumé..... | 7 |
| Acknowledgements..... | 9 |
| Contribution to original knowledge | 10 |
| Contribution of authors | 11 |
| List of publications | 11 |
| List of Figures | 13 |
| | |
| CHAPTER 1 – Literature review | 15 |
| THE IMMUNOLOGICAL SYSTEM | 15 |
| Cellular players of the immune system | 15 |
| Bridging of innate and adaptive immunity by dendritic cells | 17 |
| In vitro generation of dendritic cells | 20 |
| Key dendritic cell functions in immunity..... | 21 |
| Recognition of pattern-associated and danger-associated molecular patterns | 21 |
| Migration | 22 |
| T cell priming | 24 |
| CELLULAR METABOLISM IN THE REGULATION OF IMMUNE CELL FUNCTION AND ACTIVATION | 25 |
| Metabolic networks | 27 |
| Key metabolic regulators..... | 27 |
| Glycolysis | 27 |
| Oxidative metabolism..... | 29 |
| Lipid metabolism..... | 30 |
| Dendritic cell metabolism | 31 |
| Dendritic cell metabolism during development | 31 |
| Metabolic mechanisms regulating dendritic cell activation | 32 |
| Dendritic cell metabolism in tolerance..... | 33 |
| Regulation of mitochondrial metabolism by transcriptional coactivator PGC-1 β | 37 |
| PGC-1 coactivator targets and regulation..... | 37 |
| PGC-1 coactivators in immunity | 39 |
| THE IMPACT OF DIET-INDUCED OBESITY IN IMMUNITY | 41 |
| Changes to immune cells in obesity | 41 |
| Adipose tissue-associated dendritic cells | 42 |
| Rationale and objectives | 44 |

| | |
|--|-----------|
| CHAPTER 2 – Glycolysis is essential for CCR7 oligomerization and dendritic cell migration | 46 |
| Preface | 46 |
| Abstract | 46 |
| Introduction | 47 |
| Results | 49 |
| Differentially-activated DCs display distinct bioenergetic profiles | 49 |
| Early glycolytic flux is a hallmark of both weak and strong DC activators | 53 |
| Loss of coupled respiration directly correlates with iNOS expression and NO production | 56 |
| Weakly inflammatory DCs lack long-term glycolytic reprogramming | 56 |
| Induction of glycolysis is required for DC motility and migration..... | 60 |
| Discussion | 65 |
| Experimental procedures | 71 |
| Supplementary figures | 81 |
| | 83 |
| References | 86 |

| | |
|---|------------|
| CHAPTER 3 – The role of PGC-1β in oxidative metabolism and immune function of dendritic cells | 90 |
| Abstract | 90 |
| Introduction | 91 |
| Results | 93 |
| Metabolic profiling of differentially-activated DCs | 93 |
| PGC-1 β -deficient DCs have impaired oxidative metabolism and increased glycolysis..... | 94 |
| Effect of PGC-1 β on metabolic phenotype of differentially-activated DCs | 98 |
| PGC-1 β -deficient DCs exhibit reduced FAO but unchanged total mitochondrial mass | 100 |
| PGC-1 β -deficient DCs have reduced mitophagy and increased autophagic flux | 102 |
| PGC-1 β -deficient DCs have reduced pro-inflammatory cytokine production and promote T cell expansion and Th2 differentiation | 103 |
| Discussion | 104 |
| Experimental procedures | 109 |
| Supplementary Figures | 114 |
| References | 119 |

| | |
|--|------------|
| CHAPTER 4 – Characterization of conventional dendritic cell subsets at homeostasis and in high fat-diet induced obesity | 122 |
| Introduction | 123 |
| Results | 125 |

| | |
|---|------------|
| Comparison of metabolic phenotypes of cDC subsets in lymphoid and non-lymphoid tissues | 125 |
| Comparison of metabolic phenotypes of migratory and tissue-resident cDC subsets in the lymph node | 127 |
| Changes in cDC proportion and activation over time in high fat diet-fed mice | 129 |
| Changes in cDC proportion, activation, and metabolic phenotype in high fat diet-fed mice | 132 |
| Mitochondrial changes in cDC subsets after weight loss following HFD challenge..... | 133 |
| Discussion | 137 |
| Experimental procedures..... | 142 |
| Supplementary figures | 145 |
| References | 149 |
| | |
| CHAPTER 5 – Discussion..... | 153 |
| Summary | 153 |
| The relationship between cellular metabolism and the cytoskeleton | 154 |
| The influence of diet on immune responses | 158 |
| Dietary regulation of PGC-1 proteins | 160 |
| Challenges in studying metabolism in DCs | 161 |
| Clinical implications | 164 |
| Cancer immunotherapy | 164 |
| Metabolic induction of tolerogenic DCs | 166 |
| Final conclusion | 168 |
| | |
| References | 169 |
| | |
| List of abbreviations | 186 |

Abstract

Dendritic cells (DCs) are innate immune cells that are specialized to sense their microenvironment, integrate the signals they receive, and convey this message to initiate adaptive immunity, thereby shaping the nature of the immune response. Cellular metabolism has been established to be a critical molecular mechanism regulating the function and activation of immune cells, including those of DCs. In this thesis, I highlight our findings on how different aspects of metabolism, including glycolysis, oxidative metabolism, and changes in whole-body metabolism, influence DC function and activation. Strong Toll-like receptor stimulation has previously been shown to rapidly induce glycolysis to fuel fatty acid synthesis and consequent membrane expansion. We show that weak activation of DCs also increases their early glycolytic activity, suggesting that enhanced glycolysis is a hallmark of DC activation regardless of the strength of stimulation. Only the highly pro-inflammatory DCs, however, undergo long-term glycolytic reprogramming that is associated with active HIF-1 α , a transcription factor that promotes glycolysis. We then assessed the role of glycolysis in a fundamental process of DCs—cellular migration. We found that glycolysis is required for spontaneous DC motility as well as chemokine-induced DC migration by promoting oligomerization of the chemokine receptor CCR7. In addition, we show that inhibition of glycolysis impairs DC migration in a house dust mite-induced allergic asthma model *in vivo*. While glycolytic regulation of DC function and activation has been relatively well-studied, there is less known about the role of mitochondrial metabolism. Therefore, we next investigated the role of a major regulator of mitochondrial metabolism, the transcriptional co-activator PGC-1 β , in DCs. Bioenergetic profiles of PGC-1 β -deficient DCs reveal an impairment of oxidative metabolism and concurrent increase in glycolytic activity. Lipopolysaccharide-activated DCs, which downregulate PGC-1 β gene

expression and lose oxidative capacity over time, do not rely on PGC-1 β for their bioenergetics. In contrast, interferon- β -treated DCs maintain PGC-1 β gene expression and mitochondrial metabolism, and rely on PGC-1 β for optimal bioenergetic capacity. PGC-1 β deficiency also affects the immune function of DCs by promoting T cell expansion and type 2 T helper cell differentiation. We next examined conventional DC (cDC) subsets *in vivo*, comparing and characterizing their mitochondrial and lipid content across different tissues. We found that these metabolic features differ between cDC subsets across tissues, establishing that the specific tissue microenvironment they reside in influences these phenotypes. When challenged with a metabolic perturbation such as high-fat diet feeding, levels of intracellular lipid increase considerably, while mitochondrial mass is greatly diminished. Collectively, our findings both expand our understanding and underscore the importance of metabolic programming in regulating DC biology.

Résumé

Les cellules dendritiques (CD) sont des cellules du système immunitaire inné qui sont spécialisées pour réagir à leur microenvironnement, à intégrer des signaux qu'elles reçoivent et à transmettre les messages pour déclencher le système immunitaire adaptatif. Un mécanisme essentiel pour l'activation des cellules immunitaires, incluant les CD, est le métabolisme cellulaire. Dans cette thèse, nous soulignons les différents aspects du métabolisme qui influence l'activation et la fonction des CD. Cela inclut la glycolyse, le métabolisme oxydatif et le métabolisme général. Au préalable, il a été démontré qu'une forte stimulation du récepteur de type Toll est impliquée dans l'augmentation de la glycolyse pour induire la biosynthèse des acides gras responsable de l'expansion de la membrane. Nous avons démontré qu'une faible activation des CD augmente les premières étapes de la glycolyse, suggérant que l'augmentation de la glycolyse est une caractéristique de l'activation des CD. Néanmoins, seules les CD pro-inflammatoires vont suivre une reprogrammation glycolytique à long terme, associée avec l'activation du facteur de transcription HIF-1 α , promouvant la glycolyse. Nous avons donc étudié le rôle de la glycolyse dans la migration cellulaire qui est un processus fondamental pour les CD. Nous avons trouvé que la glycolyse est nécessaire pour la motilité spontanée des CD, ainsi que pour leur migration induite par l'activation et l'oligomérisation de récepteurs chimiokine CCR7. De plus, nous avons montré que l'inhibition de la glycolyse limite la migration des CD dans un modèle *in vivo* d'asthme allergique induit par les acariens. Bien que la régulation de la glycolyse dans la fonction et l'activation des CD a déjà bien été étudiée, le rôle du métabolisme mitochondrial reste peu connu. Nous avons donc décidé d'investiguer le rôle d'un co-activateur transcriptionnel important dans le métabolisme mitochondrial : le PGC-1 β . Nous avons trouvé au travers des profils bioénergétiques que les CD déficientes en PGC-1 β

ont un métabolisme oxydatif réduit et présente une augmentation de la glycolyse. Les CD8 activées par les lipopolysaccharides, ont une expression réduite du gène PGC-1 β qui est associée à une perte de la capacité oxydative, et ne dépendent pas de l'action de PGC-1 β pour leur besoin bioénergétique. À l'opposé, les CD8 traitées avec l'interféron β ont la capacité de maintenir l'expression génique de PGC-1 β et le métabolisme mitochondrial et repose sur l'expression de PGC-1 β pour avoir des capacités bioénergétiques optimales. De plus, le manque de PGC-1 β affecte aussi la fonction immunitaire des CD8 en induisant l'expansion des cellules T et la différenciation de lymphocyte Th2. Nous avons ensuite étudié le sous-ensemble des CD8 conventionnelles (CD8c) *in vivo*, en comparant et caractérisant leur composition mitochondriale et lipidique à travers différents tissus. Nous avons trouvé que les caractéristiques métaboliques diffèrent entre les CD8c selon leur tissu d'origine, montrant que le microenvironnement des CD8c influence leur phénotype. Lorsque les modèles animaux ont été soumis à des perturbations métaboliques telles qu'un régime riche en graisse, nous avons observé que la quantité de lipides intracellulaires augmente de manière importante alors que la masse mitochondriale diminue fortement. En conclusion, ces recherches accroissent nos connaissances sur la programmation métabolique et souligne son importance sur la régulation des CD8c.

Acknowledgements

I would like to thank my supervisor, Dr. Connie Krawczyk, for her invaluable mentorship, patience, and understanding throughout my PhD. I am grateful for her trust in me and for providing me with space for growth both as a scientist and as an individual.

I would like to thank all past and present Krawczyk lab members for fostering a warm and collaborative lab environment. I am more grateful than I can express in words to have had Giselle as not only a lab mate but also an amazing friend. Her sense of humor always kept me entertained, her curiosity and enthusiasm for science was contagious, and her kindness and generosity inspiring. I am also thankful to my other lab mates at McGill for making the lab an enjoyable place to be, including Anisa for her fearlessness and affection, So Yoon for all the laughs, Brendan for his infectious enthusiasm, Mario for the countless science chats, Kristin for her abundant positivity, and Benedeta for her wit and wisdom. I would also like to thank my lab mates at Van Andel Research Institute, including Alex, Paula, Lukai, and Catherine, for their outstanding help and effort in building up the lab at Grand Rapids. I am so grateful to Mario for coming along to Grand Rapids and help establish the lab again. Having a familiar face around made the transition much easier. I am also incredibly thankful to members of the Jones lab, namely Eric, Takla, and Said, for all of their help. I especially acknowledge Eric for his boundless generosity and collaboration, both at McGill as well as at VARI. I would also like to thank others at McGill for their friendship, including Victor, Logan, and Song.

I would like to thank my mom, dad, and sister Esther for their endless love and support. Esther has always kept me balanced and I am so fortunate to have had her company for most of PhD journey.

I also thank my committee members Dr. Rusty Jones, Dr. Ana Nijnik, Dr. Martin Richer, and past member Dr. Julie St-Pierre, for all the helpful advice and input on my project. I also acknowledge financial support from MICRTP and FRQS.

Contribution to original knowledge

- Differentially-activated DCs exhibit an increase in early glycolytic activity regardless of the strength of the inflammatory phenotype.
- Strongly-activated DCs, but not weakly-activated DCs, exhibit increased HIF-1 α and iNOS expression, and undergo long-term glycolytic reprogramming.
- Glycolysis is required for optimal CCR7 oligomerization and therefore, chemokine-induced migration by DCs. This process is not dependent on mitochondrial bioenergetics.
- PGC-1 β deficiency in DCs leads to increased glycolysis and impaired oxidative metabolism, which is in part due to reduced fatty acid oxidation.
- PGC-1 β deficiency in DCs promotes T cell expansion and Th2 differentiation.
- Migratory cDCs have greater mitochondrial mass compared to resident cDCs in the LN.
- HFD challenge increases the frequency of all cDC subsets in white adipose tissue, with a proportionally larger increase in cDC2A and cDC2B subsets compared to cDC1.
- HFD challenge in mice leads to a substantial drop in mitochondrial mass and increase in intracellular lipid content in adipose tissue-associated DCs.
- Weight loss after HFD-induced obesity does not completely restore mitochondrial mass in adipose tissue-associated DCs.

Contribution of authors

Chapter 2: Eric Ma performed and analyzed the GC-MS experiments in Fig. 2C on samples I prepared. Sara Al Habyan, Maia Al-Masri, and Luke McCaffrey helped with performing and analyzing live imaging studies in Fig. 5 on I cells prepared. Haya Aldossary performed the experiments in Fig. 6G. So Yoon Won and Thomas Ying helped with miscellaneous experiments for the project (not shown in manuscript figures). I performed and analyzed all other experiments presented in this chapter. Dr. Connie Krawczyk, Dr. Russell Jones, and I wrote and edited the manuscript.

Chapter 3: I performed and analyzed all experiments. I wrote the manuscript.

Chapter 4: I performed and analyzed all experiments. Some technical support was provided by Alex Vanderark, Paula Davidson, and Lukai Zhai. I wrote the manuscript.

Dr. Connie Krawczyk supervised all work in this thesis and edited all manuscripts.

List of publications

The work presented in this thesis is published or is in preparation to be published as follows:

Chapter 1 (excerpts): Guak H, Krawczyk CM. Implications of cellular metabolism for immune cell migration. *Immunology*. 2020 Sep 13;161(3):200–8.

Chapter 2: Guak H, Al Habyan S, Ma EH, Aldossary H, Al-Masri M, Won SY, et al. Glycolytic metabolism is essential for CCR7 oligomerization and dendritic cell migration. *Nature Communications*. 2018 Jun 25;9(1):2463.

Chapter 3: Guak H, Krawczyk CM. The role of PGC-1 β in oxidative metabolism and immune function of dendritic cells. *Manuscript in preparation*.

Chapter 4: Guak H, Krawczyk CM. Characterization of conventional dendritic cell subsets at homeostasis and in high fat-diet induced obesity. *Manuscript in preparation*

Chapter 5 (excerpts): Guak H, Krawczyk CM. Implications of cellular metabolism for immune cell migration. *Immunology*. 2020 Sep 13;161(3):200–8.

Other published research contributions and review articles that do not appear in this thesis:

Boukhaled GM*, Corrado M*, **Guak H***, Krawczyk CM. Chromatin Architecture as an Essential Determinant of Dendritic Cell Function. *Front Immunol*. 2019;10. * These authors have contributed equally to this work

Ma EH, Bantug G, Griss T, Condotta S, Johnson RM, Samborska B, Mainolfi N, Suri V, **Guak H** et al. Serine Is an Essential Metabolite for Effector T Cell Expansion. *Cell Metabolism*. 2017 Feb 7;25(2):345–57.

Won S-Y, Hunt K, **Guak H**, Hasaj B, Charland N, Landry N, et al. Characterization of the innate stimulatory capacity of plant-derived virus-like particles bearing influenza hemagglutinin. *Vaccine*. 2018 Dec 18;36(52):8028–38.

Boukhaled GM, Cordeiro B, Deblois G, Dimitrov V, Bailey SD, Holowka T, Domi A, **Guak H** et al. The Transcriptional Repressor Polycomb Group Factor 6, PCGF6, Negatively Regulates Dendritic Cell Activation and Promotes Quiescence. *Cell Reports*. 2016 Aug 16;16(7):1829–37.

Contreras I, Estrada JA, **Guak H**, Martel C, Borjian A, Ralph B, et al. Impact of *Leishmania mexicana* Infection on Dendritic Cell Signaling and Functions. *PLOS Neglected Tropical Diseases*. 2014 Sep 25;8(9):e3202.

List of Figures

Chapter 1

| | |
|---|----|
| Figure 1 – Hematopoiesis of immune cells and development of DC subsets..... | 18 |
| Figure 2 – Metabolic pathways of the cell..... | 26 |

Chapter 2

| | |
|--|----|
| Figure 1 – Bioenergetic profiles of differentially-activated DCs | 52 |
| Figure 2 – Weakly-activated DCs undergo early glycolytic flux | 55 |
| Figure 3 – iNOS expression and NO production is correlated with loss of coupled respiration...58 | |
| Figure 4 – Weakly activated DCs lack long-term metabolic reprogramming. | 59 |
| Figure 5 – Glycolysis is required for DC motility and morphology..... | 61 |
| Figure 6 – Inhibition of glycolysis impairs CCR7 oligomerization and reduces DC migration to the draining lymph node. | 64 |
| Figure S1 – Surface marker expression and cytokine production by differentially-activated DCs. | 81 |
| Figure S2 – Rapid oxygen consumption induced by Zym and ZymD is primarily non-mitochondrial. | 82 |
| Figure S3 – Early glycolytic flux by LPS and HDM is prevented by AKT inhibition..... | 83 |
| Figure S4 – Inhibition of glycolysis results in rounded cell morphology..... | 84 |
| Figure S5 – CCR7 expression on DCs..... | 85 |
| Figure S6 – Inhibition of glycolysis does not affect phagocytosis of HDM by DCs. | 85 |

Chapter 3

| | |
|--|-----|
| Figure 1 – Metabolic profiling of differentially-activated DCs..... | 94 |
| Figure 2 – PGC-1 β -deficient DCs have impaired oxidative metabolism and increased glycolysis | 97 |
| Figure 3 – Effect of PGC-1 β on metabolic phenotype of differentially-activated DCs | 99 |
| Figure 4 – PGC-1 β -deficient DCs exhibit reduced fatty acid oxidation, but unchanged total mitochondrial mass | 101 |
| Figure 5 – PGC-1 β -deficient DCs have reduced mitophagy and enhanced autophagic flux | 103 |

| | |
|---|-----|
| Figure 6 – PGC-1 β -deficient DCs promote T cell expansion and Th2 differentiation | 106 |
| Figure S1 – NOS2 expression does not affect <i>Ppargc1b</i> expression | 114 |
| Figure S2 – PGC-1 β knockdown efficiency and bioenergetic phenotype of PGC-1 β KO DCs | 115 |
| Figure S3 – CPT-1a protein levels are reduced in PGC-1 β -deficient DCs | 116 |
| Figure S4 – Frequency of apoptotic cells are not affected by PGC-1 β deficiency..... | 117 |
| Figure S5 – Immune phenotype of PGC-1 β KO DCs | 118 |

Chapter 4

| | |
|--|-----|
| Figure 1 – Comparison of mitochondrial and lipid content in cDC subsets across tissues | 127 |
| Figure 2 – Comparison of mitochondrial and lipid content in migratory and lymphoid-resident cDC subsets..... | 130 |
| Figure 3 – HFD-induced changes to cDC proportions and activation over time..... | 131 |
| Figure 4 – HFD-induced changes to mitochondrial and lipid content in cDC subsets of the spleen and adipose tissue | 135 |
| Figure 5 – Mitochondrial changes in cDC subsets of the spleen and adipose tissue after weight loss following HFD challenge | 136 |
| Figure S1 | 145 |
| Figure S2..... | 146 |
| Figure S3..... | 146 |
| Figure S4..... | 147 |
| Figure S5..... | 148 |

THE IMMUNOLOGICAL SYSTEM

Cellular players of the immune system

The immune system encompasses an intricate network of anatomical barriers, chemical defenses, and cellular players that comprise innate and adaptive immunity (1). Innate immunity is the early line of defense that includes physical barriers such as skin and mucosal epithelia, chemical signals such as cytokines, and a range of cells with limited specificity to recognize conserved molecular patterns or danger signals (1). Innate immune cells include monocytes, macrophages, neutrophils, dendritic cells (DCs), mast cells, natural killer (NK) cells, and innate lymphoid cells (ILCs) (2). These cells express germline-encoded pattern recognition receptors (PRRs) that are stimulated by pathogen-associated molecular patterns (PAMPs) such as viral RNA or bacterial endotoxins, and danger-associated molecular patterns (DAMPs), which are molecules such as ATP that are released from dying cells and signal tissue damage (1). Several innate immune cells, including macrophages and neutrophils, are phagocytic and have the ability to engulf and clear pathogens and dead host cells (1).

In contrast, adaptive immune cells, which comprise T cells and B cells, express diverse receptors that recognize specific antigens (1). T cells require context for their cognate antigen in the form of major histocompatibility complex (MHC) molecules. For CD8⁺ T cells, antigen is recognized in the context of MHC class I (MHC I) molecules expressed by all nucleated cells, while MHC class II (MHC II) expressed by professional antigen-presenting cells (APCs), such as DCs, is required for CD4⁺ T cells (1). B cells, however, possess their own antigen-presenting abilities, and take up and present their cognate antigen to T helper (Th) cells, which in turn

provide activating signals to the B cells. Some types of antigen, predominantly polysaccharides from bacteria, can induce B cell activation independent of any T cell help (1). Upon activation, effector T cells or B cells proliferate and differentiate to mount targeted immune responses. Long-lived memory cells are also formed, poised to rapidly respond to previously encountered pathogens (2).

Within adaptive immunity, cell-mediated immunity involves T cells, while B cells engage in humoral immunity (2). $CD4^+$ T cells differentiate into different lineages of Th cells, producing specific cytokines that influence other immune cells and help shape the nature of the immune response (1). $CD4^+$ T cells can also differentiate into regulatory T (Treg) cells, which have anti-inflammatory roles (1). $CD8^+$ T cells become cytotoxic T lymphocytes (CTLs) that directly kill cells by secreting cytotoxic molecules such as granzymes or perforin, and inducing apoptosis through cell surface interactions with target cells—making CTLs particularly effective for immune responses against tumors and intracellular pathogens (1). In humoral immunity, B cells produce antigen-specific molecules known as antibodies, which coat microbes expressing the unique antigen and target them for phagocytosis (2). Antibodies can also activate the complement system, which consists of a cascade of plasma proteins initiated by recognition of antigen-antibody complexes by complement and resulting in lysis of the target cell and recruitment of phagocytes (1). Together, these immune cell types and mediators execute a context-specific immune response in a precisely balanced manner. Any loss of this balance can lead to excessive inflammation and damage to the host or failure to remove the pathogen or tumor.

These immune cells develop from hematopoietic stem cells (HSCs) in the yolk sac during fetal development and in the bone marrow after birth (1). HSCs are multipotent cells that give

rise to two main lineages: lymphoid, which includes T cells, B cells, NK cells, and ILCs, and myeloid, which includes macrophages, monocytes, granulocytes (neutrophils, basophils, eosinophils), DCs, mast cells, and erythrocytes (1) (Figure 1). The primary lymphoid organs are the bone marrow, where HSCs develop into most immune cell types, and the thymus, where T cell precursors from the bone marrow migrate to and mature (2). Secondary lymphoid organs, which mainly include the spleen and lymph nodes, are sites of initiation for adaptive immunity where cells are precisely organized for optimal interactions (1,3). Here, DCs play a major role in this initiation.

Bridging of innate and adaptive immunity by dendritic cells

DCs bridge the innate and adaptive arms of immunity by migrating from peripheral tissues to draining lymph nodes to communicate with T cells and instruct the immune response that ensues (2). There are also DCs that are resident to lymphoid tissues and receive antigen via lymphatic drainage or transfer from other cells (3,4). DCs comprise the subsets known as conventional or classical DC (cDC) 1 and cDC2, and the cDC2 subset can be further divided into the cDC2A and cDC2B subsets (5). The origin of another subset known as plasmacytoid DCs (pDCs) has been debated, with several studies implicating either lymphoid or myeloid origins. Recently, Rodrigues *et al.* has shown that pDCs are heterogeneous and primarily of lymphoid origin, with minimal contribution by the myeloid progenitors, while Dress *et al.* contend that pDCs are exclusively of lymphoid origin and do not, in fact, share a common progenitor with cDCs (6,7). In addition, cDCs and pDCs are functionally different, notably in the superiority of cDCs at antigen presentation and pDCs in production of the antiviral immune mediators, type 1 interferons (IFNs) (4).

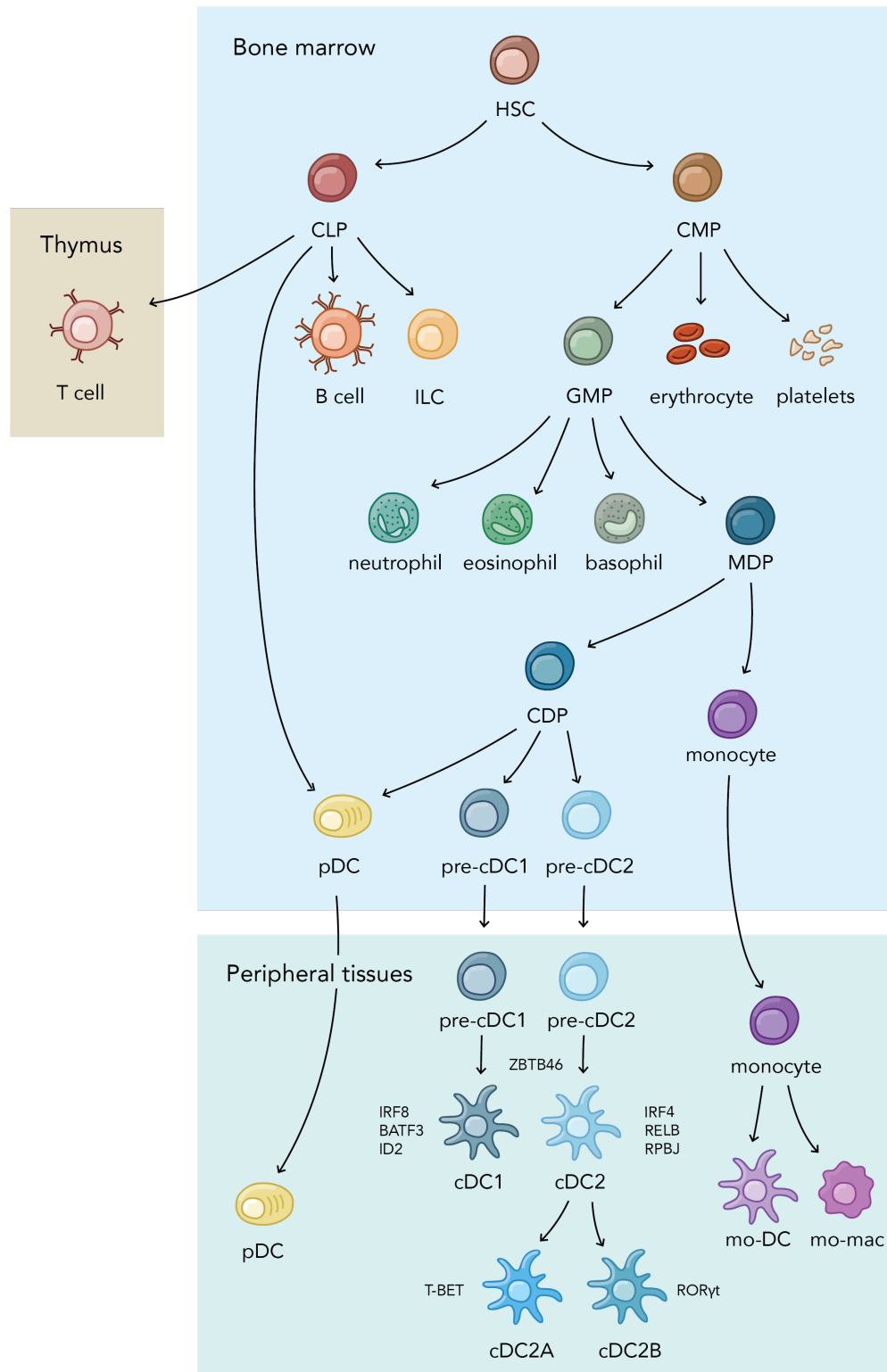


Figure 1 – Hematopoiesis of immune cells and development of DC subsets.

cDCs are defined by lineage-determining transcription factors, such as ZBTB46 for all cDCs; IRF8, BATF3, and ID2 for cDC1s; IRF4, RELB, and RBPJ for cDC2s (4,8). cDC2A are further defined by expression of TBET, while cDC2B express ROR γ t (5). Commitment of cDC precursors (pre-cDCs) to either the cDC1 or cDC2 lineages is predetermined in the bone marrow rather than in the peripheral tissues (9). The specific differentiation into cDC2A and cDC2B subsets is influenced by their tissue microenvironment (5). Pre-cDCs leave the bone marrow and seed both lymphoid and non-lymphoid tissues throughout the body, where they give rise to immature cDCs (10). DCs can also be derived from monocytes, but they differ in their ontogeny, as monocytes diverge from common DC precursors (CDPs) at the level of MDPs and can develop into either monocyte-derived DCs or monocyte-derived macrophages (10). The remainder of this review will focus on cDCs and monocyte-derived DCs.

At the cell surface, cDCs express high levels of MHC II and CD11c. However, these markers alone are not sufficient to identify DCs, as they overlap with certain macrophage populations (4). In addition, cDC1s are historically distinguished from cDC2s by their expression of CD8 α in lymphoid tissues and CD103 in non-lymphoid tissues, while cDC2s are distinguished by CD11b expression in both lymphoid and non-lymphoid tissues (4). However, these distinguishing markers are not always mutually exclusive, as intestinal cDCs have been described to express both CD103 and CD11b (4). Ginhoux and colleagues have since determined—through unsupervised high-dimensional analysis of flow cytometry and mass cytometry—a set of markers to distinguish DC subsets across different tissues and several mammalian species (including human and mouse) in a conserved manner (11). After excluding CD64⁺F4/80⁺ macrophages and including cells that are MHC II^{hi}CD11c⁺CD26⁺, cDC1s and cDC2s are distinguished by the expression of XCR1 and CD172a, respectively (11). In the

spleen, cDC2A are ESAM⁺CLEC12A⁻, while cDC2B are ESAM⁻CLEC12A⁺ (5). The individual cDC subsets have both distinct and overlapping functions (discussed in section Key dendritic cell functions in immunity).

In vitro generation of dendritic cells

Dendritic cells are a relatively rare immune cell type, with cDC1s and cDC2s each generally comprising less than 1% of immune cells in most tissues at steady state. Exceptions include the lung and skin, with cDC2s making up approximately 1.5% and 25% of CD45⁺ immune cells, respectively (12). Human cDC1s and cDC2s found in blood make up 0.6% and 0.05% of peripheral blood mononuclear cells (PBMCs), respectively (13). Due to the scarcity of DCs *in vivo*, most studies on DC biology have been performed on DCs that have been differentiated *in vitro*.

A commonly utilized method for *in vitro* DC generation involves growing HSCs from murine bone marrow in the presence of the cytokine granulocyte-macrophage colony-stimulating factor (GM-CSF) (14). Due to the different hematopoietic progenitors that exist in the bone marrow, the resulting cell composition from GM-CSF culture consists of a heterogeneous mix of DCs and macrophages (15). Helft *et al.* have identified that the population with high MHC II expression primarily contains DC-like cells, while those with intermediate MHC II expression are more similar to macrophages (15). While heterogeneity within these cultures is important to acknowledge, varied cell purity and extent of heterogeneity between studies occurs due to variations in culture conditions (16). In addition, immature DCs must also be considered, as they express comparatively lower levels of MHC II and upregulate MHC II upon activation (1). Another common method, which includes IL-4 with GM-CSF for differentiating bone marrow, partially limits but does not prevent the development of macrophages in the study by Helft *et al*

(15). *In vitro* human DCs are most commonly generated from monocytes of PBMCs following culture with GM-CSF and IL-4 as well (4).

Another method to generate DCs *in vitro* is to culture bone marrow cells with FMS-like tyrosine kinase 3 ligand (FLT3L). The populations generated developmentally resemble the cDC1, cDC2, and pDC subsets (4). The disadvantage to this method, however, is that the cell yield is relatively poor. A recent report introduces a system to improve the yield and immune functions of the cDC1-like cells by using Notch ligand-expressing OP9 cell lines to engage Notch signaling of these cells (17). Overall, these culture methods provide valuable *in vitro* strategies to study a rare cell type.

Key dendritic cell functions in immunity

Recognition of pattern-associated and danger-associated molecular patterns

DCs express a wide range of germline-encoded PRRs to recognize conserved molecular patterns. Upon engagement of PRRs, intracellular signaling directs DCs to adopt context-specific activation phenotypes, which then determine the differentiation of the T cells they stimulate. Toll-like receptors (TLRs) are membrane-bound receptors that are found at the cell surface or on intracellular endolysosomes (18). These receptors recognize a range of PAMPs primarily found on bacteria and viruses, as well as several types of DAMPs. For example, TLR4 recognizes lipopolysaccharide (LPS), a component on the outer membrane of Gram-negative bacteria. The TLRs found intracellularly, which are TLR3, 7, 8, and 9, recognize nucleic acids derived from bacteria or viruses (18). DAMPs released by dead or dying cells mainly engage TLRs, but some bind other PRRs as well. Examples include mitochondrial DNA, which engage TLR9, and nuclear histones, which activate TLR2 and TLR4 (19). Other intracellular PRRs include the

cytosolic receptors retinoic acid-inducible gene (RIG)-I-like receptors (RLRs), which are enhanced upon viral infection and recognize viral double-stranded RNA, and NOD-like receptors (NLRs), which recognize bacterial peptidoglycans (18).

C-type lectins are a large family of proteins with a very broad range of functions (20). Membrane-bound C-type lectins (C-type lectin receptors; CLR) bind a broad range of ligands, but were initially named for their ability to bind carbohydrates (20). Importantly, they are the primary PRRs that mediate anti-fungal immunity by recognizing carbohydrates on cells walls of fungi. A common example is the CLR dectin-1, which mediates anti-fungal responses to *Candida albicans* (21). Activation by PRR signaling instructs DCs about the type of pathogen or danger signal that has been encountered, and allows them to respond appropriately.

Different cDC subsets express distinct sets of PRRs. For example, RNA sequencing reveals that splenic cDC1s exclusively express TLR3, TLR11 and TLR12, while both cDC2A and cDC2B have greater expression of TLR1, TLR5, and TLR7 (5). Compared to cDC2A, cDC2B preferentially express TLR2, TLR6, TLR8, and TLR9 (5). By proteomics, lymphoid-resident cDC2s were determined to more highly express RIG-I, which recognizes double-stranded RNA, and NOD1, which recognizes bacterial peptidoglycan, compared to cDC1s (22). These differing profiles of PRR expression indicate divergent functions between the cDC subsets.

Migration

From the bone marrow, pre-cDCs distribute via blood circulation to tissues throughout the body (10). Within the tissues, the pre-cDCs differentiate into cDCs and continuously sample their microenvironment by using long dendrite-like projections (10). Upon sensing of a threat, they become activated, increasing C-C chemokine receptor 7 (CCR7) expression to migrate to

the draining LN via the lymphatic system (10). Both cDC1s and cDC2s require CCR7 expression to migrate and initiate an adaptive immune response, such as in the context of anti-tumor immunity for cDC1s (23), and during allergic asthma for cDC2s (24). DCs also migrate under homeostatic conditions, presenting antigen derived from the host to promote the generation of Treg cells and immune tolerance to self (25). CCR7 detects the chemokines C-C motif chemokine ligand 19 and 21 (CCL19 and CCL21), which are expressed by lymphatic endothelial cells and high endothelial venules, forming a gradient of chemokines that directs DCs to the draining LN (26). Adhesion molecules, such as integrins and their ligands, also help mediate DC migration along endothelial cells of the vasculature. An important study in mice with integrin-deficient DCs reveals that while integrins are required for movement along a two-dimensional surface such as endothelial or epithelial linings, they are dispensable for extravasation through interstitial environments (27). Once the DC is within the tissue, it moves by protrusive flow of actin. When the environment is especially dense, contraction of the trailing edge is mediated by myosin II in order to push along the relatively inflexible nuclei (27). Chemokines further instruct intranodal migration, segregating cDC1s and cDC2s to position them for optimal T cell interactions (3). cDC1s continue CCR7-dependent migration deep into the T cell zone, guided by a network of fibroblastic reticular cells that produce CCL21 (3). Compared to cDC1s, cDC2s, however, express a higher ratio of C-X-C motif chemokine receptor 5 (CXCR5) to CCR7, positioning them at the T cell-B cell border mediated by a gradient of the CXCR5 ligand CXCL13 produced by follicular dendritic cells (which are not related to cDCs nor of hematopoietic origin) (28).

T cell priming

Several signals are provided by DCs to activate T cells in a context-specific manner. First, antigen is presented on MHC I or MHC II to CD8⁺ or CD4⁺ T cells, respectively, that possess the antigen-specific TCR (1). Proteins from intracellular pathogens are degraded by proteasomes to generate peptides that are loaded onto MHC I molecules. DCs also have the ability to ingest tumor cells or infected cells and present peptides from the ingested cells on MHC I in a process known as cross-presentation (1). Extracellular proteins that have been internalized by DCs are digested enzymatically in endosomes and lysosomes and primarily presented on MHC II molecules (1). The type of MHC molecule in antigen presentation is important for instructing the type of T cell response that takes place; activation of CTLs leads to direct killing of cells that express the specific antigen, while activation of Th cells induces cytokine production that stimulates other cells, such as B cells, macrophages, and CTLs, to further enhance the immune response (1). In general, cDC1s are known to activate CD8⁺ T cells while cDC2s activate CD4⁺ T cells (4). An exception to this is cDC1 induction of Th1 responses (29–31). cDC2B are generally more pro-inflammatory than cDC2A, as cDC2B induce more Th1 and Th17 cells, while cDC2A induce more Th2 cells (5). Both cDC1s and cDC2s are capable of activating both T cell subsets *in vitro*, but they are restricted *in vivo* based on spatial organization of DCs and T cells in the lymph node (3).

The second signal is the engagement of co-stimulatory molecules, which are required for optimal T cell activation (1). Without co-stimulation, the T cell either fails to respond or enters a state of hyporesponsiveness (1). There are multiple types of co-stimulatory molecules expressed by antigen-presenting cells that engage corresponding ligands expressed by T cells (32).

Commonly studied examples are CD80 and CD86, which can increase upon activation and

engage CD28 on T cells (32). The T cells also express inhibitory receptors CTLA-4 and PD-1, which engage CD86 and PD-L1, respectively, on DCs to restrict inflammatory responses, although inappropriate expression can lead to immune tolerance (32).

The final signal is cytokines, which determine the differentiation of the T cell by activating specific transcription factors. Intracellular pathogens such as *Listeria* or *Leishmania* promote IL-12 production by DCs, which induces Th1 and CTL differentiation (1). These T cells are defined by TBET expression and IFN- γ production (1). Th2 responses develop against allergens and helminths, are defined by STAT6 and GATA-3 expression, and are associated with the production of IL-4, IL-5, and IL-13 (1). Th2 cells stimulate and recruit other immune cells, such as eosinophils and macrophages, to eliminate the threat and repair host tissue (1). IL-1, IL-6, and TGF- β production induced by extracellular bacteria or fungi promote Th17 differentiation defined by the transcription factor ROR γ t and production of IL-17 (33). Together, these context-dependent signals from DCs help orchestrate the immune response.

CELLULAR METABOLISM IN THE REGULATION OF IMMUNE CELL FUNCTION AND ACTIVATION

The vast and complex network of metabolic pathways found in the cell provides energy, biosynthetic intermediates, as well as metabolites that act as signaling molecules or substrates for enzymes (Figure 2). Engagement of specific metabolic pathways by immune cells has been shown to be crucial for their precise development, differentiation, and function.

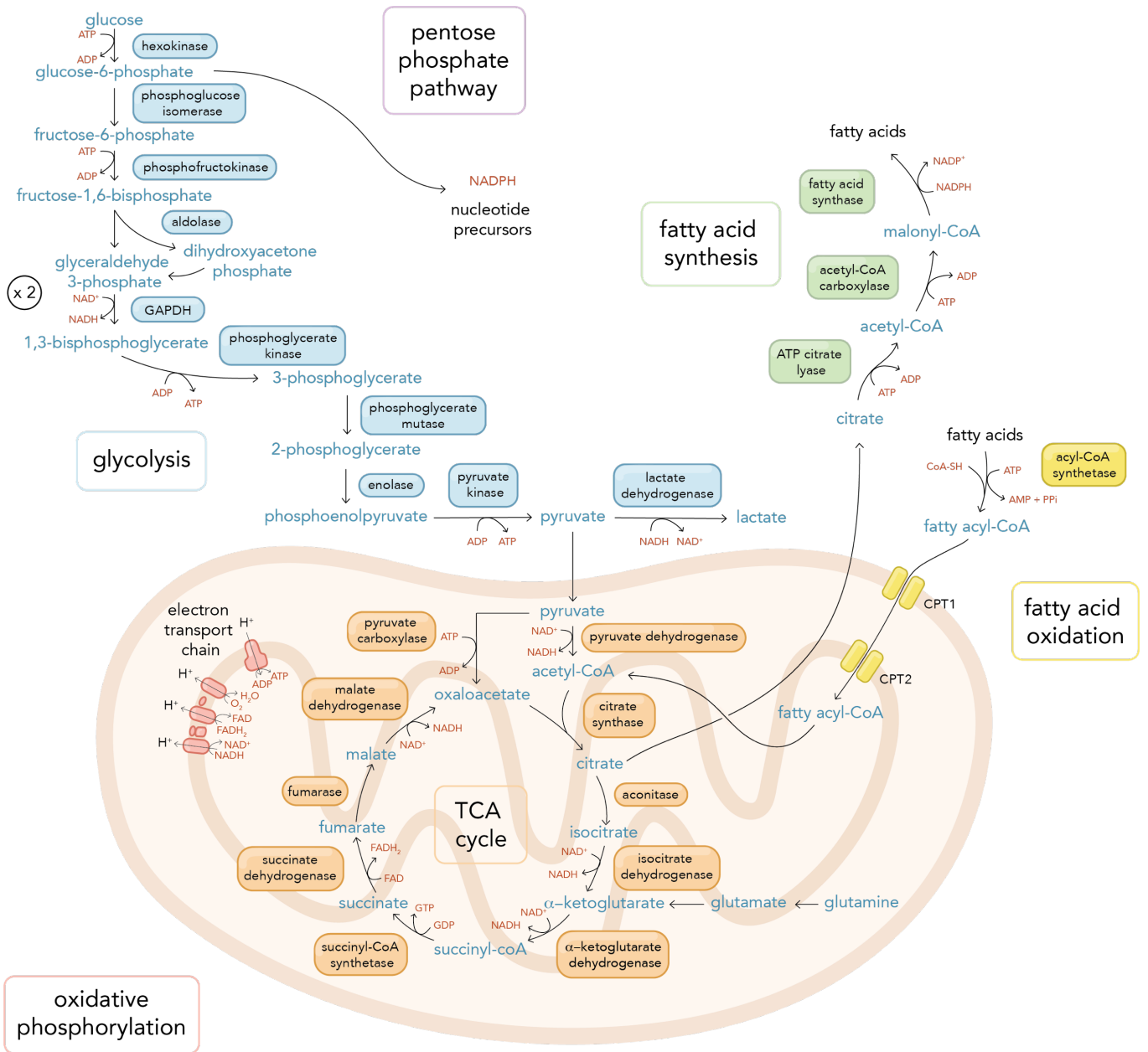


Figure 2 – Metabolic pathways of the cell.

Some metabolic pathways of the cell, including glycolysis, oxidative phosphorylation and tricarboxylic (TCA) cycle, fatty acid oxidation, fatty acid synthesis, and pentose phosphate pathway. Select metabolites, enzymes, use and production of reducing agents and energy, are shown.

Metabolic networks

Key metabolic regulators

Several proteins are central in the regulation of cellular metabolism by sensing and integrating both intracellular and environmental changes. Some have been well-studied in a variety of systems and play key roles in immunity. One such protein is mammalian target of rapamycin (mTOR), which is a serine/threonine kinase and a core component of mTOR complex 1 (mTORC1) and mTOR complex 2 (mTORC2) (34). These complexes are activated by signaling induced by the nutrient status of the cell, or by extracellular cues such as growth factors, TLR ligands, or cytokines (34,35). They regulate many metabolic processes, including protein synthesis, mitochondrial biogenesis, and glucose and lipid metabolism (36). mTORC1 can promote glycolysis through hypoxia-inducible factor 1 α (HIF-1 α), which is a transcription factor that induces the expression of glycolysis-related genes, and mTORC2 can promote glycolysis through AKT (34). AMP-activated protein kinase (AMPK) is a glucose- and energy-sensing factor that promotes catabolism, while inhibiting mTORC1 activity and other anabolic processes (37). These metabolic regulators play key roles in immune cell function and activation.

Glycolysis

Glucose is a major source of carbon for the cell. Glycolysis involves a series of steps converting glucose into pyruvate, which can then become lactate or be shuttled into the mitochondria to enter the tricarboxylic acid (TCA) cycle (38). The TCA cycle then generates reducing agents to power oxidative phosphorylation (OXPHOS). From a bioenergetic perspective, glycolysis is much less efficient than oxidative metabolism. However, advantages to glycolysis are the more rapid generation of energy and production of specific biosynthetic

intermediates. The reducing agent and substrate cofactor, NADH, is produced during glycolysis, and the reduction of pyruvate to lactate re-generates NAD^+ needed to maintain glycolytic flux and TCA cycle activity (38). In addition, there are intermediates that are common to other metabolic pathways; importantly, glucose-6-phosphate branches off into the pentose phosphate pathway, which generates nucleotide precursors as well as NADPH that is used in anabolic pathways such as fatty acid synthesis (38).

The Warburg effect, which is also known as aerobic glycolysis, is the engagement of glycolysis despite the presence of sufficient oxygen, and is often observed in tumor cells and activated immune cells (38). DCs, for example, experience a dramatic increase in glycolytic flux, which is necessary for the pro-inflammatory functions induced by TLR ligands (39,40). In addition, macrophages exhibit strongly elevated glycolysis following LPS-mediated activation (41). The expression of glycolytic genes and inflammatory genes, notably IL-1 β , is promoted by enhanced stabilization and activity of HIF-1 α by succinate and pyruvate kinase M2 (PKM2) (41,42). Inhibition of glycolysis using the glucose analog 2-deoxyglucose impairs the polarization of macrophages to an M1 phenotype, instead promoting the production of IL-10, which is associated with an M2 phenotype (42). Further, effector T cells require an increase in glycolysis for optimal IFN- γ production upon activation (43,44). Glucose transporter 1 (GLUT1) expression is necessary for the growth and survival of effector T cells, but not for Treg cells (45). In fact, Th17 differentiation requires HIF-1 α -dependent glycolysis, while HIF-1 α deficiency or inhibition of glycolysis promote Treg differentiation (46). These examples demonstrate the importance of glycolysis for bioenergetic and biosynthetic needs, and importantly, for the differentiation and specific immune functions of many inflammatory immune cells.

Some metabolic pathways of the cell, including glycolysis, oxidative phosphorylation and tricarboxylic (TCA) cycle, fatty acid oxidation, fatty acid synthesis, and pentose phosphate pathway. Select metabolites, enzymes, use and production of reducing agents and energy, are shown.

Oxidative metabolism

The TCA cycle generates reducing agents as well as several metabolic intermediates that intersect numerous other pathways. The reducing agents provide electrons to the electron transport chain (ETC), generating membrane potential and consequently powering ATP production in the process of OXPHOS (38). Many different carbon sources can fuel the TCA cycle. Glutamine, for example, contributes α -ketoglutarate to the TCA cycle. Acetyl coenzyme A (acetyl-CoA) primarily derives from either pyruvate that is processed from carbohydrates or from the oxidation of fatty acids (38). To oxidize fatty acids, the fatty acids in the cytosol must be transported into the mitochondria (47). The mitochondrial membranes are permeable to short-chain fatty acids, but not to medium- and long-chain fatty acids, which require the addition of a CoA group (creating fatty acyl-CoA), and then carnitine-dependent translocation into the mitochondria coordinated by carnitine palmitoyltransferase 1 and 2 (CPT1 and CPT2) (47). Units of acetyl-CoA are removed in a series of reactions, shortening the acyl-CoA by two carbons and generating NADH and FADH₂ in each round (47). The acetyl-coA can then join the TCA cycle for the generation of energy and biosynthetic intermediates.

Preference for mitochondrial metabolism is often associated with steady-state and regulatory immune phenotypes (48). In macrophages, for example, M2 polarization relies on glutamine metabolism, while M1 polarization does not (49). In addition, OXPHOS, but not glycolysis, is required for M2 differentiation (50). Although the TCA cycle for M2-like

macrophages can use glucose-derived pyruvate, in the absence of glucose other carbon sources like glutamine may be used, demonstrating metabolic flexibility of the cells (50). The importance of oxidative metabolism is also demonstrated by immune cells in tumor microenvironments, often displaying dysregulated oxidative metabolism associated with their suppressed functions. For example, immunosuppressive neutrophils of 4T1 tumor-bearing mice exhibit greater mitochondrial mass and respiration, and elevated ROS production (51). In a glucose-restricted tumor microenvironment, this metabolic adaptation allows the neutrophils to engage in ROS-mediated suppression of T cells with ROS produced by NADPH oxidase using NADPH from mitochondria rather than glucose and or the pentose phosphate pathway (51). In other instances, mitochondria of immune cells are dysfunctional, as in the example of TILs of clear cell renal carcinoma, which have fragmented, hyperpolarized mitochondria that generate large amounts of ROS (52). Treatment with a mitochondrial ROS scavenger can partially restore T cell activation (52). These examples show that oxidative metabolism and modulation of these pathways can determine immune phenotypes.

Lipid metabolism

Lipids have multiple purposes, serving as a source of energy, a component of membranes, and metabolic precursors for certain signaling molecules and immune mediators (48). Fatty acids can be synthesized by the cell or taken up from the environment, and excess fatty acids are stores in lipid bodies in the cytosol (47). Synthesis of fatty acids requires citrate, a metabolic intermediate generated by the TCA cycle, and NADPH, a reducing agent made by the pentose phosphate pathway (38). Lipids can be enzymatically released from the lipid bodies by lipolysis when needed (38). One study shows that lipolysis by the enzyme lysosomal acid lipase supports CD8⁺ memory T cell development by hydrolyzing lipid molecules in free fatty acids to

use in fatty acid oxidation (FAO) (53). T cells also engage fatty acid synthesis for building their membranes during growth and proliferation, with Th17 cells using *de novo* fatty acid synthesis from glucose-derived citrate, while Treg cells preferentially uptake exogenous fatty acids (54). Inhibition of key fatty acid synthesis enzyme acetyl-CoA carboxylase 1 (ACC1) attenuates Th17-mediated autoimmune disease (54), further confirming the importance of engaging specific metabolic pathways for immune cell differentiation and activation.

Dendritic cell metabolism

Dendritic cell metabolism during development

During DC development, there is an increase in anabolic programs, such as mitochondrial biogenesis, to support the expansion of progenitors (38). Monocyte-derived DCs, for example, have greater mitochondrial mass and respiration compared to the monocytes they differentiate from (55). A major regulator of mitochondrial biogenesis, PGC-1 α , rapidly increases in expression early during monocyte differentiation into DCs, triggering the activation of its target transcription factors, NRF-1 and TFAM (56). Fatty acid synthesis is required for normal DC development as well, as inhibition of the process leads to reduced proliferation and elevated apoptosis (57).

During both GM-CSF- and FLT3L-driven DC development, anabolic metabolism is coordinated by mTOR (58,59). Inhibition of mTOR with rapamycin impairs DC development, with a more profound effect on cDC1 compared to cDC2 in FLT3L-driven differentiation (58). Deletion of PTEN, a negative regulator of PI3K upstream mTOR, accelerates cDC1 development mediated by mTOR, emphasizing the precise regulation that is required for homeostatic maintenance of DC composition (58). Although inhibition of anabolism impairs FLT3L-induced

proliferation of DC progenitors, catabolism also has a role in DC differentiation by controlling the balance of cDC subsets (60). Inhibition of catabolic processes by blocking FAO or AMPK activity, for example, leads to increased cDC2 differentiation and reduced cDC1 differentiation, while the total cDC frequency remains unchanged (60). Conversely, presence of mitochondrial ROS favors cDC2 differentiation, and scavenging the ROS increases the ratio of cDC1 to cDC2. ROS is required for the development of monocyte-derived DCs as well (55), which aligns with evidence that monocyte-derived DCs have many overlapping features with cDC2s (5,61). The exact mechanism by which mitochondrial ROS controls DC differentiation is not well understood, but may involve its role as a secondary messenger (55).

Metabolic mechanisms regulating dendritic cell activation

Upon TLR activation, DCs dramatically shift their metabolic activity to glycolysis (39,40). The early increase in glycolytic flux is controlled by TBK1-IKK ϵ signaling and provides glucose-derived pyruvate for the generation of citrate, which is used for *de novo* fatty acid synthesis. This supports the expansion of the endoplasmic reticulum and Golgi membranes that are required for the production and secretion of inflammatory mediators (40). CLR engagement by β -glucans also induces early glycolytic reprogramming that depends on PI3K/TBK1/AKT signaling (62). Intracellular stores of glucose in the form of glycogen contribute to early TLR activation of DCs as well, with carbons from glycogen preferentially supporting citrate production that is used for fatty acid synthesis (63).

During late activation of bone marrow-derived DCs (BMDCs), glycolysis remains elevated and promotes optimal activation and cell survival (39). Due to the expression of inducible nitric oxide synthase (iNOS or NOS2), which is promoted by TLR stimulation,

BMDCs have gradually diminishing mitochondrial function due to inhibition of the ETC by nitric oxide (64). This results in upregulation of glycolysis, likely to compensate for the loss in mitochondrial ATP production. cDCs, however, do not express iNOS, and BMDCs are more similar to iNOS-expressing inflammatory monocyte-derived DCs, which have been shown to also require glycolysis for survival *in vivo* (64). Despite this difference, cDC stimulation by poly I:C, a viral RNA mimic and TLR3 agonist, similarly reduces oxidative metabolism and increases glycolysis by inducing type I IFN-dependent HIF-1 α gene expression (65). While glycolysis is generally associated with DC activation, the presence of glucose after activation has been shown to be inhibitory for the capacity of DCs to induce T cell proliferation and IFN- γ production (66). Through an mTOR/HIF-1 α /iNOS signaling circuit, glucose sensing by DCs determines their functional outputs (66). This mechanism is thought to enhance DCs stimulation of T cells within the lymph node, where they may face nutrient limitation due to high cellular density and competition.

In DCs, HIF-1 α , which promotes the expression of certain glycolytic genes, can be stabilized by hypoxia or by TLR ligands like LPS under normoxia (67). HIF-1 α -induced glycolysis is activated by different pathways depending on the stimulus; while HIF-1 α activity by LPS activation requires MYD88-dependent NF- κ B activity, HIF-1 α activity promoted by hypoxia does not (67,68). HIF-1 α -controlled glycolytic metabolism is essential for the immunogenicity of DCs (65), further highlighting the importance of glycolysis in DC activation.

Dendritic cell metabolism in tolerance

Immune tolerance exists as a measure to prevent inflammatory responses towards self or non-pathogenic antigens, such as dietary antigens. Tolerogenic DCs induce immune tolerance by

inhibiting effector T cell function while promoting Treg cell expansion, supported by the production of regulatory cytokines like IL-10 and TGF- β , and the expression of inhibitory surface molecules like PD-L1 and CTLA-4 (69). Disrupting the balance in the regulation of tolerance can result in autoimmune disease or a suboptimal response against pathogens or tumors.

Reprogramming of DC metabolism to induce tolerance is one of many mechanisms tumors use to evade the immune system. Several amino acids or their metabolic derivatives have an inhibitory effect on immune cell function. Melanoma-derived signaling protein WNT5A promotes FAO in DCs by triggering β -catenin signaling, which induces PPAR- γ -driven expression of CPT-1A (70). This elevated FAO activity fuels heme biosynthesis that is needed to support the enzymatic activity of indoleamine 2,3-dioxygenase 1 (IDO), an immunoregulatory enzyme that is involved in tryptophan catabolism (70). Kynurenine, a metabolite derived from tryptophan, promotes the differentiation of Treg cells from naïve CD4⁺ T cells, further establishing an immunosuppressive tumor microenvironment (70). Another way tumors induce IDO expression in DCs is via myeloid-derived suppressor cells (MDSCs) (71), which are generated during cancer progression by the action of tumor-derived factors on myeloid progenitors (72). MDSCs express high levels of arginase 1 (ARG1), and polyamines produced during decarboxylation of the ARG1 product ornithine can induce IDO expression in DCs, promoting their tolerization (71). TGF- β alone can also act on DCs to increase their ARG1 expression, producing the necessary metabolites required to upregulate IDO expression and confer immunosuppressive properties on the DCs (71). In addition, tumor-infiltrating DCs of spontaneous mammary adenocarcinomas uptake relatively high levels of L-arginine compared to splenic DCs (73). L-arginine metabolism by ARG1 in the tumor-infiltrating DCs suppresses anti-

tumor CD8⁺ T cell function, and pharmacological inhibition of ARG1 largely restores T cell proliferation (73). Mutations in the TCA cycle enzyme isocitrate dehydrogenase is found in several tumor types and produces the oncometabolite D-2-hydroxyglutarate, which inhibits IL-12 secretion by human monocyte-derived DCs (74). The metabolic reprogramming induced by LPS is affected in the presence of D-2-hydroxyglutarate, with reduced lactate production and enhanced cell respiration (74). These studies demonstrate that some amino acids or metabolite derivatives may act on or be secreted by DCs to induce immune tolerance.

Another metabolite that has inhibitory properties is lactate, a metabolite that is often abundant in the microenvironment of highly glycolytic tumor types. Tumor-associated macrophages, for example, polarize to an M2-like phenotype when exposed to high levels of lactic acid, thus favoring tumor growth (75). Lactic acid also reduces effector function and tumor infiltration by T cells and NK cells, as demonstrated by improved tumor control in mice with tumors expressing lower levels of lactate dehydrogenase A (LDHA) (76). Tumor-associated DCs have impaired maturation and IL-12 secretion, which is prevented if lactic acid production by melanoma cells is blocked by oxamic acid, an inhibitor of LDH activity (77). Conditioning by lactic acid also reduces DC production of IL-12p70 and IFN- α , as well as cross-presentation and anti-tumor immunity *in vivo* (78). The lactate produced by developing monocyte-derived DCs cultured at higher density is inhibitory to their differentiation and acquisition of inflammatory functions, with increased IL-10 production, but reduced pro-inflammatory cytokine production and ability to induce Th1 polarization (79). Tolerogenic DCs themselves have been shown to secrete high levels of lactate, which inhibits proliferation of CD4⁺ T cells (80). In all, lactate has inhibitory effects on DCs and other immune cells.

Tumors can also induce immune tolerance by promoting lipid accumulation in DCs. Under physiological conditions, lipid bodies in DCs are not typically associated with impairment of DC function. For example, two populations of hepatic DCs distinguished by their lipid content have contrasting phenotypes: the population with high lipid content has much greater immunogenicity, while the population with lower lipid levels induces tolerance by promoting Treg cell generation (81). Inhibition of fatty acid synthesis in the DCs with high lipid content impairs pro-inflammatory cytokine production and effector T cell activation, demonstrating a direct role for lipids in promoting their immunogenicity (81). Lipid bodies in CD8 α^+ cDC1s also play a critical role in cross-presentation (82). In the tumor microenvironment, however, lipid accumulation in DCs leads to their dysfunction, as defined by their reduced capacity to process antigen and stimulate T cells (83). Here, increased lipid uptake and fatty acid synthesis both contribute to lipid accumulation. Pharmacological inhibition of fatty acid synthesis improves DC function and therefore anti-tumor immunity (83). Another study has demonstrated that the lipids that accumulate in tumor-associated DCs are oxidized, and that these oxidized lipids block cross-presentation by preventing the trafficking of peptide-MHC I complexes to the cell surface (83,84). The electrophilic properties of oxidized lipids, which endogenous non-oxidized lipid bodies lack, cause the binding of oxidized lipids to heat shock protein 70 (HSP70) (84). This impedes the interaction between HSP70 and peptide-MHC I complexes, resulting in the peptide-MHC I complexes remaining co-localized at lysosomes and not at the cell surface (84). The sources of the oxidized lipids in tumor-associated DCs have been shown to be through the uptake of oxidized lipids in the tumor microenvironment via the scavenger receptor CD204, as well as further triglyceride synthesis driven by the activation of ER stress factor XBP1 (83,85,86). In summary, these studies establish that the type of lipids that accumulate in DCs are significant to

their function; while oxidized lipids limit the immunogenic capacity of DCs, neutral lipids generally do not.

Regulation of mitochondrial metabolism by transcriptional coactivator PGC-1 β

PGC-1 coactivator targets and regulation

Transcription factors bind DNA in a sequence-specific manner in order to regulate gene expression. They often require additional proteins that do not possess DNA-binding domains but are necessary for carrying out enzymatic activities such as chromatin remodeling and recruitment of RNA polymerase II. An example of such a regulator of transcription factors is the peroxisome proliferator-activated receptor gamma coactivator 1 (PGC-1) family of transcriptional coactivators, which consists of PGC-1 α and PGC-1 β , homologs that share extensive sequence identity, and PGC-related coactivator (PRC), a less closely related member (87). PGC-1 α and PGC-1 β have crucial roles in cellular metabolism as coactivators of numerous transcription factors responsible for regulating the expression of nuclear-encoded mitochondrial genes. Stimulation of these genes results in the increased metabolic activity by the mitochondria, including β -oxidation of fatty acids and OXPHOS.

The PGC-1 coactivators target multiple transcription factors, including NRF-1 and NRF-2, which promote the transcription of mitochondrial biogenesis and anti-oxidative genes; PPAR- $\alpha/\beta/\delta$, which induce FAO; PPAR- γ , which regulates lipid uptake and storage; SREBP-1a/1c/2, which promote lipogenesis; and several others (87). The expression levels of the PGC-1 proteins and their functions vary depending on the tissue that they are expressed. For example, PGC-1 α expression is induced by cold exposure in brown adipose tissue and targets PPAR- γ to stimulate programs of adaptive thermogenesis while PGC-1 β expression remains unchanged (88,89). In

contrast, PGC-1 β expression is induced by dietary lipids in the liver to a much greater extent than PGC-1 α , coactivating the SREBP family of transcription factors (90). In skeletal muscle, PGC-1 α expression is induced by exercise, while PGC-1 β expression is largely unchanged despite being highly expressed (91,92). Skeletal muscle-specific deficiency of PGC-1 α results in largely normal mitochondria, although simultaneous knockout of both PGC-1 α and PGC-1 β leads to reduced oxidative metabolism but no change in mitochondrial mass, suggesting there is some redundancy of these proteins (93). PGC-1 expression also promotes health and proper tissue function in other tissues with high metabolic activity, such as the heart and brain (93,94).

Regulation of PGC-1 proteins occurs at both the post-translational and transcriptional level (93). Their expression and activity are tightly and dynamically regulated to respond efficiently to physiological cues. In skeletal muscle, AMPK directly phosphorylates PGC-1 α , promoting its stability, in conditions of energy deficiency such as during exercise (95,96). PGC-1 α is also protective to neural cells by promoting the expression of anti-oxidative genes (97). Glycogen synthase kinase 3 β (GSK3 β), which phosphorylates PGC-1 α to favor its ubiquitination and subsequent degradation, is inhibited by oxidative stress, allowing PGC-1 α to promote the expression of anti-oxidative genes in this setting (97). In addition, the histone deacetylase SIRT1 deacetylates PGC-1 α in response to fasting signals in the liver (98). SIRT1 regulates the expression of gluconeogenic and glycolytic genes through PGC-1 α , but does not affect the mitochondrial genes that PGC-1 α can target (98). p38 MAPK plays a role in thermogenesis by phosphorylating both ATF-2 and PGC-1 α to induce uncoupling protein 1 (UCP-1) expression (99). The promoter for the PGC-1 α gene has a binding site for ATF-2, and therefore, activated ATF-2 also promotes the gene expression of PGC-1 α in brown adipose

tissue, further elevating PGC-1 α activity (99). Other binding sites at the promoter of the PGC-1 α gene include FOXO1 and cAMP response element-binding protein (CREB), which allow factors that are responsive to cold, exercise, insulin, and more, to stimulate PGC-1 α expression (100). PGC-1 β expression in the liver is induced by dietary lipids, but the exact mechanism regulating this is not yet known (90). Further, while the regulation of PGC-1 β expression has not been carefully examined in comparison to studies on PGC-1 α , there are likely similarities in regulatory mechanisms due to their close homology.

PGC-1 coactivators in immunity

Currently, studies on the role of PGC-1 proteins in immunity is largely focused on PGC-1 α , with few on PGC-1 β . In T cells, an important role for PGC-1 α has been established in maintaining metabolic fitness and function in the context of disease. Upon activation, T cells increase glycolytic activity, mitochondrial biogenesis, and mitochondrial respiration (101). Metabolic defects can develop from pathological environments, such as in cancer or chronic infection, and severely impact their function. For example, CD8⁺ T cells from patients with chronic lymphocytic leukemia (CLL) display elevated mitochondrial respiration and membrane potential, but upon activation, mitochondrial biogenesis and glucose uptake are impaired (102). PGC-1 α expression is lower in CLL CD8⁺ T cells compared to the healthy control, which may explain the impairment of mitochondrial biogenesis (102). Examination of chimeric antigen receptor (CAR)-T cells prior to infusion into CLL patients reveals a positive correlation between greater mitochondrial mass and complete response to CAR-T cell therapy (102). There have also been recent studies that modulate the metabolic activity of dysfunctional T cells in order to improve immune responses. Tumor-infiltrating lymphocytes (TILs) have reduced mitochondrial

mass and mitochondrial function, and enforcing PGC-1 α expression improves their anti-tumor effector functions (103). Overexpression of PGC-1 α also favors the formation of central memory rather than resident-memory CD8⁺ T cells, promoting persistence of the cells and stronger anti-tumor immunity in a mouse melanoma model (104). Exhausted virus-specific T cells in mice infected with chronic lymphocytic choriomeningitis virus (LCMV) also exhibit metabolic defects, with greater mitochondrial mass but increased mitochondrial depolarization occurring early in the infection and resulting in bioenergetic insufficiencies (105). PD-1 and PD-L1 interactions were shown to repress the expression of PGC-1 α , and blocking this interaction with α PD-L1 improved the metabolic fitness of the T cells (105). Similar to the studies on TILs, overexpressing PGC-1 α in exhausted T cells also helps reverse some of their metabolic defects and counteract exhaustion (105). These studies highlight the crucial role PGC-1 α serves in mitochondrial biogenesis and optimal T cell function, and as a promising target in therapeutic strategies.

The role of PGC-1 β in immunity has been examined in a few different cell types across tissues. In macrophages, PGC-1 β is necessary for alternative activation induced by IL-4 by promoting FAO (106). STAT6, which mediates the transcriptional responses induced by IL-4, also promotes PGC-1 β expression, which in turn co-activates STAT6 in a feed-forward manner (106). In addition, expression of PGC-1 α and PGC-1 β by skeletal muscle cells *in vivo* dampens NF- κ B signaling induced by LPS injection and increases the levels of anti-inflammatory cytokines such as IL-10 and decreases pro-inflammatory cytokine IL-12 in the microenvironment (107,108). In cardiomyocytes, LPS reduces both PGC-1 α and PGC-1 β expression, suppressing FAO and promoting lipid accumulation (109). Restoring PGC-1 β expression rescues FAO in these cells and reduces LPS-induced ROS production (109). In the

brain, promotion of kynurenine aminotransferase 4 by NRF-2 and PGC-1 β results in production of kynurenic acid, which is known to be neuroprotective during sepsis (110). In human disease, gout patients that possess a genetic variant of *PPARGC1B* with a missense single-nucleotide polymorphism (SNP) have elevated IL-1 β in plasma and higher *NLRP3* expression in their PBMCs compared to gout patients without this SNP (111). Overall, existing studies demonstrate that PGC-1 β expression is associated with an anti-inflammatory phenotype.

THE IMPACT OF DIET-INDUCED OBESITY IN IMMUNITY

Changes to immune cells in obesity

With adipose tissue expansion, extensive changes occur in the composition and number of immune cells within the tissue. Chronic inflammation that results from these changes significantly contributes to metabolic pathologies commonly associated with obesity, including insulin resistance (112). Macrophages are the most abundant immune cell type found in adipose tissue, where a spectrum of activation phenotypes exists (113). This includes alternatively-activated M2-like macrophages that secrete immunomodulatory molecules like IL-10 and clear apoptotic cells, maintaining homeostasis (113). During obesity, adipose tissue hyperplasia leads to increased adipocyte stress and death, which results in adipose tissue macrophages surrounding dead adipocytes and forming clusters known as crown-like structures (114). In addition, the number of inflammatory macrophages increases as tissue-resident macrophages proliferate and circulating monocytes are recruited into the tissue by inflammatory factors and differentiate into macrophages (113). These macrophages adopt an inflammatory “metabolically-activated” phenotype, which is an activation state distinct from M1- or M2-like macrophages, and is

induced by stimuli, such as glucose, insulin, and fatty acids, that are associated with metabolic syndrome (115). Macrophage accumulation associated with obesity directly promotes the development of inflammation and systemic insulin resistance (116,117).

T cells are the next most abundant immune cell type in the adipose tissue after macrophages (118). In fact, adipose tissue is a major reservoir for memory T cells (119). In an obese setting, inflammatory CD8⁺ T cells, Th1 cells, and Th17 cells accumulate in the adipose tissue, while Treg cells decrease in frequency (120). The infiltration of CD8⁺ T cells in adipose tissue occurs before the accumulation of macrophages, with the CD8⁺ T cells participating in the recruitment and differentiation of macrophages (121). In contrast, Treg cells that express abundant levels of IL-10 help maintain homeostasis in adipose tissue of lean mice (122). Other immune cell types that contribute to establishing an anti-inflammatory environment include Th2 cells, invariant NKT cells and ILC2s (113).

Adipose tissue-associated dendritic cells

While adipose tissue-associated dendritic cells have not been extensively studied, emerging evidence has established their roles in both maintaining homeostasis and driving inflammation related to obesity. A major challenge has been distinguishing adipose tissue-resident cDCs from macrophages due to their largely overlapping set of surface markers used for identification, including CD11c, CD11b, MHC II, and F4/80 (4). One report discerns macrophages from cDCs with CD64, using gene profiling to confirm the enrichment of macrophages in the population of CD45⁺CD64⁺CD11c^{+/-} cells, and cDCs in the CD45⁺CD64⁻CD11c⁺ cells (123). A high fat diet challenge leads to CCR7-dependent accumulation of cDCs in adipose tissue that augments inflammation and insulin resistance, suggesting most cDCs are recruited during obesity-related inflammation (123). Adipose tissue-associated DCs have also

been found to contribute to inflammation by inducing Th17 differentiation (124) and promoting macrophage infiltration of adipose tissue during obesity (125).

Another group further confirms the role of cDCs in adipose tissue homeostasis and inflammation by focusing on cells expressing ZBTB46, a transcription factor that distinguishes cDCs from other immune cells, and dividing them into the cDC1 and cDC2 subsets based on CD103 and CD11b expression, respectively (126). They found that cDC1s and cDC2s engage the Wnt/ β -catenin and the PPAR- γ pathways, respectively, to promote an anti-inflammatory microenvironment and maintenance of homeostatic conditions (126). Inhibition of these pathways exacerbates the inflammation associated with diet-induced obesity, and consequently increases insulin resistance in mice. Chronic over-nutrition reduces the level of Wnt ligands available in the adipose environment for cDC1s and PPAR- γ expression in cDC2s, leading to increased cDC activation, as well as additional recruitment of cDCs and other inflammatory cells into the adipose tissue (126). A subpopulation of DCs containing perforin also has an important regulatory role in maintaining immune homeostasis, as animals lacking these cells exhibit weight gain, dyslipidemia, inflammation, and reduced insulin sensitivity independent of diet—symptoms that were further exacerbated with high-fat diet feeding (127). Perforin-containing DCs are known to selectively delete self-reactive T cells (128), and accordingly, animals lacking this DC subpopulation were found to have increased CD4⁺ and CD8⁺ T cell numbers in the adipose tissue directly responsible for the increased inflammation and consequent metabolic pathologies (127). Together, these studies support the importance of adipose tissue-associated cDCs and their ability to independently drive obesity-related inflammation, providing a firm foundation for further study on the clinical implications of these cells in both health and disease.

Rationale and objectives

As an abundant number of studies have clearly demonstrated (section Dendritic cell metabolism), the metabolism of DCs and other immune cells is intimately involved in regulating their development, activation, and function, and is therefore imperative in shaping an immune response. I hypothesized different metabolic profiles correspond to specific inflammatory phenotypes and that metabolism regulates multiple aspects of DC function. To further investigate this, I explored several aspects of metabolism and their importance in DC biology.

To date, most studies on DC metabolism have focused on activated DCs that display strongly pro-inflammatory phenotypes. In Chapter 2, we explored the metabolic changes in DCs stimulated by a range of stimuli. We found that DCs increase their early glycolytic activity across a range of inflammatory phenotypes. Based on this finding, we next investigated the importance of glycolysis in a crucial function common to DCs regardless of the strength of activation: cellular migration.

In Chapter 3, we aimed to examine mitochondrial metabolism in DCs, as its role is not well-studied in DCs. Moreover, the major mitochondrial regulator and transcriptional co-activator, PGC-1 β , has not yet been examined in DCs. Interestingly, in many tissues, including brown adipose tissue and skeletal muscle, PGC-1 α expression is more dynamically regulated by physiological cues compared to PGC-1 β (93). In contrast, our early data showed that PGC-1 β drastically changes with LPS stimulation of bone marrow-derived DCs. Thus, in Chapter 3, we investigated the role of PGC-1 β in regulating the metabolic status of DCs and its influence on DC function and activation.

The importance of DCs in adipose tissue—both for maintaining homeostasis and for driving obesity-associated inflammation—has recently been established but few studies have

examined their metabolism. In Chapter 4, we sought to characterize cDC subsets, including the previously unexamined cDC2A and cDC2B subsets, in adipose tissue with an improved strategy to distinguish cDCs from macrophages. We measured metabolic features such as mitochondrial and lipid content in cDCs, and the changes that occur due to whole-body metabolic perturbation caused by high fat diet (HFD)-induced obesity in mice.

CHAPTER 2 – Glycolysis is essential for CCR7 oligomerization and dendritic cell migration

Preface

The work presented in Chapter 2 has been published as an original research article:

Guak H, Al Habyan S, Ma EH, Aldossary H, Al-Masri M, Won SY, et al. Glycolytic metabolism is essential for CCR7 oligomerization and dendritic cell migration. *Nature Communications*. 2018 Jun 25;9(1):2463.

Abstract

Dendritic cells (DCs) are first responders of the innate immune system that integrate signals from external stimuli to direct context-specific immune responses. Current models suggest that an active switch from mitochondrial metabolism to glycolysis accompanies DC activation to support the anabolic requirements of DC function. We show that early glycolytic activation is a common program for both strong and weak stimuli, but that weakly-activated DCs lack long-term HIF-1 α -dependent glycolytic reprogramming and retain mitochondrial oxidative metabolism. Early induction of glycolysis is associated with activation of AKT, TBK and mTOR, and sustained activation of these pathways is associated with long-term glycolytic reprogramming. We show that inhibition of glycolysis impaired maintenance of elongated cell shape, DC motility, CCR7 oligomerization and DC migration to draining lymph nodes. Together, our results indicate that early induction of glycolysis occurs independent of pro-inflammatory phenotype, and that glycolysis supports DC migratory ability regardless of mitochondrial bioenergetics.

Introduction

Dendritic cells (DCs) are among the first responding immune cells to any infection, injury or threat. DCs express a wide variety of pattern recognition receptors (PRRs), which are germline-encoded receptors that recognize conserved moieties such as non-self microbe/pathogen-associated molecular patterns (M/PAMPs) and danger-associated molecular patterns (DAMPs), often released during cell death or injury. Membrane-bound PRRs include Toll-like receptors (TLRs) and C-type lectin receptors (CLRs). DCs adopt different activation phenotypes depending on the combination of receptors engaged and the context in which activation occurs; this process is known as differential activation. Differential activation enables DCs to transmit context-specific information to other cells of the immune system and consequently direct the nature of inflammatory responses.

Regardless of their activation phenotype, DCs migrate from peripheral tissues to the draining lymph node (LN) where they interact with other cells of the immune system. For example, the activation phenotype of DCs directly determines T helper (Th) cell differentiation. DCs that are stimulated with TLR ligands such as lipopolysaccharide (LPS) stimulate a pro-inflammatory phenotype characterized by production of cytokines such as IL-12, IL-6, TNF- α , and moderate amounts of IL-10, and promote the differentiation of naïve Th cells into IFN- γ -producing Th1 cells (1). DCs stimulated by the yeast component zymosan (Zym), which engages TLR2, TLR6, and the CLR Dectin-1, produce less IL-12 and more IL-10 relative to LPS-stimulated DCs, and promote the induction of Th17 cells (2,3). DCs that encounter the allergen house dust mite (HDM) engage TLR2, TLR4, and Dectin-2, and produce very little pro-inflammatory cytokines, but are able to promote the activation and differentiation of Th2 and Th17 cells (4,5).

In recent years, cellular metabolism has become recognized as an important determinant of immune cell inflammatory phenotype and function (6–12). Glycolysis and oxidative phosphorylation (OXPHOS) are the main bioenergetic catabolic pathways, taking place in the cytosol and mitochondria, respectively. Glucose-derived pyruvate can either be converted to lactic acid and expelled from the cell, or completely oxidized in the mitochondria via the tricarboxylic acid (TCA) cycle. The TCA cycle fuels OXPHOS by providing reducing agents to drive the electron transport chain (ETC), consuming oxygen as the final electron acceptor. Although OXPHOS supports a higher yield of ATP per molecule of glucose, induction of glycolytic metabolism despite the presence of oxygen (i.e. the Warburg effect) is observed in many cell types (13). We and others have shown that TLR-mediated DC activation results in a striking Warburg-like metabolic shift to glycolysis, which is necessary to support their pro-inflammatory phenotype (7,14,15). The immediate increase in glycolytic activity in TLR-activated DCs was found to be required for *de novo* fatty acid synthesis to expand the endoplasmic reticulum and Golgi to support the increased production and secretion of immune mediators (14). In long-term activation of inducible nitric oxide synthase (iNOS)-expressing DCs, TLR-induced nitric oxide (NO) production was shown to block electron transport, resulting in the cessation of OXPHOS (15). Thus, in NO-producing cells, the increase in glycolysis was found to be only necessary in the absence of OXPHOS (15). In DCs lacking iNOS, a long-term shift to glycolytic metabolism also occurs, although this is thought to be driven by autocrine type I interferon signaling through HIF-1 α (16).

The importance of metabolic programming for the function of DCs has largely been shown for highly pro-inflammatory DCs; however, activated DCs can take on distinct activation phenotypes. We therefore examined the metabolic profiles of DCs activated by a more diverse

range of stimuli, including both weak and strong activators of DCs, to determine the impact of glycolytic metabolism on DC function. We found that regardless of activation stimulus, DCs increase their glycolytic activity following stimulation. DCs activated with strong stimuli such as LPS or Zym display increased glycolysis with a corresponding decrease in OXPHOS. However, we found that HDM-activated DCs, which display a weak pro-inflammatory phenotype, also rapidly increased glycolysis early following stimulation, but lacked long-term metabolic reprogramming. TBK, AKT, and mTOR signaling pathways, which are known to regulate glycolysis in DCs, were activated in DCs with either a weak or strong pro-inflammatory phenotype. However, long term activation of these pathways and increased HIF-1 α activation occurred only in DCs with a highly pro-inflammatory phenotype. We demonstrate that glycolysis, and not mitochondrial metabolism, is important for DC motility and migration, as inhibition of glycolysis impaired the maintenance of elongated cell shape, DC motility, and DC migration to draining lymph nodes *in vivo*. Importantly, glucose metabolism is also necessary for CCR7 oligomerization, which is essential for efficient DC migration. These findings reveal that glycolysis induction occurs independent of acquisition of a pro-inflammatory phenotype and supports the migratory capacity of DCs.

Results

Differentially-activated DCs display distinct bioenergetic profiles

Stimulation of DCs with strong TLR agonists such as LPS promotes metabolic reprogramming to glycolysis with concomitant loss of ATP-coupled mitochondrial respiration (7,14,15). To assess whether this is a universal effect of PRR stimulation, we examined the bioenergetic

profile of DCs stimulated with a range of activators that engage different PRRs (Table 1), resulting in different inflammatory phenotypes. We measured surface expression of the co-stimulatory molecules CD80, CD86, CD40, and MHC II (Fig. 1A, Supplementary Fig. 1A), as well as the production of cytokines IL-12p40, TNF- α , IL-6, and IL-10 (Fig. 1B, Supplementary Fig. 1B) following stimulation with these activators. “Strong” activators (i.e. LPS, Zym, and curdlan) induced much greater surface marker expression and cytokine secretion compared to “weak” activators (i.e. HDM and zymosan depleted of its TLR ligands (ZymD)).

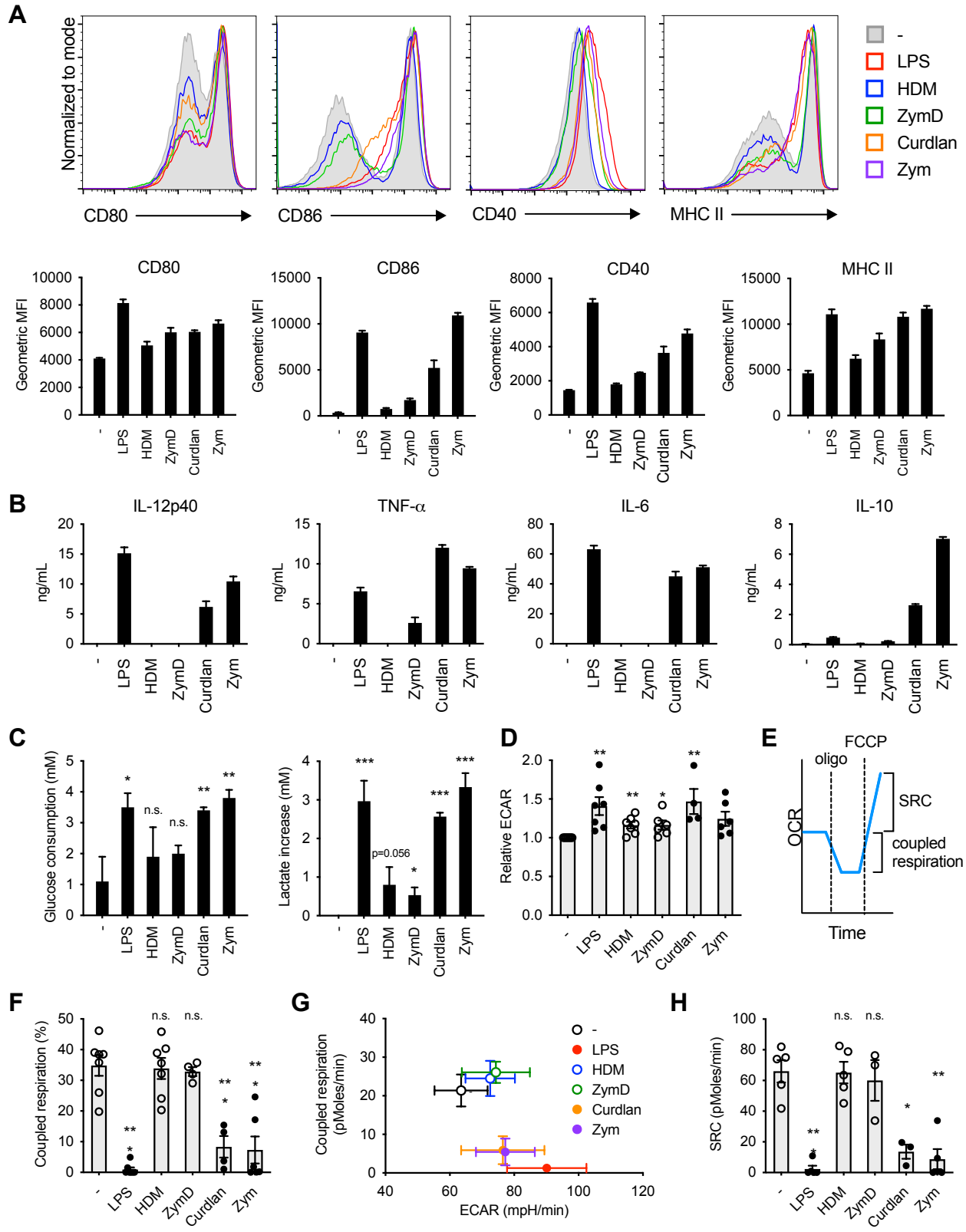
Table 1 – DC activators

| Activator | PRRs engaged | Concentration |
|--------------------------|------------------|---------------------|
| Lipopolysaccharide (LPS) | TLR4 | 10 or 100 ng/mL |
| House dust mite (HDM) | TLR2/4, Dectin-2 | 50 μ g/mL |
| Curdlan | Dectin-1 | 25 or 50 μ g/mL |
| Zymosan | TLR2/6, Dectin-1 | 5 or 10 μ g/mL |
| Zymosan-depleted (ZymD) | Dectin-1 | 10 or 25 μ g/mL |

To assess metabolic reprogramming induced by these activators, we examined glucose consumption and lactate production in DCs 18 h following stimulation with either strong or weak DC activators. All DC activators stimulated increased glucose consumption and lactate production relative to resting DCs, with strong DC activators generally displaying higher levels of glucose metabolism than weaker activators (Fig. 1C). We next used Seahorse profiling, measuring the extracellular acidification rate (ECAR, a measure of glycolysis) and oxygen consumption rate (OCR, Fig. 1E), to determine the bioenergetic profiles of differentially-activated DCs. Consistent with previously published reports (7,14,15), resting DCs engaged both

OXPPOS and glycolysis, while LPS-treated DCs no longer displayed ATP-coupled mitochondrial respiration and exclusively used glycolysis for ATP production (Fig. 1D,F,G). Similar to LPS, stimulation with the highly pro-inflammatory activators curdlan and Zym increased ECAR and decreased coupled respiration (Fig. 1D,F). Interestingly, weak DCs agonists (HDM, ZymD) induced slight but consistent increases in ECAR while retaining coupled respiration (Fig. 1D,F).

The difference in maximal mitochondrial respiratory capacity, measured after FCCP treatment, and basal respiration is known as the spare respiratory capacity (SRC) (Fig. 1E,H). DCs stimulated with strong activators (LPS, curdlan, Zym) most often displayed negligible SRC, although in some experiments DCs stimulated with curdlan and Zym retained SRC, while the SRC of weakly activated DCs was consistently similar to resting DCs (Fig. 1H). These data indicate that differential DC activators can induce intermediate bioenergetic phenotypes in DCs, resulting in the stimulation of glycolysis while retaining varying degrees of OXPPOS and mitochondrial respiratory capacity.



(legend on next page)

Figure 1 – Bioenergetic profiles of differentially-activated DCs

(A, B) Activation marker expression (CD80, CD86, CD40, and MHC II) and cytokine production (IL-12p40, TNF- α , IL-6, and IL-10) were measured following 18 h activation with indicated activators. (C) Glucose consumption (left) and lactate increase compared to the unstimulated condition (right) were measured 18 h following stimulation. (D, F-H) ECAR and OCR were measured using a Seahorse Bioanalyzer following an 18h stimulation. (E) Coupled respiration is represented by the decrease in OCR from baseline after oligomycin treatment, and is therefore the OCR attributed to ATP production. Spare respiratory capacity (SRC) is represented by the increase in OCR from baseline after FCCP treatment. (F) Coupled respiration as a percentage of total respiration. (G) Mean coupled respiration versus mean ECAR. (H) SRC. Data shown in (A-C) are from 1 experiment representative of at least 3 independent experiments (mean and s.d. of triplicates (A,C) or duplicates (B)). Data shown in (D, F-H) are from 3 to 7 experiments (depending on condition) (mean and s.e.m.). LPS: Lipopolysaccharide; HDM: house dust mite; ZymD: Zymosan depleted of TLR ligands; Zym: Zymosan; ECAR: Extracellular acidification rate; OCR: Oxygen consumption rate. Data were analyzed using *t*-test, comparing each condition relative to the control. *** $p < 0.001$, ** $p < 0.01$, * $p < 0.05$

Early glycolytic flux is a hallmark of both weak and strong DC activators

Given that both strongly and weakly activated DCs increase glycolysis, regardless of their pro-inflammatory nature, we monitored the bioenergetic states (ECAR and OCR) of differentially-activated DCs in real-time following PRR stimulation. All differentially-activated DCs, including those weakly activated by HDM or ZymD, displayed increased ECAR immediately after stimulation (Fig. 2A, left). Short-term activation did not change the OCR of differentially-activated DCs, except those stimulated with Zym and ZymD (Fig. 2A, right). The increase in oxygen consumption observed with these stimuli was determined to be largely non-mitochondrial (Supplementary Fig. 2), which is consistent with literature demonstrating that Zym stimulates NADPH oxidase activity and the consequent production of reactive oxygen species (3,17). The serine/threonine protein kinase AKT is known to be required for glycolytic activity in TLR-activated DCs (14). Analysis of phospho-AKT (Ser473) levels following

stimulation for 1h revealed increased, albeit variable, AKT activation in differentially-activated DCs regardless of inflammatory stimulus (Fig. 2B). Thus, the downregulation of OXPHOS observed in strongly-stimulated DCs is a long-term adaptation to PRR stimulation, while AKT activation and increased glycolysis is an early event following activation and is independent of a pro-inflammatory phenotype.

To further characterize glucose metabolism following DC activation, we investigated the fate of ^{13}C -labeled glucose in activated DCs using stable isotope tracer analysis (SITA, Fig. 2C) (18). DCs were activated with LPS, HDM, or Zym for 2h and pulsed with U- ^{13}C -glucose for an additional 2h (Fig. 2C). Zym- and LPS-stimulated DCs displayed hallmark profiles of Warburg metabolism, characterized by increased conversion of ^{13}C -glucose to ^{13}C -pyruvate and ^{13}C -lactate (Fig. 2C). Consistent with their bioenergetic profile (Fig. 1), HDM-stimulated DCs displayed increased ^{13}C -lactate production from ^{13}C -glucose, although at lower levels than observed in LPS- or Zym-stimulated DCs (Fig. 2C). Moderate but consistent increases in ^{13}C -glucose-derived TCA cycle intermediates were observed in activated DCs (Fig. 2C), suggesting evidence of glucose conversion to acetyl-CoA. Of note was an increased abundance of unlabeled α -ketoglutarate and succinate in strongly activated DCs (Fig. 2C), suggesting an alternative carbon source is contributing to the increased production of these metabolites. DCs also converted a significant amount ($\sim 30\%$) of ^{13}C -glucose to alanine, indicating that glucose-derived pyruvate has several metabolic fates – lactate, alanine, and acetyl-CoA – which are all produced independent of pro-inflammatory phenotype.

Loss of coupled respiration directly correlates with iNOS expression and NO production

Increased glycolytic metabolism in LPS-stimulated DCs has been reported to be required for energy production due to the inhibition of mitochondrial respiration by NO (15). To determine whether loss of mitochondrial metabolism also correlates with NO production in differentially-activated DCs, iNOS expression and NO production were measured in DCs activated by various stimuli. iNOS expression increased in a dose-dependent manner for curdlan and Zym (levels plateaued after 10 µg/mL for Zym) (Fig. 3a), with corresponding increases in nitrite levels (Fig. 3B). In these strongly-activated DCs, the increase in iNOS expression and NO production correlated with the loss of coupled respiration (Fig. 3C). Inhibition of mitochondrial oxidative metabolism was further reflected by the little to no SRC remaining in the strongly-activated DCs (Fig. 3D). No appreciable levels of iNOS or NO were induced by HDM or ZymD stimulation of DCs (Fig. 3A-B), and both coupled respiration and SRC were maintained in these activated DCs (Fig. 3C-D). Together, these data show that iNOS expression and NO production correlates with the loss of coupled respiration in differentially-stimulated DCs and that an early increase in glycolysis can occur regardless of whether iNOS is later induced.

Weakly inflammatory DCs lack long-term glycolytic reprogramming

Metabolic reprogramming in immune cells is reinforced by changes in expression of key metabolic pathway genes that underlie changes at the biochemical level. To assess the impact of different TLR agonists on DC metabolic reprogramming, we examined the kinetics of gene expression of key enzymes in glycolysis following activation. During early stages of DC activation (4 h post-stimulation), minor changes in the expression of *Glut1* and *Hk2* were observed, but expression of distal components of glycolysis (*Pkm2*, *Gapdh*, and *Ldha*) were unchanged (Fig. 4A, left).

However, at late time points (18 h post-stimulation), DCs activated with pro-inflammatory stimuli (LPS, curdlan and Zym) showed increased expression of glycolytic genes, whereas DCs stimulated with “weak” activators HDM and ZymD showed little or no change in the expression of these enzymes relative to resting DCs (Fig. 4A, right). These results suggest that increased early glycolysis induced by stimulation occurs independent of large-scale changes in metabolic gene expression. Metabolic reprogramming at the level of transcription occurs following long-term DC activation in strongly pro-inflammatory DCs, but not in weakly-activated DCs.

The TBK- $\text{IKK}\epsilon$ signaling pathways have been identified as key kinases important for early induction of glycolysis in DCs (14). We found that early activation of TBK, AKT and mTORC1 occurred regardless of the activation phenotype (Fig. 4B). However long-term activation of both mTORC1 (measured by phospho-S6K and phospho-S6 levels) and mTORC2 (measured by phospho-AKT Ser473 levels) was associated only with the presence of a pro-inflammatory phenotype (Fig. 4B). Analysis of the time course revealed that AKT and mTORC1 activity was progressively lost in HDM-stimulated DCs around 8-12 h following activation (Fig. 4C). Early glycolysis induction by HDM, like LPS (14), could be prevented by AKT inhibition (Supplementary Fig. 3). Interestingly, TBK phosphorylation levels were maintained in HDM-stimulated cells (Fig. 4C). Stable HIF-1 α protein expression was observed in LPS-stimulated DCs between 8-18 h post-activation, but absent in HDM-stimulated DCs at all time points (Fig. 4C). Consistent with the role of HIF-1 α in glycolytic reprogramming, the absence of detectable HIF-1 α protein levels in DCs stimulated with weak agonists correlated with the lack of significant long-term induction of HIF-1 α -dependent glycolytic gene expression (*Hk2*, *Ldha*) (19) in these cells (Fig. 4A). Induction of iNOS was also absent in HDM-stimulated DCs (Fig. 4D). These data are

consistent with evidence linking mTORC1 to long-term commitment to glycolysis by induction of iNOS and HIF-1 α (20).

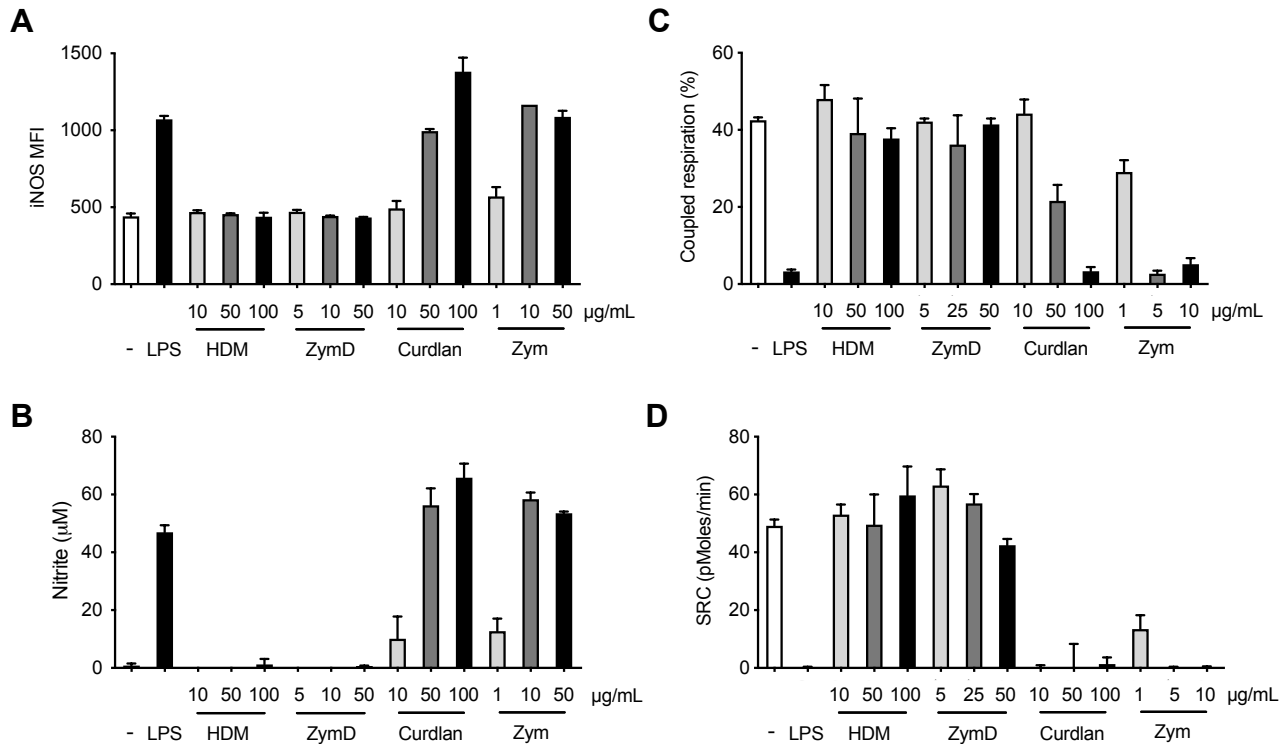


Figure 3 – iNOS expression and NO production is correlated with loss of coupled respiration

DCs were stimulated for 18 h by activators at the indicated doses (µg/mL). (A) Geometric MFI of iNOS, (B) nitrite (NO₂⁻) production, (C) coupled respiration and (D) SRC were measured as described in Materials and Methods and in Figure 1. Data shown are from 1 experiment representative of 3 experiments (mean and s.d. of duplicates (A,B), s.e.m. of 4 to 6 replicates (C,D)). Data were analyzed using a one-way ANOVA. ***p<0.001, **p<0.01

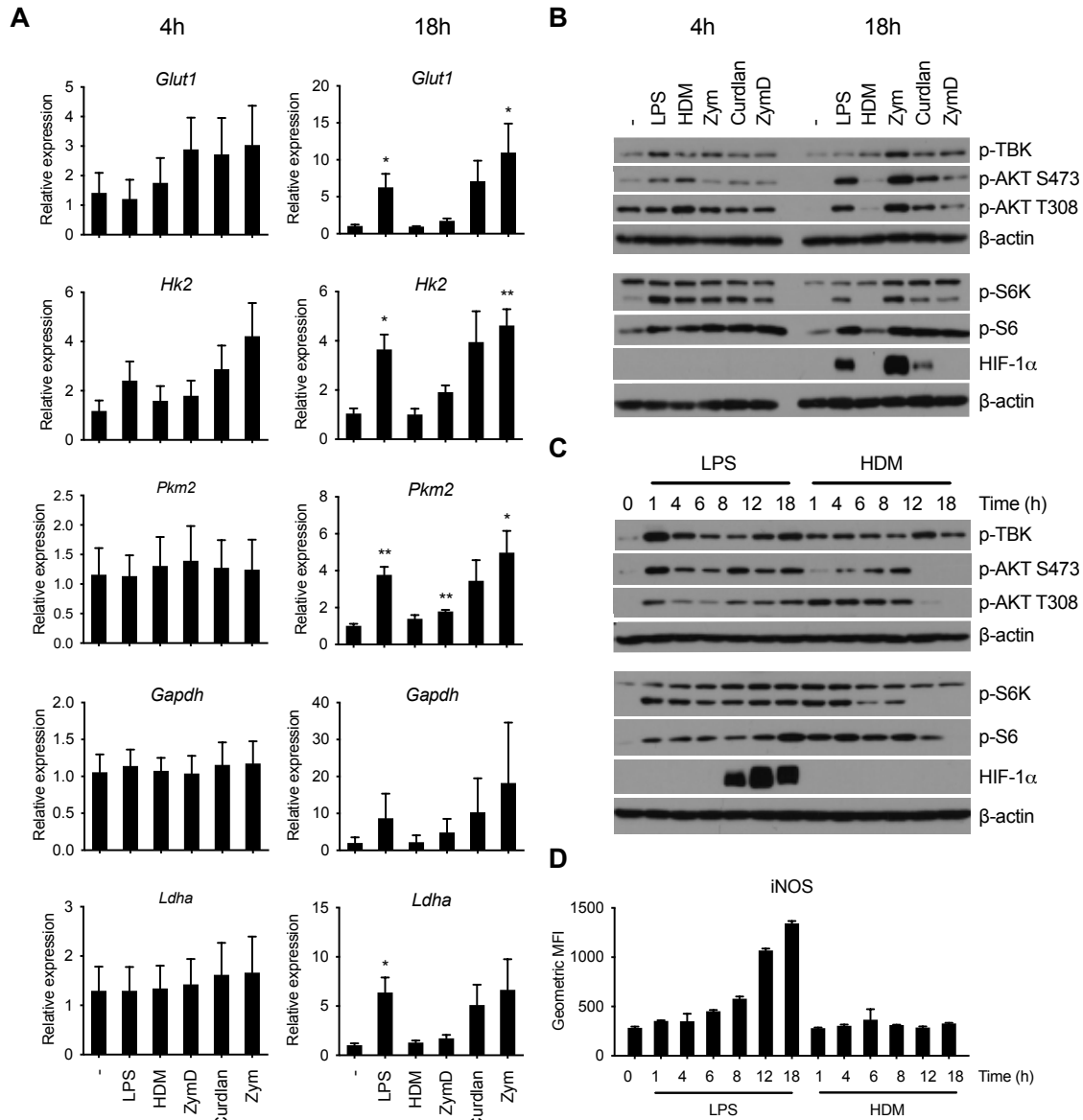


Figure 4 – Weakly activated DCs lack long-term metabolic reprogramming.

(A) Gene expression of glucose transporter *Glut1* and glycolytic enzymes *Hk2*, *Pkm2*, *Gapdh*, and *Ldha* by DCs were measured after differential activation for 4 h (left) and 18 h (right). (B,C) Immunoblot for p-AKT (Ser473), p-AKT (Thr308), p-TBK (Ser172), p-S6K, p-S6, HIF-1α, and β-actin following (B) differential activation for 4 h and 18 h, and (C) activation by LPS or HDM over a time course from 1 h to 18 h. (D) Geometric MFI of iNOS in DCs activated by LPS or HDM over a time course from 1 h to 18 h. Data shown in (A) are fold changes from 3 experiments, (B,C) 1 experiment representative of 3 experiments, and (D) 1 experiment representative of 2 experiments (mean and s.e.m. (A) and s.d. (D) of triplicates). Data were analyzed using *t*-test, comparing each condition relative to the control. *** $p < 0.001$, ** $p < 0.01$, * $p < 0.05$

Induction of glycolysis is required for DC motility and migration

Our results indicate that early glycolytic flux is necessary for an aspect of DC function beyond sustaining a pro-inflammatory phenotype. Activated DCs, regardless of activation phenotype, must migrate to the draining LN to stimulate immune responses. Therefore, we examined the impact of glucose availability on DC migration. Using live imaging via confocal microscopy, we determined the cell velocity and displacement (distance travelled) in the presence or absence of glucose in culture medium. Under glucose limiting conditions, DCs exhibited dramatic reductions in motility, characterized by both reduced velocity and shorter overall distance travelled (Fig. 5A, Supplementary Movie 1). To ensure that reduced DC motility was not due to reduced cell viability, we cultured DCs in glucose-free medium and measured their motility upon the addition of glucose (10 mM). DCs immediately increased both velocity and displacement upon addition of glucose, displaying motility equal to that of DCs initially cultured in the presence of glucose (Fig. 5B,C, Supplementary Movie 2). Adding the glycolytic inhibitor 2-deoxyglucose (2-DG) significantly decreased DC velocity and displacement (Fig. 5C), implicating glycolysis in this process. Culturing DCs without glucose or with 2-DG also impacted DC morphology, stimulating the cells to become more round with retraction of dendrites (Fig. 5D, Supplementary Fig. 4). When glycolytic activity was reduced, either by glucose withdrawal or culture with 2-DG, DCs displayed metabolic compensation to mitochondrial OXPHOS (Fig. 5E), allowing DCs to maintain cellular ATP levels (Fig. 5F). These data demonstrate that DCs are capable of metabolic plasticity (shifting between glycolysis and OXPHOS) to maintain ATP production. However, increased OXPHOS is not sufficient to restore DC motility, and thus glycolysis is essential for DC motility. These data suggest that glycolysis is necessary for cytoskeletal changes that support cell shape and motility.

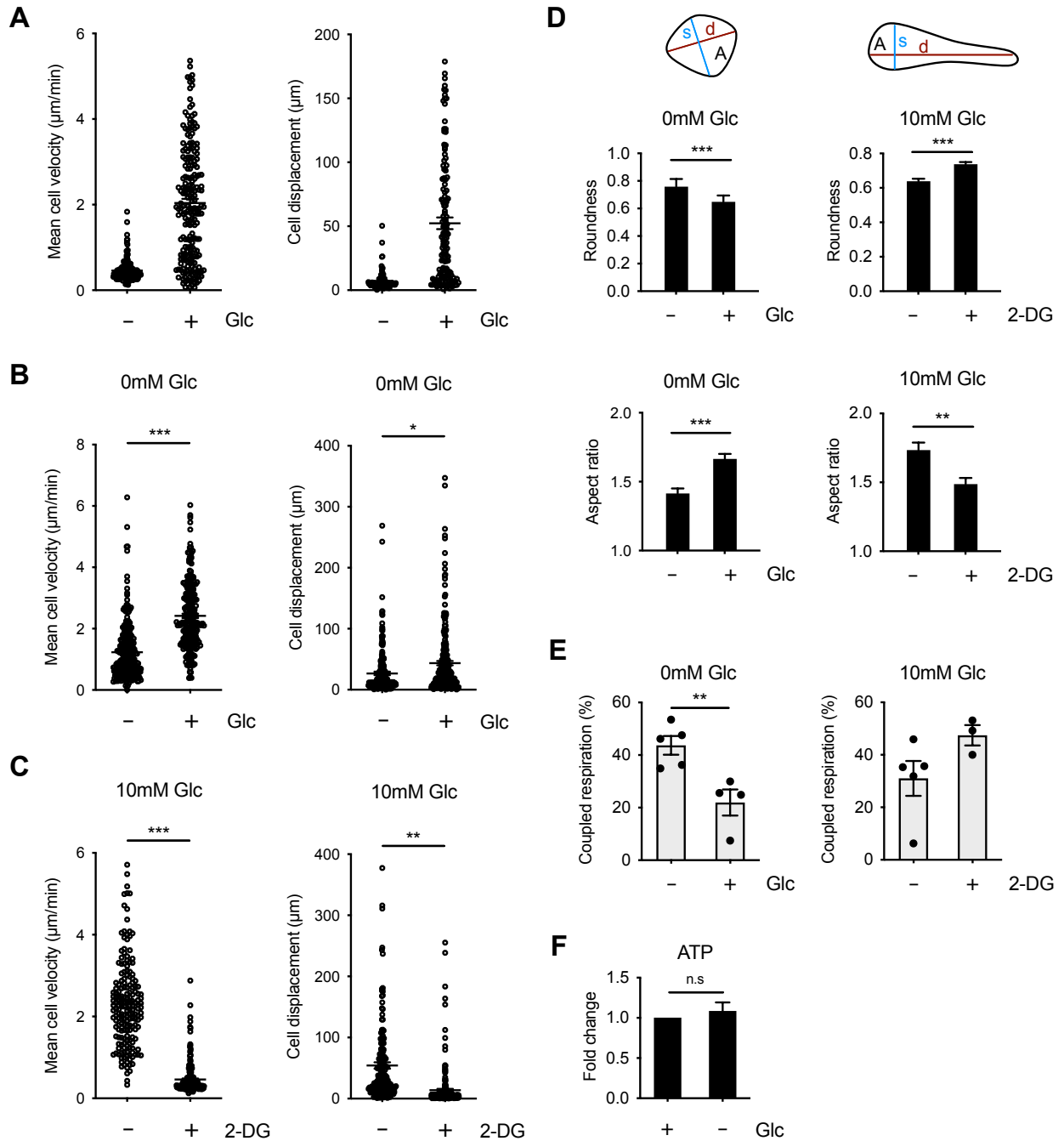


Figure 5 – Glycolysis is required for DC motility and morphology.

Images of DCs were captured over time using confocal microscopy. **(A)** Mean cell velocity (left) and cell displacement (right) of DCs in the presence or absence of 10 mM glucose after 4h. **(B)** Mean cell velocity (left) and cell displacement (right) of DCs cultured in the absence of glucose following the addition of media with or without 10 mM glucose. **(C)** Mean cell velocity (left) and cell displacement (right) of DCs cultured in the presence of glucose after the addition of

media with or without 10 mM 2-deoxyglucose (2-DG). **(D)** Roundness ($4 \times A/(\pi \times d^2)$; top left) and aspect ratio (d/s ; bottom left) of DCs cultured without glucose after the addition of media with or without 10 mM glucose, and roundness (top right) and aspect ratio (bottom right) of DCs cultured in the presence of glucose after the addition of media with or without 10 mM 2-DG. **(E)** Coupled respiration as a percentage of total respiration of DCs cultured without glucose and following the addition of glucose (left), and of DCs cultured in the presence of glucose and following the addition of 2-DG (right). **(F)** Fold change of ATP levels in DCs cultured with or without glucose relative to glucose condition. Data in **(A)** represent 164 to 210 cells. Data in **(B-D)** represent 179 to 268 cells from 1 experiment representative of 2 experiments. Data in **(E)** are 3-5 experiments (depending on condition) (mean and s.e.m.). Data in **(F)** are fold changes of 3 experiments (mean and s.e.m.). Data were analyzed using unpaired *t*-tests. *** $p < 0.001$, ** $p < 0.01$, * $p < 0.05$

In vivo, upregulation of CCR7, the receptor for the chemokines CCL21 and CCL19, in response to activating stimuli is necessary for DC migration to the draining lymph node. We found that *in vitro*, glucose was essential for DC migration toward CCL21 (Fig 6A). Glucose limitation had little effect on overall CCR7 expression on either resting or activated DC populations, however decreased CCR7 expression on CCR7⁺ DCs was observed (Fig. 6B, Supplementary Fig. 5). Oligomerization of CCR7 monomers enables efficient DC migration more so than expression levels, and is necessary to guide DCs to the draining lymph node (21). By fluorescence resonance energy transfer (FRET), we determined that CCR7 oligomerization on DCs was significantly impaired under conditions of reduced glucose availability, both in the absence and presence of activating stimuli (Fig. 6C). Finally, we examined DC migration toward CCL21 by splenic DCs, and found that, like BMDCs, splenic DC migration toward CCL21 was reduced upon glucose limitation or when glycolysis was blocked by 2-DG (Fig. 6D).

To determine the impact of glycolysis on DC migration *in vivo*, we first examined the ability of differentially-activated DCs injected in the footpad to migrate to draining lymph nodes. CFSE-labeled DCs were left unstimulated or stimulated with either LPS or HDM, and then injected subcutaneously into the footpads of mice. The size of the draining LNs increased

following injection of DCs compared to the PBS-injected control mice, but activated DCs migrated to a greater extent to the LN than unstimulated DCs (Fig. 6E). Notably, LPS and HDM promoted DC migration to a similar extent (Fig. 6E, right), indicating that migratory ability was not entirely dependent on a pro-inflammatory phenotype. HDM-activated DCs treated with 2-DG prior to injection displayed reduced migration to the draining LN (Fig. 6F), establishing a requirement for glycolysis for effective DC migration *in vivo*. We confirmed this decrease in migratory ability after 2-DG treatment was not due to reduced uptake of HDM by the DCs (Supplementary Fig. 6).

Finally, to examine the migration of endogenous DCs *in vivo*, we administered HDM intranasally and monitored DC migration from the lung to the mediastinal LN (22). At the time of stimulation, animals were treated with or without i.p. administration of 2-DG (23). Administration of 2-DG during allergic inflammation induced by HDM did not significantly impair the migration and accumulation of total immune cells (Fig. 6G). However, consistent with our adoptive transfer experiment (Fig. 6F), 2-DG administration reduced the migration of endogenous CD11c⁺MHCII^{hi} DCs to the lung in response to HDM (Fig. 6G). Together these data indicate that induction of glycolysis in DCs *in vivo* is essential to support DC motility and CCR7 oligomerization necessary for DC migration, regardless of PRR stimulus and activation phenotype.

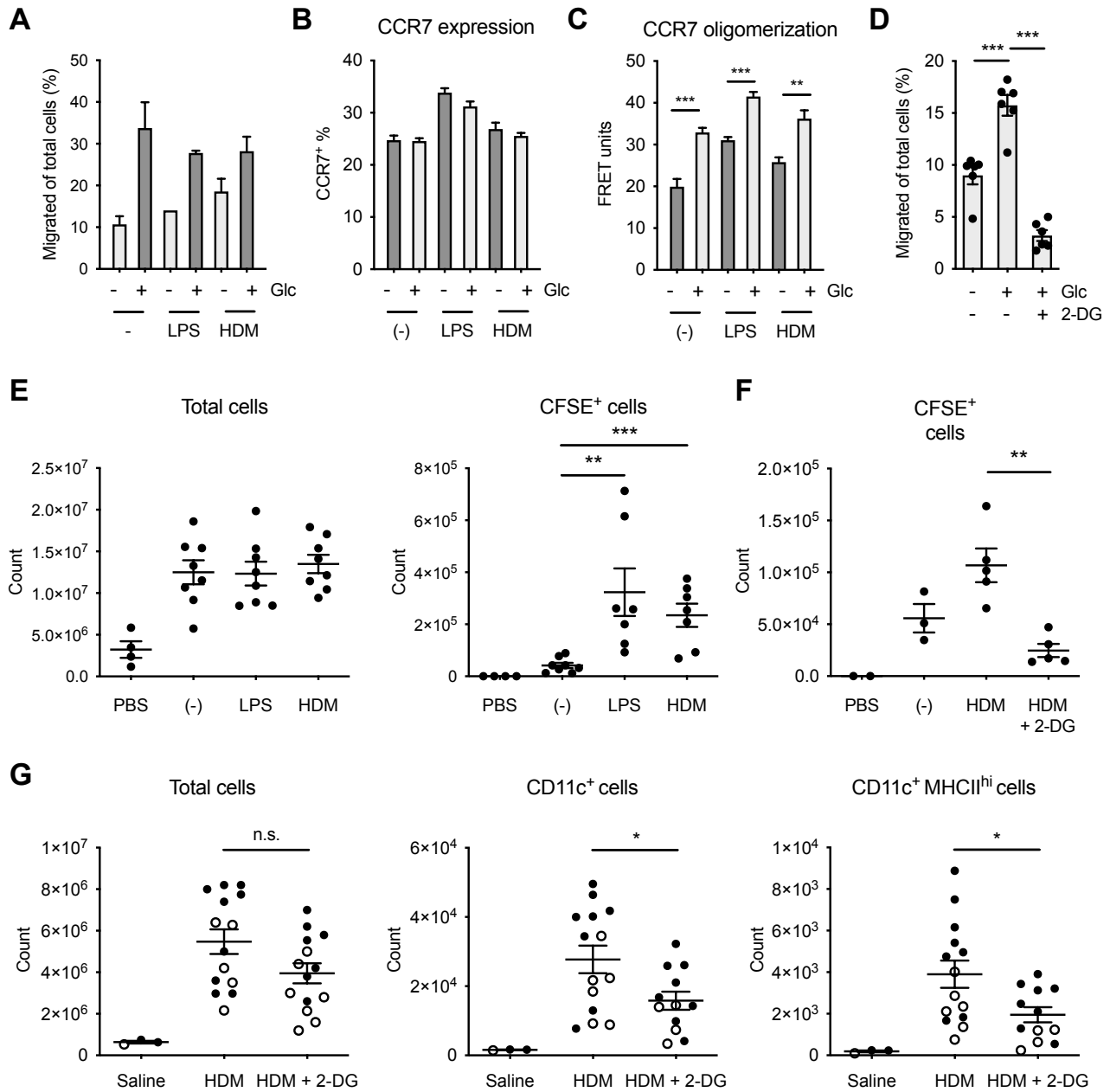


Figure 6 – Inhibition of glycolysis impairs CCR7 oligomerization and reduces DC migration to the draining lymph node.

(A) DCs incubated with or without 10 mM glucose for 4h migrate towards CCL21 for 2h. (B) Total CCR7 expression levels were measured and (C) CCR7 oligomerization was determined by FRET of DCs left unstimulated or stimulated with LPS or HDM with or without 10 mM glucose for 6h. (D) DCs isolated from the spleen were cultured with or without 10 mM glucose or 2-DG for 6h, then migrate towards CCL21 for 2h. (E) CFSE-labeled DCs stimulated were injected subcutaneously into the footpads of mice and the popliteal LNs were harvested after 45h. Total

cell number (left) and CFSE⁺ cells (right) from dLNs were determined. (F) CFSE-labeled DCs were stimulated with HDM with or without 10 mM 2-DG prior to footpad injection and LN harvest as in (E). (G) Cell numbers from mediastinal LNs of mice treated i.n. with 40 µg HDM or saline, and i.p. with 2-DG or saline. Data in (A-C) are from 1 experiment representative of 3 experiments (mean and s.d. of triplicates). Data in (d,e) are from 2 experiments (mean and s.e.m. of 6 mice (D), 4 mice for PBS control and 8 mice for other conditions (E)). Data shown in (F) are from 1 experiment representative of 3 experiments (mean and s.e.m. of 2 mice (PBS), 3 mice (unstimulated), or 4 to 5 mice (other conditions)). Data in (G) are from 2 experiments, with closed and open circles representing mice from different experiments (mean and s.e.m. of 3 mice for saline control and 14 mice for other conditions). Data were analyzed using one-way ANOVA. *** p<0.001, ** p<0.01, * p<0.05

Discussion

Reprogramming of cellular metabolism following immune cell activation is integral to support their activation and function. The majority of studies examining cellular metabolism in DCs use TLR agonists that induce strongly pro-inflammatory activation states (7,14,15,24), which collapses mitochondrial respiration and promotes aerobic glycolysis. By examining DCs stimulated with differential TLR agonists, we demonstrate that the bioenergetic profile of DCs is far more heterogeneous than previously reported. While strong pro-inflammatory activators, such as LPS, Zym, and curdlan, collapse ATP-coupled mitochondrial respiration and promote a prominent switch to glycolysis, DCs activated with TLR agonists that promote alternative DC activation with low inflammatory potential retain mitochondrial respiration. Using ¹³C-glucose tracing techniques, we demonstrate differential use of glucose-derived carbon in DCs stimulated with differential DC agonists, indicating diverse metabolic pathways usage by DCs depending on activation stimulus. The common metabolic link between highly- and weakly-inflammatory DCs is the immediate induction of glycolysis. We demonstrate that glycolysis is required for DCs to efficiently migrate *in vitro*, to retain their characteristic dendritic morphology, and to home to

secondary lymphoid organs *in vivo*. Mechanistically, CCR7 oligomerization, which is essential for efficient DC migration (21), was found to be highly dependent on glycolysis. Together our data implicate the early upregulation of glycolysis as a key mechanism supporting DC migration, in addition to supporting a pro-inflammatory phenotype of strongly activated DCs.

Previous work has established that inflammatory signals promote a metabolic shift to glycolysis in DCs (7,14). Our data here indicate that induction of glycolysis is not limited to DCs that acquire a highly pro-inflammatory phenotype. DCs treated with HDM, which induce Th2 differentiation (22), did not exhibit a detectable inflammatory phenotype, but strongly induced the activation of TBK, AKT, mTORC1 and mTORC2, and showed an early increase in glycolysis (Fig. 2, 4C) (14). In contrast to LPS stimulation, HDM-activated DCs maintained OXPHOS and SRC similar to unstimulated DCs. SRC is linked to the total mitochondrial capacity available to cells, and can be used under conditions of stress to produce energy and maintain cell viability (25). The lack of SRC in LPS-stimulated DCs limits their adaptability when glucose levels are limiting (15). Thus, while early glycolysis stimulated by all TLR agonists supports DC migration, the greater SRC in alternatively activated DCs argues that they can engage mitochondrial respiration for ATP production and are more metabolically flexible than pro-inflammatory DCs. In fact, in many experiments, Zym- and curdlan-activated DCs retained some coupled respiration while increasing glycolysis (Fig. 1C) suggesting that complete loss of OXPHOS may be unique to inflammatory DCs stimulated with certain agonists such as LPS. Of note, results obtained using ZymD were highly variable depending on the batch of ZymD. When ZymD was weakly activating, DCs acquired inflammatory and metabolic phenotypes similar to HDM-activated DCs; however more stimulatory batches of ZymD

sometimes led to a stronger pro-inflammatory phenotype with metabolic characteristics more similar to Zym-activated DCs.

Despite the fact that HDM induces no appreciable pro-inflammatory phenotype in DCs (as measured by upregulation of MHC, costimulatory molecules, and cytokine production), HDM stimulated the activation of TBK, AKT, and mTORC1/2. Whether these pathways regulate cell shape and motility in DCs beyond their involvement in glycolysis will be the subject of future study. Despite the activation of mTORC1 in HDM-activated DCs, we did not observe significant stabilization of HIF-1 α or induction of iNOS. Interestingly, TBK phosphorylation levels were maintained in HDM-stimulated cells even after AKT and mTORC1/2 activity had subsided suggesting that TBK may have another role in HDM-activated DCs at later time points.

We confirm that long-term metabolic reprogramming is modulated in part by HIF-1 α in pro-inflammatory DCs (20,26). HIF-1 α is stabilized under conditions of hypoxia and promotes expression of glycolytic genes to allow cells to generate more energy by glycolysis in the absence of oxygen. In several immune cell types, including DCs, HIF-1 α can be stabilized by LPS stimulation even under normoxic conditions, consequently promoting aerobic glycolysis (27–29). Jantsch *et al.* demonstrated that HIF-1 α regulates DC activation by LPS (24), and our results here demonstrate that HIF-1 α protein also accumulates when DCs are stimulated by other strong activators like LPS, Zym and curdlan. These results are in line with a recent report demonstrating that HIF-1 α is responsible for sustained glycolytic reprogramming in DCs (20). Weakly-activated DCs, such as those stimulated by HDM or ZymD, did not significantly increase HIF-1 α protein expression, in agreement with the lack of glycolytic reprogramming we observed in these DCs.

The induction of NOS triggered by TLR agonists and subsequent NO production is known to inhibit mitochondrial respiration (15), and NO promotes HIF-1 α stabilization under normoxic conditions (20,30). We show here that the expression of iNOS and production of NO induced by a variety of DC activators, including those that engage CLR, is directly correlated with the loss of coupled respiration. Pro-inflammatory DCs reduced coupled respiration in a dose-dependent manner, while DCs stimulated by weak activators HDM and ZymD did not appreciably increase iNOS or NO levels even at higher doses, thus maintaining coupled respiration. Therefore, we hypothesize that NO simultaneously inhibits mitochondrial function and stabilizes HIF-1 α , reducing mitochondrial metabolism and promoting glycolysis, respectively. The differential usage of these metabolic pathways in DCs was dependent on the strength of activation, which was based on the nature and dose of the particular stimuli. Long-term metabolic programming at the transcriptional level stimulated by strong agonists likely depends on the presence of NO. DCs that do not express iNOS have been shown to similarly alter their metabolic activity in the presence of exogenous NO, which can be derived from other cells such as inflammatory macrophages (15,20), indicating that environmental factors beyond TLR agonists can help shape DC metabolism.

Here we show that glycolysis is important for the elongated shape of DCs and their ability to migrate. Migration is a crucial aspect of DC function; DCs that encounter foreign antigen must migrate to the draining LN to alert the adaptive immune system regardless of the strength or type of activation. One of our key observations is that mitochondrial bioenergetics is not sufficient to support these cellular features, but rather early activation of glycolysis is essential. Following activation, DCs upregulate CCR7, the receptor for CCL19 and CCL21, which enables them to be guided to the lymph nodes by CCL21 produced by lymphatic

endothelial cells. Recently, CCR7 oligomerization has been shown to be essential for efficient DC migration by forming a signaling hub to optimize signal transduction (21). We found that CCR7 oligomerization was specifically dependent on glucose availability in DCs. Accordingly, blocking glycolysis was sufficient to disrupt optimal DC migration to the draining LN. However, this defect in migration is not solely due to CCR7 oligomerization but also due to a defect in motility. *In vitro*, we observed that DCs possess a rounded morphology in the absence of glucose, while adopting a more dynamic and elongated phenotype when glucose is present, implying strongly that glycolysis may play a crucial role in cytoskeletal remodeling.

In human prostate and breast cancer cell lines, cell migration is exploited to facilitate metastasis, and increased glycolytic activity has been shown to be associated with greater cytoskeletal rearrangements and therefore cell motility (31). Interestingly, the ATP generated from OXPHOS was not sufficient to support cell shape and migration. A possible explanation for this requirement for glucose-derived ATP is that local ATP is used for actin polymerization at specific areas of the cytoskeleton such as for the formation of actin-rich structures lamellipodia, filopodia, and podosomes. This compartmentalization of glycolytic activity allows for rapid ATP production locally at the cytoskeleton rather than throughout the cell for the energetically-demanding remodeling processes (32). Vessel branching via migrating endothelial cells has been shown to be regulated by glycolysis, with glycolytic activator PFKFB3 playing a major role (33). PFKFB3 was found to be enriched in lamellipodia, promoting local glycolytic activity to generate ATP at these actin-rich structures (33). In addition to bioenergetic requirements, another mechanism for glycolytic control of cytoskeletal remodeling involves the association of the glycolytic enzyme aldolase to the cytoskeleton. A recent study describes the regulation of glycolysis by phosphoinositide 3-kinase (PI3K), which activates the GTPase RAC to mobilize

the cytoskeleton, and consequently releasing the actin-bound aldolase (34). Our data show that without glycolysis, there is little motility of the cytoskeleton, suggesting a feed-forward loop may exist where glycolytic activity is needed for cytoskeletal reorganization necessary to release aldolase to further increase glycolysis. Additional work will be necessary to reveal how glycolysis can support the cytostructure and motility of DCs.

Inhibiting glucose availability may also alter signaling pathways in DCs that affect their migratory responses. AMPK, a cellular energy sensor that is activated in response to increased AMP:ATP or ADP:ATP ratios, can antagonize mTORC1 activity (35). mTORC1 inhibition can affect cytoskeletal dynamics by preventing the protein expression of small GTPases (36). mTORC2 also regulates cytoskeletal reorganization via protein kinase C ζ activity (37). Therefore, altered AMPK and/or mTOR activity could contribute to the observed defects in cell shape, motility and migration following glucose deprivation or 2-DG treatment. Additionally, since *in vivo* administration of 2-DG can affect multiple cell types, it is possible that defects in other cells are contributing to the migratory defect observed in these experiments.

Defined metabolic pathways are increasingly being shown to direct specific cellular functions. Previously, induction of glycolysis was thought to primarily support the bioenergetic and catabolic demands of a highly pro-inflammatory phenotype (14). We demonstrate that regardless of activation phenotype, DCs increase glycolysis upon activation, and that glycolysis, and not mitochondrial bioenergetics, is essential to maintain DC cell shape, promote oligomerization of the chemokine receptor CCR7, and enable DC migration. Our data suggest that nutrient competition in chronic inflammatory and in particular, tumour microenvironments, in addition to inhibiting DC activation, may also interfere with DC migratory capacity, limiting their ability to migrate to draining lymph nodes to orchestrate adaptive immune responses.

Experimental procedures

Mice

Female wild-type C57BL/6 mice or BALB/C were purchased from Charles Rivers Laboratories at 6-8 weeks of age (Montreal, QC Canada). Animals were maintained in a specific pathogen-free environment. All experiments were conducted following the guidelines of the Canadian Council of Animal Care, as approved by the McGill University Animal Care Committee. Animals were randomly assigned to the different treatment groups. Investigators were not blinded.

In vitro bone marrow-derived DC generation and stimulation

Bone marrow extracted from C57BL/6 mice was cultured in the presence of 20 ng/mL GM-CSF (PeproTech) in “complete DC medium” (CDCM) containing RPMI-1640 (Corning) medium with 10% fetal calf serum (FCS) (Hyclone), 2 mM L-glutamine (Wisent), 100 U/mL penicillin-streptomycin (Wisent), and 0.01% β -mercaptoethanol (Gibco). After 8 to 10 days, DCs were collected, seeded at 2 million cells/mL, and stimulated where indicated with lipopolysaccharide (LPS; O111:B4 Sigma-Aldrich), house dust mite (HDM; low endotoxin from Greer Laboratories), curdlan (InvivoGen), zymosan (InvivoGen), or zymosan-depleted (38) (InvivoGen). HDM was labeled with Alexa Fluor 647 in indicated experiments with the Alexa Fluor 647 Protein Labeling Kit (Invitrogen). Glucose-withdrawal experiments used glucose-free RPMI-1640 (Wisent) supplemented with 10% dialyzed FCS (Wisent), 2 mM L-glutamine, 100 U/mL penicillin-streptomycin, and 0.01% β -mercaptoethanol.

Splenic DC isolation

Flt3L-expressing B16 cells were subcutaneously injected into C57BL/6 mice (3.5×10^5 cells/mouse) in order to expand the DC population (39). After approximately 2 weeks, the tumor-bearing mice were sacrificed and the spleens were harvested for DCs. Spleens were digested with 1 mg/mL collagenase and 10 μ g/mL DNase I (Roche), and red blood cells lysed with ACK lysis buffer. Splenic DCs were purified using the Pan DC Isolation Kit (Miltenyi), according to the manufacturer's protocol.

Seahorse assay

An XF-96 Extracellular Flux Analyzer (Seahorse Bioscience) was used to analyze real-time changes of the extracellular acidification rate (ECAR) and oxygen consumption rate (OCR). DCs were seeded in XF-96 cell culture plates at 7.5×10^4 cells/well in CDCM with or without stimuli. After incubation for the indicated time points, the media was removed and replaced with warmed unbuffered "Seahorse medium" (XF Assay Base Medium with 10 mM glucose, unless specified glucose-free, 10% FCS, and 2 mM L-glutamine) at pH 7.4. Where indicated, the DCs were treated with 1 μ M oligomycin, 1.5 μ M fluoro-carbonyl cyanide phenylhydrazone (FCCP), and 100 nM rotenone with 1 μ M antimycin A (all Sigma-Aldrich). For analyzing real-time changes in ECAR and OCR immediately upon activation, DCs were plated in XF-96 cell culture plates at 7.5×10^4 cells/well in "Seahorse medium", and the stimuli were injected into the wells by the XF analyzer.

Metabolite analysis

Nova Bioanalyzer

Supernatant was collected from BMDCs stimulated for 18h, and spun down to remove any cells and debris. Supernatants were then run on the Nova Bioanalyzer to measure the levels of various metabolites, including lactate and glucose.

GC-MS analysis of ¹³C metabolites

Gas chromatography-mass spectrometry (GC-MS) metabolite analysis was conducted as previously described (40). Briefly, 5×10^6 BMDCs were cultured with indicated activators in CDCM for 2h. Following activation, the medium was changed to glucose-free RPMI (with 10% dialyzed FCS, Wisent) containing 11 mM U-[¹³C]-glucose (Cambridge Isotope Laboratories) for 2h. Metabolites were extracted from cells using dry ice-cold 80% methanol, followed by sonication and removal of cellular debris by centrifugation at 4°C. Metabolite extracts were dried, derivatized as tert-butyldimethylsilyl (TBDMS) esters, and analyzed via GC-MS as previously described (41). Uniformly deuterated myristic acid (750 ng/sample) was added as an internal standard following cellular metabolites extraction, and metabolite abundance was expressed relative to the internal standard and normalized to cell number. Mass isotopomer distribution was determined using a custom algorithm developed at McGill University (42).

LC-MS analysis of nucleotides

Nucleotide levels were determined by liquid chromatography-mass spectrometry (LC-MS), as previously described (18). BMDCs were cultured with or without glucose for 4h, and then washed with cold 150 mM ammonium formate solution pH of 7.4 and extracted with 600 μ L of

31.6% MeOH/36.3% ACN in H₂O (v/v). Cells were lysed and homogenized by bead-beating for 2 minutes at 30Hz using a 5 mm metal bead (TissueLyser II – Qiagen). Cellular extracts were partitioned into aqueous and organic layers following dimethyl chloride treatment and centrifugation. Aqueous supernatants were dried by vacuum centrifugation with sample temperature maintained at -4°C (Labconco, Kansas City MO, USA). Pellets were subsequently resuspended in 25 µl of H₂O as the injection buffer. For semi-quantitative targeted metabolite analysis of mono-, di-, and tri-phosphate nucleoside, samples were injected onto an Agilent 6430 Triple Quadrupole (Agilent Technologies, Santa Clara, CA, USA). Chromatography was achieved using a 1290 Infinity ultra-performance LC system (Agilent Technologies, Santa Clara, CA, USA) consisting of vacuum degasser, autosampler and a binary pump. Separation was performed on a Scherzo SM-C18 column 3 µm, 3.0×150mm (Imtakt Corp, JAPAN) maintained at 10°C. The chromatographic gradient started at 100% mobile phase A (5 mM ammonium acetate in water) with a 5 min. gradient to 100% B (200 mM ammonium acetate in 20% ACN / 80% water) at a flow rate of 0.4 ml/min. This was followed by a 5 min hold time at 100% mobile phase B and a subsequent re-equilibration time (6 min) before next injection. A sample volume of 5 µL of sample was injected for analysis. Sample temperature was maintained at 4°C before injection.

The mass spectrometer was equipped with an electrospray ionization (ESI) source and samples were analyzed in positive mode. Multiple reaction monitoring (MRM) transitions were optimized on standards for each metabolite quantitated. Transitions for quantifier and qualifier ions are described in the table below. Gas temperature and flow were set at 350°C and 10 l/min respectively, nebulizer pressure was set at 40 psi and capillary voltage was set at 3500V. Relative concentrations were determined by integrating area under the curve for the quantifying MRM

transition and compared to external calibration curves. Data were analyzed using MassHunter Quant (Agilent Technologies, Santa Clara, CA, USA).

| Compound | Precursor ion (m/z) | Quantifier ion (m/z) | Qualifier ion (m/z) |
|-----------------|--------------------------------|---------------------------------|--------------------------------|
| ATP | 508.0 | 136.0 | 410.1 |
| ADP | 428.0 | 136.0 | 348.1 |
| AMP | 348.0 | 136.1 | 118.9 |
| CTP | 484.0 | 112.1 | 97.1 |
| CDP | 404.0 | 112.0 | 69.0 |
| CMP | 324.0 | 112.1 | 69.1 |
| TTP | 483.0 | 81.1 | 53.0 |
| TDP | 403.0 | 81.1 | 207.0 |
| TMP | 323.0 | 207.1 | 126.9 |
| GTP | 524.0 | 152.0 | 134.9 |
| GDP | 444.0 | 152.0 | 97.0 |
| GMP | 364.0 | 152.1 | 97.0 |
| ITP | 509.0 | 137.0 | 97.1 |
| IDP | 429.0 | 137.0 | 97.0 |
| IMP | 349.0 | 137.0 | 110.0 |
| UTP | 485.0 | 97.1 | 113.0 |
| UDP | 405.0 | 97.0 | 69.2 |
| UMP | 325.0 | 97.0 | 113.0 |

All LC/MS grade solvents and salts were purchased from Fisher (Ottawa, Ontario Canada): dichloromethane (DCM), water (H₂O), acetonitrile (ACN), methanol (MeOH) and ammonium acetate. The authentic metabolite standards were purchased from Sigma-Aldrich Co. (Oakville, Ontario, Canada).

Enzyme-linked immunosorbent assay

The cytokines IL-6, IL-12p40, TNF α , and IL-10 were measured in the supernatant of activated cells as described in the Ready-Set-Go![®] ELISA protocol from eBioscience.

Flow cytometry

Antibodies used for flow cytometry analysis of surface marker expression on BMDCs are the following: anti-CD11c (N418), anti-CD40 (1C10), anti-CD80 (16-10A1), anti-CD86 (GL1), and anti-I-A/I-E (M5/114.15.2) (all eBioscience). Antibodies used for flow cytometry analysis of cells from mediastinal LNs are the following: anti-CD19 (eBio1D3), anti-F4/80 (BM8) (eBioscience), anti-CD3 ϵ (145-2C11), anti-CD45 (30-F11), anti-CD11c (N418), and anti-I-A/I-E (M5/114.15.2) (BioLegend). For staining of intracellular protein iNOS (C-11) (Santa Cruz Biotechnology), samples were first fixed with IC Fixation Buffer (eBioscience) and stained in Permeabilization Buffer (eBioscience). Samples were acquired on the BD LSR Fortessa and data analyzed using FlowJo software.

Live imaging

DCs were seeded at 3×10^4 cells per well in complete DC medium with or without 10 mM glucose in an 8-chamber cover glass plate (Lab-Tek). Cells were allowed to settle at 37°C for 4h, and then imaged using a ZEISS LSM700 confocal microscope and a 20X 0.8NA objective lens. Cells were imaged every 3 minutes for 2h in a humidified chamber with 5% CO₂ and heated to 37°C. Either 10 mM glucose or 10 mM 2-DG was added as a bolus where indicated, and imaged for another 3h. ZEN black was used to obtain images from ZEISS LSM700 confocal microscope and movies were analyzed using ZEN blue and ImageJ/Fiji software (National Institute of Health). Shape descriptors were calculated using the Analyze Particles tool in ImageJ/Fiji and in-house custom macros. Aspect ratio was calculated as the ratio of the major axis (d) to the minor axis (s) ($AR = d/s$) and values are equal to or greater than 1. Roundness was calculated by the equation $R = 4A/(\pi d^2)$, where A is area, and has values between 0 (oblong) and 1 (perfect circle).

Immunoblot

Protein lysates were prepared in 1% CHAPS lysis buffer with protease inhibitor and phosphatase inhibitor, then quantified by BCA assay (Pierce). Samples were run on 10% gels by SDS-PAGE, and proteins were transferred by electrophoretic wet transfer to PVDF membranes. Membranes were blot for p-TBK Ser172 (D52C2), p-AKT Ser473 (D9E) and Thr308 (D25E6), total AKT (C67E7), p-S6K Thr389, p-S6 Ser240/244, β -actin (all Cell Signaling), and HIF-1 α (Cayman Chemicals), all diluted to 1:1000 except for HIF-1 α (1:500). Incubation with primary antibody overnight was followed by incubation with horseradish peroxidase–linked antibody to rabbit IgG for 45 minutes. Enhanced chemiluminescence (Perkin Elmer or Amersham) was used to develop the blots. Scans of the original blots are in Supplementary Fig. 7.

Quantitative RT-PCR

RNA was purified from cells using TRIzol (Invitrogen) and cDNA was synthesized with a reverse transcription kit (Applied Biosystems) to perform a SYBR-based real-time PCR (Applied Biosystems) with primers from Integrated DNA Technologies. Data was generated using the $\Delta\Delta Cq$ method. Relative gene expression was normalized to that of HPRT.

Primers

| Gene | Sequence |
|--------------|--|
| <i>Glut1</i> | Forward: CTG GAC CTC AAA CTT CAT TGT GGG |
| | Reverse: GGG TGT CTT GTC ACT TTG GCT GG |
| <i>Hk2</i> | Forward: CCG TGG TGG ACA AGA TAA GAG AGA ACC |
| | Reverse: GGA CAC GTC ACA TTT CGG AGC CAG |
| <i>Pkm2</i> | Forward: GGT ATC GCA GCA GGA ACC GAA GTA C |
| | Reverse: GCT GGG TCT GAA TGA AGG CAG TC |
| <i>Gapdh</i> | Forward: GTC GGT GTG AAC GGA TTT G |
| | Reverse: TAG ACT CCA CGA CAT ACT CAG CA |
| <i>Ldha</i> | Forward: TGT CTC CAG CAA AGA CTA CTG T |
| | Reverse: GAC TGT ACT TGA CAA TGT TGG GA |

Transwell assay

DCs incubated for 4 to 6h in specified conditions were seeded in the inserts of 24-well Transwell plates (5 μ m polycarbonate membrane; Costar) at 4×10^5 cells per insert. CCL21 (250 ng/mL) in media with or without glucose was added to the bottom chambers. Cells were allowed to migrate for 2h at 37°C. Cells that migrated into the bottom chambers and cells remaining in the insert were collected and counted on the BD LSR Fortessa using counting beads (123count eBeads, eBioscience). Results are expressed as the percentage of cells that migrated of total cells.

In vivo migration experiments

Footpad injection

BMDCs were stained with carboxyfluorescein succinimidyl ester (CFSE) and stimulated for 6h with the indicated activators. After 6h, cells were collected and resuspend in PBS at 20×10^6

cells/mL. 5×10^5 (25 μ L) cells were injected subcutaneously into each rear footpad of C57BL/6 mice. After 45h, the draining popliteal lymph nodes were isolated (popliteal lymph nodes from each mouse were pooled) and digested with DNase I (10 μ g/mL) and collagenase D (1 mg/mL). CFSE⁺ cells in the dLNs were detected by flow cytometry and cells were counted using 123count eBeads (eBioscience).

HDM-induced allergic asthma model

To investigate effects of 2-DG on DC activation and migration, female Balb/c (7 to 8 weeks) were briefly anaesthetized with isoflurane and treated intranasally with 40 μ g of low endotoxin HDM (LE-HDM; Greer) in a volume of 30 μ L. Mice were injected intraperitoneally with 500 mg/kg body weight 2-DG or control saline in a volume of 200 μ L, daily, starting one day prior to LE-HDM delivery. Mice were sacrificed 72h after application of LE-HDM, and mediastinal LNs were collected for flow cytometry analysis. CD11c⁺MHCII^{hi} cells were gated on viable CD45⁺ cells from which cells expressing CD19, CD3 ϵ , and F4/80 were excluded.

Fluorescence resonance energy transfer (FRET)

CCR7 oligomerization was determined by FRET. BMDCs were stimulated in the presence or absence of glucose (10 mM) or 2-DG (10 mM) for 6h. Cells were stained for 45 minutes with PE-labeled CCR7 and APC-labeled CCR7 (clone 4B12; eBioscience) at a 1:200 dilution in the presence of Fc block at 37°C. Samples were washed and acquired on the BD LSR Fortessa without compensation. FRET was calculated as previously described (43), using the following formula:

$$\text{FRET unit} = (E3_{\text{both}} - E3_{\text{none}}) - ([E3_{\text{APC}} - E3_{\text{none}}] \times [E2_{\text{both}}/E2_{\text{APC}}]) - ([E3_{\text{PE}} - E3_{\text{none}}] \times [E1_{\text{both}}/E1_{\text{PE}}])$$

where $E1$ is the fluorescence detected at 580 nm upon excitation at 561 nm, $E2$ is the fluorescence detected at 670 nm upon excitation at 640 nm, and $E3$ is the fluorescence detected at 670 nm upon excitation at 561 nm. The positive population percentage was used for E stained with neither PE nor APC (E_{none}), PE only (E_{PE}), APC only (E_{APC}), or both PE and APC (E_{both}).

Statistical analysis

Data were analyzed using GraphPad Prism software (version 6). An unpaired student's t-test was performed to determine statistical significance between two samples and significance was considered to be when p values were less than 0.05. Stars without lines indicate significance when compared to control. A one-way ANOVA was performed to determine statistical significance between multiple groups.

Data availability

The authors declare that the data supporting the findings of this study are available within the paper and its Supplementary Information files.

Supplementary figures

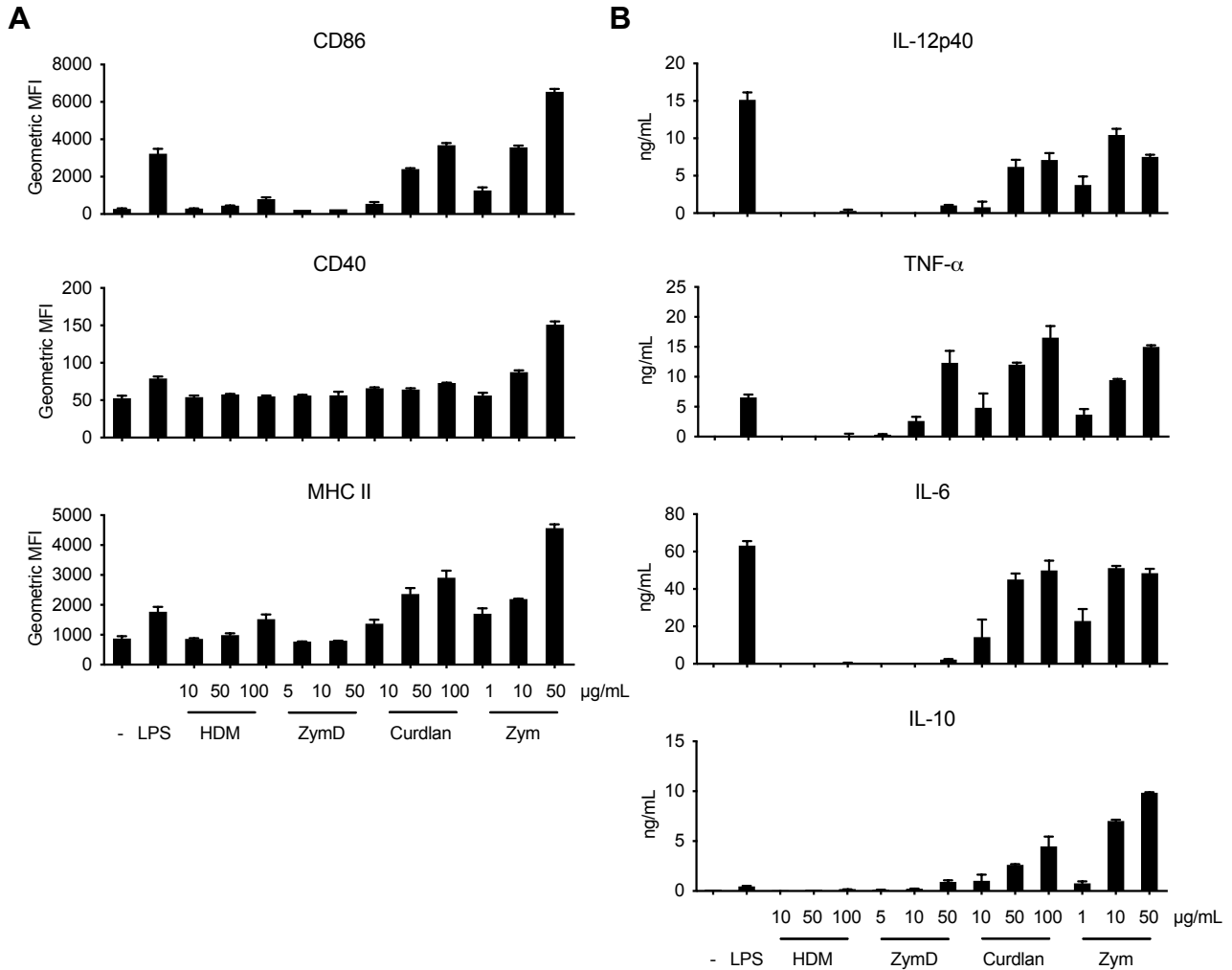


Figure S1 – Surface marker expression and cytokine production by differentially-activated DCs.

(A) Expression of surface markers CD86, CD40, and MHC II and (B) production of cytokines IL-12p40, TNF-α, IL-6, and IL-10, were determined after stimulation with increasing doses of activators for 18h. Data in (A,B) are 1 experiment representative of at least 3 experiments (mean and s.d. of duplicates).

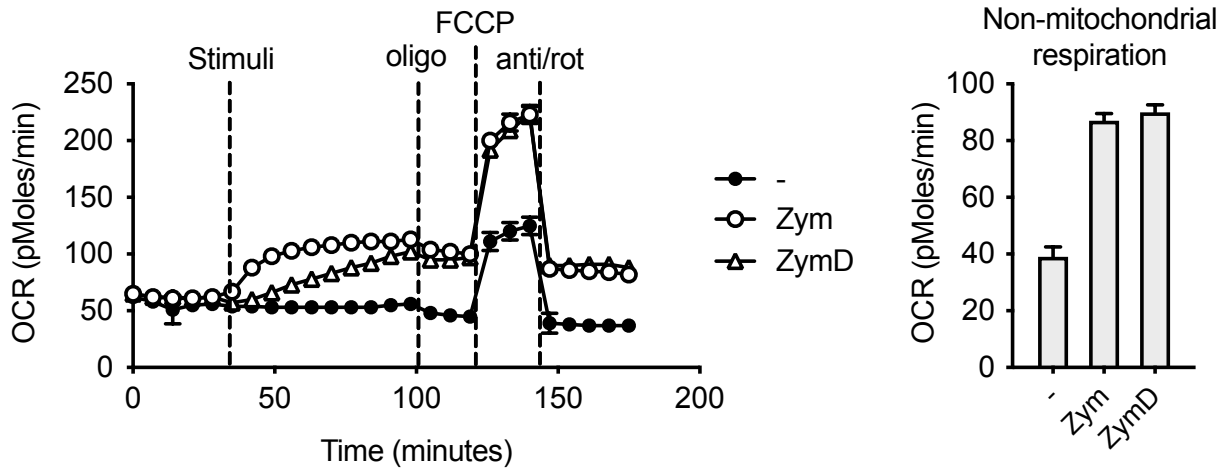


Figure S2 – Rapid oxygen consumption induced by Zym and ZymD is primarily non-mitochondrial.

DCs were untreated or stimulated with Zym and ZymD, followed by treatment with oligomycin, FCCP, and antimycin/rotenone. The antimycin and rotenone inhibit mitochondrial respiration, and the remaining oxygen consumption is non-mitochondrial. Data shown are 1 experiment representative of 3 experiments (mean and s.e.m. of 6 replicates).

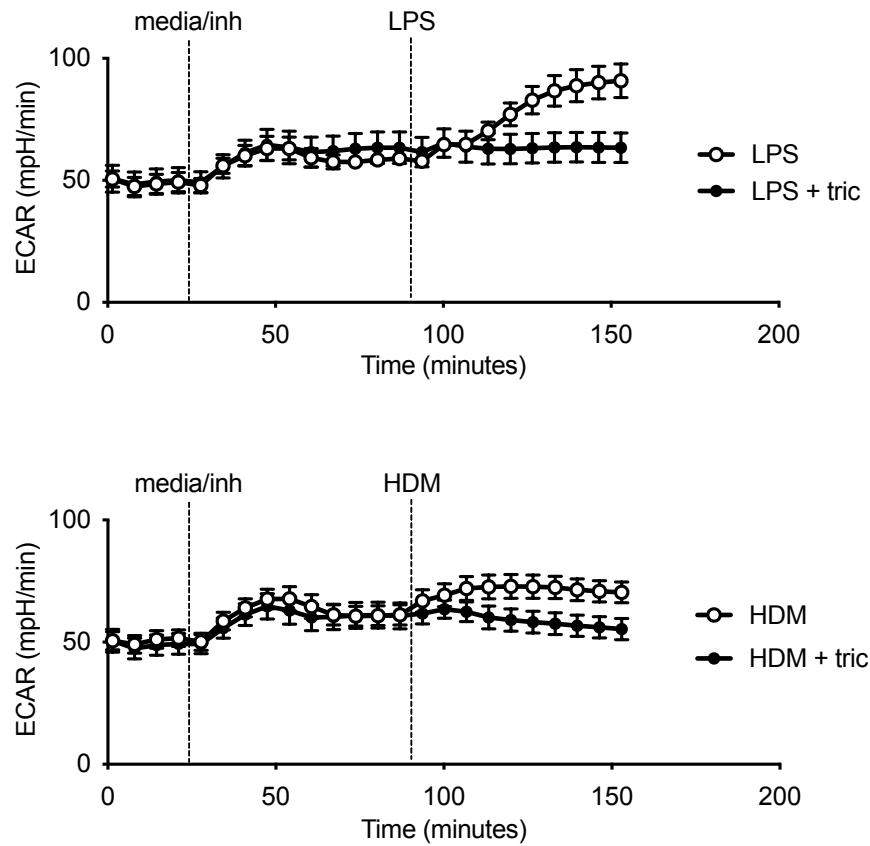


Figure S3 – Early glycolytic flux by LPS and HDM is prevented by AKT inhibition.

ECAR of DCs treated with or without AKT inhibitor triciribine for 1h and stimulated with LPS (top) or HDM (bottom) for 1h. Data are of 1 experiment representative of 2 independent experiments (mean and s.e.m. of 6 replicates).

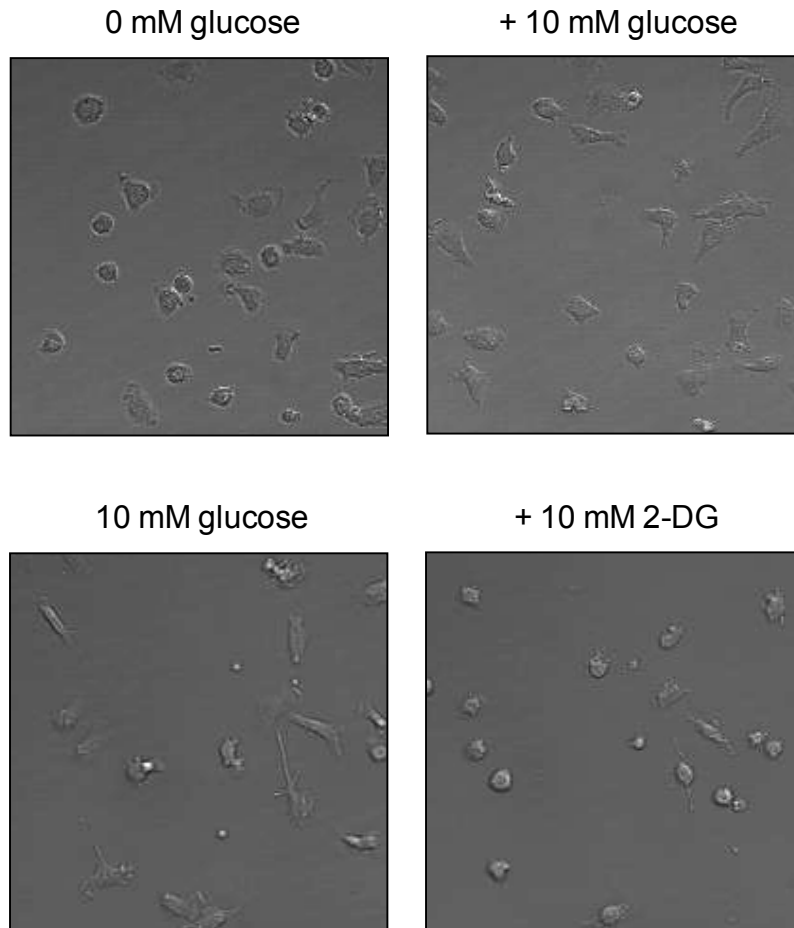


Figure S4 – Inhibition of glycolysis results in rounded cell morphology.

Representative images from the live imaging experiment analyzed in Fig. 5. DCs cultured in the absence of glucose (top), and in the presence of glucose (bottom). Glucose and 2-DG were added to the top and bottom conditions, respectively, and cell shape was examined.

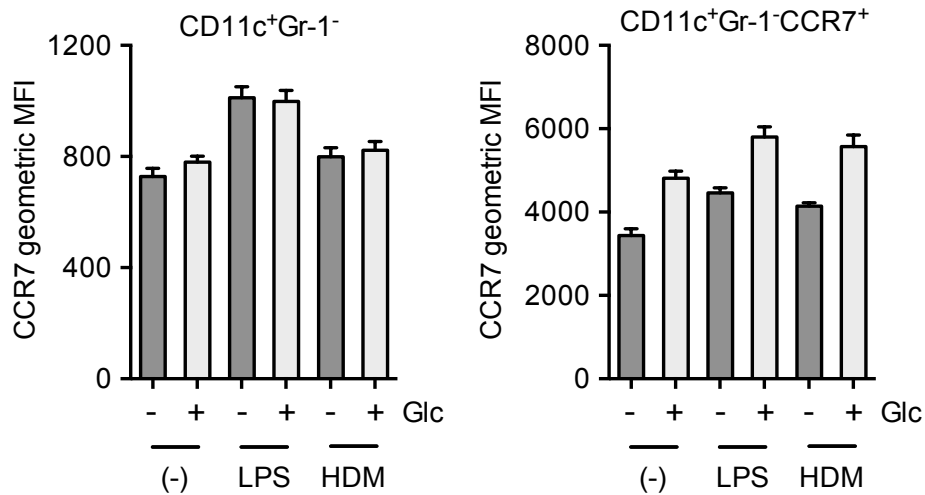


Figure S5 – CCR7 expression on DCs.

Geometric MFI of CCR7 in the CD11c⁺Gr-1⁻ (left) and CD11c⁺Gr-1⁻CCR7⁺ (right) populations of DCs left unstimulated or activated 6h with LPS or HDM in the presence or absence of glucose. Data are of 1 experiment representative of 3 independent experiments (mean and s.d. of triplicates).

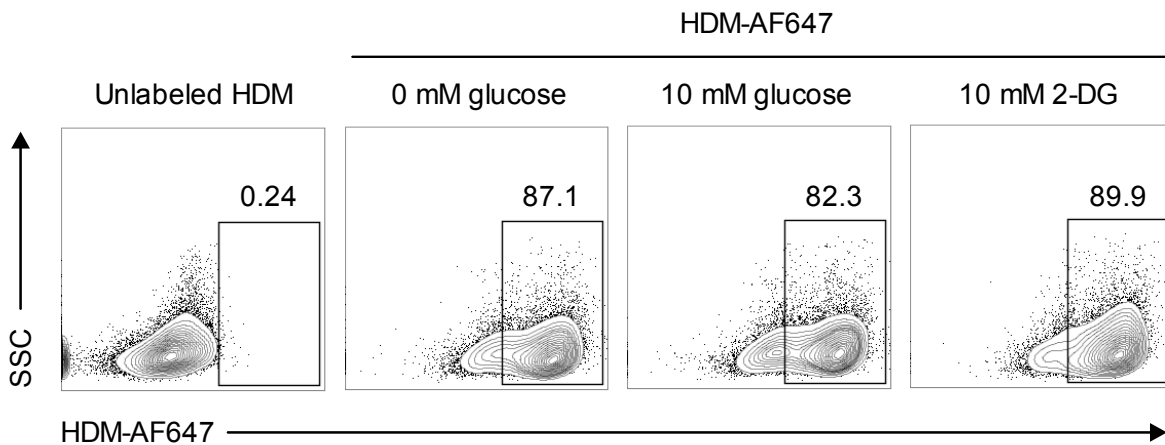


Figure S6 – Inhibition of glycolysis does not affect phagocytosis of HDM by DCs.

HDM labeled with Alexa Fluor 647 (AF647) dye was added to DCs cultured in the presence or absence of glucose or 2-DG for 4h. Data shown are of 1 experiment representative of 2 experiments.

References

1. Kawai T, Akira S. The role of pattern-recognition receptors in innate immunity: update on Toll-like receptors. *Nat Immunol.* 2010 May;11(5):373–84.
2. Ozinsky A, Underhill DM, Fontenot JD, Hajjar AM, Smith KD, Wilson CB, et al. The repertoire for pattern recognition of pathogens by the innate immune system is defined by cooperation between Toll-like receptors. *Proc Natl Acad Sci U S A.* 2000 Nov 28;97(25):13766–71.
3. Gantner BN, Simmons RM, Canavera SJ, Akira S, Underhill DM. Collaborative Induction of Inflammatory Responses by Dectin-1 and Toll-like Receptor 2. *J Exp Med.* 2003 May 5;197(9):1107–17.
4. Hammad H, Plantinga M, Deswarte K, Pouliot P, Willart MAM, Kool M, et al. Inflammatory dendritic cells—not basophils—are necessary and sufficient for induction of Th2 immunity to inhaled house dust mite allergen. *J Exp Med.* 2010;207(10):2097.
5. Norimoto A, Hirose K, Iwata A, Tamachi T, Yokota M, Takahashi K, et al. Dectin-2 Promotes House Dust Mite–Induced T Helper Type 2 and Type 17 Cell Differentiation and Allergic Airway Inflammation in Mice. *Am J Respir Cell Mol Biol.* 2014 Aug 1;51(2):201–9.
6. O’Neill LAJ, Kishton RJ, Rathmell J. A guide to immunometabolism for immunologists. *Nat Rev Immunol.* 2016 Jul 11;16(9):553–65.
7. Krawczyk CM, Holowka T, Sun J, Blagih J, Amiel E, DeBerardinis RJ, et al. Toll-like receptor–induced changes in glycolytic metabolism regulate dendritic cell activation. *Blood.* 2010 Jun 10;115(23):4742.
8. Haschemi A, Kosma P, Gille L, Evans CR, Burant CF, Starkl P, et al. The Sedoheptulose Kinase CARLK Directs Macrophage Polarization through Control of Glucose Metabolism. *Cell Metab.* 2012 Jun 6;15(6):813–26.
9. Pearce EL, Walsh MC, Cejas PJ, Harms GM, Shen H, Wang L-S, et al. Enhancing CD8 T-cell memory by modulating fatty acid metabolism. *Nature.* 2009 Jun 3;460(7251):103–7.
10. Lampropoulou V, Sergushichev A, Bambouskova M, Nair S, Vincent EE, Loginicheva E, et al. Itaconate Links Inhibition of Succinate Dehydrogenase with Macrophage Metabolic Remodeling and Regulation of Inflammation. *Cell Metab.* 2016 Jul 12;24(1):158–66.
11. Cameron AM, Lawless SJ, Pearce EJ. Metabolism and acetylation in innate immune cell function and fate. *Semin Immunol.* 2016 Oct 1;28(5):408–16.
12. Ip WKE, Hoshi N, Shouval DS, Snapper S, Medzhitov R. Anti-inflammatory effect of IL-10 mediated by metabolic reprogramming of macrophages. *Science.* 2017 May 5;356(6337):513.

13. Warburg O. On the Origin of Cancer Cells. *Science*. 1956;123(3191):309.
14. Everts B, Amiel E, Huang SC-C, Smith AM, Chang C-H, Lam WY, et al. TLR-driven early glycolytic reprogramming via the kinases TBK1-IKK ϵ supports the anabolic demands of dendritic cell activation. *Nat Immunol*. 2014 Apr;15(4):323–32.
15. Everts B, Amiel E, Windt GJW van der, Freitas TC, Chott R, Yarasheski KE, et al. Commitment to glycolysis sustains survival of NO-producing inflammatory dendritic cells. *Blood*. 2012 Aug 16;120(7):1422.
16. Pantel A, Teixeira A, Haddad E, Wood EG, Steinman RM, Longhi MP. Direct Type I IFN but Not MDA5/TLR3 Activation of Dendritic Cells Is Required for Maturation and Metabolic Shift to Glycolysis after Poly IC Stimulation. *PLOS Biol*. 2014 Jan 7;12(1):e1001759.
17. Kelly EK, Wang L, Ivashkiv LB. Calcium-Activated Pathways and Oxidative Burst Mediate Zymosan-Induced Signaling and IL-10 Production in Human Macrophages. *J Immunol Baltim Md 1950*. 2010 May 15;184(10):5545–52.
18. Ma EH, Bantug G, Griss T, Condotta S, Johnson RM, Samborska B, et al. Serine Is an Essential Metabolite for Effector T Cell Expansion. *Cell Metab*. 2017 Feb 7;25(2):345–57.
19. Marín-Hernández A, Gallardo-Pérez JC, Ralph SJ, Rodríguez-Enríquez S, Moreno-Sánchez R. HIF-1 α modulates energy metabolism in cancer cells by inducing over-expression of specific glycolytic isoforms. *Mini Rev Med Chem*. 2009 Aug;9(9):1084–101.
20. Lawless SJ, Kedia-Mehta N, Walls JF, McGarrigle R, Convery O, Sinclair LV, et al. Glucose represses dendritic cell-induced T cell responses. *Nat Commun*. 2017 May 30;8:15620.
21. Hauser MA, Schaeuble K, Kindinger I, Impellizzeri D, Krueger WA, Hauck CR, et al. Inflammation-Induced CCR7 Oligomers Form Scaffolds to Integrate Distinct Signaling Pathways for Efficient Cell Migration. *Immunity*. 2016 Jan 19;44(1):59–72.
22. Plantinga M, Guilliams M, Vanheerswynghels M, Deswarte K, Branco-Madeira F, Toussaint W, et al. Conventional and Monocyte-Derived CD11b⁺ Dendritic Cells Initiate and Maintain T Helper 2 Cell-Mediated Immunity to House Dust Mite Allergen. *Immunity*. 2013 Feb 21;38(2):322–35.
23. Sukumar M, Liu J, Ji Y, Subramanian M, Crompton JG, Yu Z, et al. Inhibiting glycolytic metabolism enhances CD8(+) T cell memory and antitumor function. *J Clin Invest*. 2013 Sep 16;123(10):4479–88.
24. Jantsch J, Chakravorty D, Turza N, Prechtel AT, Buchholz B, Gerlach RG, et al. Hypoxia and Hypoxia-Inducible Factor-1 α Modulate Lipopolysaccharide-Induced Dendritic Cell Activation and Function. *J Immunol*. 2008 Apr 1;180(7):4697.

25. van der Windt GJW, Everts B, Chang C-H, Curtis JD, Freitas TC, Amiel E, et al. Mitochondrial Respiratory Capacity is a Critical Regulator of CD8(+) T Cell Memory Development. *Immunity*. 2012 Jan 28;36(1):68–78.
26. Corcoran SE, O'Neill LAJ. HIF1 α and metabolic reprogramming in inflammation. *J Clin Invest*. 2016 Oct 3; 126(10):3699–707.
27. Jantsch J, Wiese M, Schödel J, Castiglione K, Gläsner J, Kolbe S, et al. Toll-like receptor activation and hypoxia use distinct signaling pathways to stabilize hypoxia-inducible factor 1 α (HIF1A) and result in differential HIF1A-dependent gene expression. *J Leukoc Biol*. 2011 Jun 17;90(3):551–62.
28. Cheng S-C, Quintin J, Cramer RA, Shepardson KM, Saeed S, Kumar V, et al. mTOR/HIF1 α -mediated aerobic glycolysis as metabolic basis for trained immunity. *Science*. 2014 Sep 26;345(6204):1250684.
29. Tannahill GM, Curtis AM, Adamik J, Palsson-McDermott EM, McGettrick AF, Goel G, et al. Succinate is an inflammatory signal that induces IL-1 β through HIF-1 α . *Nature*. 2013 Apr 11;496(7444):238–42.
30. Metzen E, Zhou J, Jelkmann W, Fandrey J, Brüne B. Nitric Oxide Impairs Normoxic Degradation of HIF-1 α by Inhibition of Prolyl Hydroxylases. *Mol Biol Cell*. 2003 Aug 1;14(8):3470–81.
31. Shiraishi T, Verdone JE, Huang J, Kahlert UD, Hernandez JR, Torga G, et al. Glycolysis is the primary bioenergetic pathway for cell motility and cytoskeletal remodeling in human prostate and breast cancer cells. *Oncotarget*. 2015 Jan 1;6(1):130–43.
32. Zecchin A, Stapor PC, Goveia J, Carmeliet P. Metabolic pathway compartmentalization: an underappreciated opportunity? *Curr Opin Biotechnol*. 2015 Aug;34:73–81.
33. De Bock K, Georgiadou M, Schoors S, Kuchnio A, Wong BW, Cantelmo AR, et al. Role of PFKFB3-Driven Glycolysis in Vessel Sprouting. *Cell*. 2013 Aug 1;154(3):651–63.
34. Hu H, Juvekar A, Lyssiotis CA, Lien EC, Albeck JG, Oh D, et al. Phosphoinositide 3-Kinase Regulates Glycolysis through Mobilization of Aldolase from the Actin Cytoskeleton. *Cell*. 2016 Jan 28;164(3):433–46.
35. Saxton RA, Sabatini DM. mTOR Signaling in Growth, Metabolism, and Disease. *Cell*. 2017 Mar 9;168(6):960–76.
36. Liu L, Luo Y, Chen L, Shen T, Xu B, Chen W, et al. Rapamycin Inhibits Cytoskeleton Reorganization and Cell Motility by Suppressing RhoA Expression and Activity. *J Biol Chem*. 2010 Dec 3;285(49):38362–73.
37. Li X, Gao T. mTORC2 phosphorylates protein kinase C ζ to regulate its stability and activity. *EMBO Rep*. 2014 Feb;15(2):191–8.

38. Ikeda Y, Adachi Y, Ishii T, Miura N, Tamura H, Ohno N. Dissociation of Toll-Like Receptor 2-Mediated Innate Immune Response to Zymosan by Organic Solvent-Treatment without Loss of Dectin-1 Reactivity. *Biol Pharm Bull.* 2008 Jan;31(1):13–8.
39. Mach N, Gillessen S, Wilson BS, Sheehan C, Mihm M, Dranoff G. Differences in dendritic cells stimulated in vivo by tumors engineered to secrete granulocyte-macrophage colony-stimulating factor or Flt3-ligand. *Cancer Res.* 2000 Jun 15;60(12):3239–46.
40. Blagih J, Coulombe F, Vincent EE, Dupuy F, Galicia-Vázquez G, Yurchenko E, et al. The Energy Sensor AMPK Regulates T Cell Metabolic Adaptation and Effector Responses In Vivo. *Immunity.* 2015 Jan 20;42(1):41–54.
41. Faubert B, Vincent EE, Griss T, Samborska B, Izreig S, Svensson RU, et al. Loss of the tumor suppressor LKB1 promotes metabolic reprogramming of cancer cells via HIF-1 α . *Proc Natl Acad Sci U S A.* 2014 Feb 18;111(7):2554–9.
42. McGuirk S, Gravel S-P, Deblois G, Papadopoli DJ, Faubert B, Wegner A, et al. PGC-1 α supports glutamine metabolism in breast cancer. *Cancer Metab.* 2013 Dec 5;1(1):22.
43. Demotte N, Stroobant V, Courtoy PJ, Smissen PVD, Colau D, Luescher IF, et al. Restoring the Association of the T Cell Receptor with CD8 Reverses Anergy in Human Tumor-Infiltrating Lymphocytes. *Immunity.* 2008 Mar 14;28(3):414–24.

CHAPTER 3 – The role of PGC-1 β in oxidative metabolism and immune function of dendritic cells

Abstract

Dendritic cells (DCs) are innate immune cells with a crucial role of initiating adaptive immunity. Cellular metabolism has been shown to be an important regulator of dendritic cell function; however, mitochondrial metabolism in DCs is not well-studied. We found that the gene expression of PGC-1 β , a transcriptional co-activator and major regulator of mitochondrial metabolism, changes dynamically when DCs are activated with lipopolysaccharide (LPS). We then examined the role of PGC-1 β in the metabolic state of DCs, and found that PGC-1 β deficiency in DCs shifts their bioenergetic profile to be more glycolytic and less oxidative. Accordingly, PGC-1 β deficiency affects the metabolic status of IFN- β -treated DCs, which maintain their oxidative metabolism, while that of LPS-activated DCs is not significantly changed. PGC-1 β -deficient DCs also have unchanged total mitochondrial mass and components of the electron transport chain, increased autophagic flux, and impaired fatty acid oxidation, as evaluated by reduced expression of enzymes of this pathway and reduced capacity for palmitate oxidation. In addition, the immune function of DCs is altered by PGC-1 β deficiency, increasing their capacity to induce T cell expansion and Th2 differentiation. Collectively, these results demonstrate PGC-1 β regulates metabolic programming and immune function of DCs.

Introduction

Dendritic cells (DCs) are innate immune cells that act as a bridge between innate and adaptive immunity. DCs are found in most tissues throughout the body, constantly patrolling and sampling their microenvironment. When DCs encounter foreign material, such as pathogens, they migrate to the draining lymph node and activate T cells in a context-specific manner.

Numerous studies in recent years have established cellular metabolism as an essential regulator of immune cell function and activation, including that of DCs (1–3). Two of the main energy-generating pathways are glycolysis and oxidative phosphorylation. In glycolysis, glucose is broken down into pyruvate, which can become lactate or be shuttled into the mitochondria and enter the tricarboxylic (TCA) cycle. The TCA cycle produces reducing agents that fuel the electron transport chain (ETC) with oxygen as the final electron acceptor, thus consuming oxygen in the process of oxidative phosphorylation. Both glycolysis and the TCA cycle generate metabolic intermediates that intersect numerous other metabolic pathways. Fatty acids are another important source of energy and metabolic intermediates. Fatty acid oxidation (FAO) also occurs in the mitochondria, with fatty acids being processed into acetyl-coA prior to joining the TCA cycle.

At steady state, DCs engage both glycolysis and oxidative metabolism. Upon Toll-like receptor (TLR) stimulation, DCs are known to rapidly upregulate their glycolytic activity, which is required for optimal DC activation (4). At late-stage activation, glycolysis maintains survival of TLR-activated DCs (1). Conversely, an increase in FAO drives the generation of tolerogenic DCs (5,6). While the role of glycolysis in regulating DC function has been well studied (1,4,7), the role of mitochondrial metabolism in DCs requires more extensive investigation.

The peroxisome proliferator-activated receptor gamma coactivator 1 (PGC-1) group of transcriptional co-activators are major regulators of mitochondrial metabolism. This group comprises PGC-1 α and PGC-1 β , which are close homologs, and a less closely related member PGC-related coactivator (PRC) (8). PGC-1 proteins interact with and promote the activity of several transcription factors—including but not limited to PPAR $\alpha/\beta/\delta/\gamma$, NRF1/2, ERR $\alpha/\beta/\gamma$, and SREBP1a/1c/2—that regulate mitochondrial metabolism, lipid metabolism, and other aspects of cellular metabolism (reviewed in (8)). PGC-1 α and PGC-1 β regulate the expression of overlapping sets of genes but can have distinct functions in different tissues. For example, in the liver, PGC-1 α enhances the expression of genes for gluconeogenesis in response to fasting, while PGC-1 β has a key role in lipogenesis and lipoprotein secretion in response to dietary fats (9,10). In addition, PGC-1 β promotes cellular respiration that is more highly coupled to energy production in myoblasts compared to PGC-1 α (11).

Existing studies on PGC-1 proteins in the context of immunity have largely been focused on PGC-1 α , with a relatively small number on PGC-1 β . For example, PGC-1 α has been described to be important for promoting anti-tumor immunity by enforcing mitochondrial biosynthesis and metabolic fitness in T cells (12,13) In DCs, PGC-1 α drives the differentiation of human monocyte-derived DCs (14). In macrophages, PGC-1 β promotes oxidative metabolism to drive alternative activation in response to IL-4 (15). These examples illustrate that PGC-1 proteins can modulate immune cell function through metabolic reprogramming. The role of PGC-1 β in DCs, however, has not yet been described. We hypothesized that due to the importance of PGC-1 transcriptional co-activators in regulating mitochondrial metabolism, PGC-1 β would also be required for optimal mitochondrial metabolism in DCs.

Our study demonstrates the importance of PGC-1 β in maintaining oxidative metabolism in DCs. From our characterization of the metabolic and transcriptional changes that occur in DCs treated with LPS or IFN- β , we found that PGC-1 β gene expression dramatically decreases with LPS stimulation in DCs, but levels are maintained in IFN- β -treated cells. PGC-1 β deficiency impairs oxidative metabolism and shifts the bioenergetic balance towards glycolysis. The blunted mitochondrial metabolism in PGC-1 β -deficient DCs is not due to reduced mitochondrial mass or ETC components, but rather in part due to diminished FAO. PGC-1 β -deficient DCs also exhibit elevated autophagic activity. Functionally, this PGC-1 β deficiency in DCs results in enhanced CD4⁺ T cells expansion and IL-4 production. In all, PGC-1 β -mediated programming of metabolism in DCs controls their immune functions.

Results

Metabolic profiling of differentially-activated DCs

Lipopolysaccharide (LPS), a bacterial component, is well-established to induce glycolysis in DCs (1,4). In bone marrow-derived DCs, LPS stimulates nitric oxide production, which gradually inhibits oxidative phosphorylation and cause the DCs become reliant on glycolysis (19). Although the metabolic effect of the antiviral mediator interferon- β (IFN- β) is not as well-studied as that of LPS, in plasmacytoid DCs, IFN- β has been shown to promote FAO (20). To compare the metabolic profiles of LPS-activated and IFN- β -treated DCs, we measured the oxygen consumption rate (OCR) of these cells using the Seahorse bioanalyzer, with sequential treatments with mitochondrial inhibitors determining parameters of mitochondrial function (Fig. 1A). Using this assay, we confirmed that LPS- and IFN- β -treated DCs have

contrasting bioenergetic profiles (Fig. 1A), with LPS-activated cells being non-responsive to mitochondrial inhibitors as previously established (19) and IFN- β -treated DCs having greater maximal respiration than unstimulated DCs.

Ppargc1b, which encodes the protein PGC-1 β , is substantially downregulated upon LPS stimulation and mostly maintained with IFN- β treatment (Fig. 1B). This effect is independent of nitric oxide, as LPS-stimulated DCs lacking nitric oxide synthase 2 (NOS2 or iNOS) similarly downregulated *Ppargc1b* (Fig. S1).

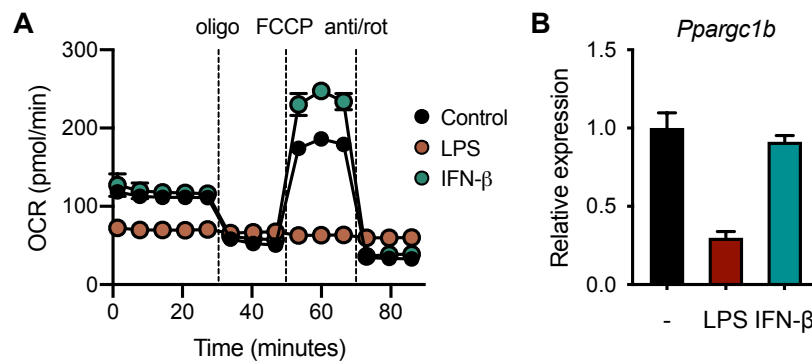


Figure 1 – Metabolic profiling of differentially-activated DCs

DCs were stimulated with LPS (100 ng/mL) or IFN- β (1000 U/mL) for 18 hours and (A) OCR was measured by Seahorse bioanalyzer over time with sequential treatments with oligomycin (oligo), FCCP, and antimycin and rotenone (anti/rot). (B) Gene expression of *Ppargc1b* relative to *Hprt*. Data are of one experiment representative of at least three experiments (mean and (A) s.d. of five replicates, (B) s.e.m. of triplicates).

PGC-1 β -deficient DCs have impaired oxidative metabolism and increased glycolysis

To determine how PGC-1 β affects the bioenergetic metabolism of DCs, we examined bone marrow-derived DCs that were deficient in PGC-1 β either by retroviral transduction with shRNA targeting *Ppargc1b* (sh*Ppargc1b*; Fig. S2A) or by differentiating bone marrow from

transgenic mice expressing loxP-flanked *Ppargc1b* and Cre under the CD11c promoter. *Ppargc1a* expression is barely detectable and does not noticeably increase to compensate for the lack of *Ppargc1b* (data not shown). We determined that DCs transduced with sh*Ppargc1b* have reduced basal OCR and spare respiratory capacity (SRC; difference between maximal OCR and basal OCR) (Fig. 2A, S2B). In contrast, the basal ECAR of PGC-1 β -deficient DCs is higher, and it is further elevated with FCCP treatment while failing to substantially raise OCR (Fig. 2B), suggesting that the PGC-1 β -deficient DCs at basal metabolism are already operating at close to maximal oxidative capacity. To determine whether this higher ECAR is due to increased glycolytic activity, we used sequential addition of glucose, oligomycin, and 2-deoxyglucose by the Seahorse bioanalyzer to measure glycolytic function (Fig. 2C, S2C). Glycolysis (difference between ECAR in the presence of glucose and non-glycolytic ECAR) and glycolytic capacity (maximal ECAR after oligomycin treatment) are indeed higher in PGC-1 β -deficient DCs (Fig. 2C, S2C). Further, gene expression of glucose transporter 1 (*Slc2a1*) is upregulated in PGC-1 β -deficient DCs compared to control DCs under conditions of glucose withdrawal (Fig. 2D), suggesting increased dependence by the cells on glycolytic metabolism.

ATP production rates attributed to oxidative phosphorylation and glycolysis were calculated using Seahorse assay measurements and demonstrate that the ATP production rate due to oxidative phosphorylation is reduced in PGC-1 β -deficient cells both basally and at maximal oxidative capacity (Fig. 2E, left). Conversely, the ATP production rate by glycolysis is greater in PGC-1 β -deficient cells at basal metabolic rates and not significantly changed at maximal oxidative capacity (Fig. 2E, right). Individual experiments display a consistent trend of higher total ATP production in PGC-1 β -deficient DCs at basal respiration, but lower at maximal oxidative capacity, suggesting that these cells have impaired capacity to generate energy (Fig.

2F). This difference is further highlighted by the reduced fold change of ATP production rates from basal metabolism to maximal oxidative capacity in PGC-1 β -deficient DCs (Fig. 2F, right). Compared to DCs transduced with sh*Ppargc1b*, DCs derived from bone marrow of *Ppargc1b*^{fl/fl} *CD11c*^{cre} mice reveal a similar metabolic profile but with smaller differences, exhibiting significantly reduced SRC, elevated glycolysis and glycolytic capacity, and consistently but insignificantly reduced J_{ATPOX} at maximal oxidative capacity, and unchanged basal metabolic activity (Fig. S2B-E). Together, these results demonstrate that PGC-1 β deficiency diminishes oxidative metabolism while augmenting glycolytic metabolism.

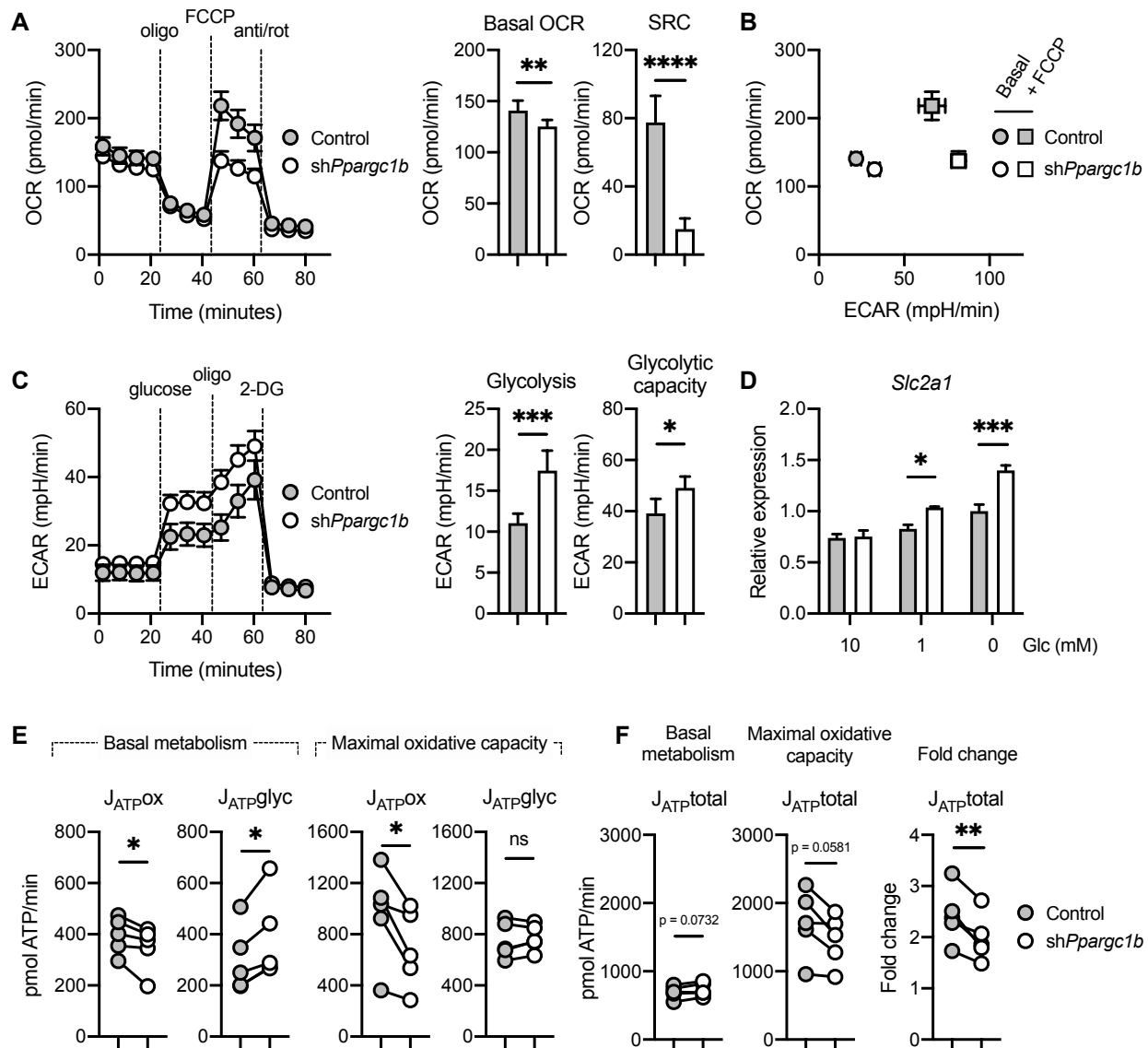


Figure 2 – PGC-1 β -deficient DCs have impaired oxidative metabolism and increased glycolysis

DCs were transduced with control shRNA or *Ppargc1b* shRNA and (A) OCR was measured by Seahorse bioanalyzer over time with sequential treatments with oligomycin (oligo), FCCP, and antimycin and rotenone (anti/rot). Basal oxygen consumption rate (OCR) and spare respiratory capacity (SRC) are determined from these measurements (right). (B) Basal and maximal (with FCCP) levels of OCR and ECAR from experiment in (A). (C) ECAR was measured over time with sequential treatments with glucose, oligomycin, and 2-deoxyglucose (2-DG). From this graph (left), glycolysis (difference between ECAR after glucose addition and non-glycolytic ECAR before glucose addition) and glycolytic capacity (maximal ECAR after oligomycin

treatment) were determined. **(D)** Gene expression of GLUT1 gene *Slc2a1* relative to *Hprt* levels in DCs cultured in 10, 1, or 0 mM glucose for 6 hours. **(E)** ATP production rates by oxidative metabolism (J_{ATPOX}) and glycolysis ($J_{ATPglyc}$) calculated from Seahorse assay measurements (see Methods) at basal (left) and maximal (right) respiratory rates. **(F)** Total ATP production rates ($J_{ATPtotal}$) at basal metabolism and maximal oxidative capacity determined by adding J_{ATPOX} and $J_{ATPglyc}$ from **(E)**, and fold change of these measurements from basal metabolism to maximal oxidative capacity represented in the rightmost graph. Data in **(A-D)** are one experiment representative of **(A-B)** five experiments and **(C)** three experiments (mean and s.d. of five to six replicates per condition). Data in **(D)** are of one experiment representative of two experiments (mean and s.e.m. of triplicates). Data in **(E)** are five experiments pooled together, with each individual experiment represented by a circle. Statistical significance was determined by **(A,C)** unpaired *t*-test, **(D)** two-way ANOVA, or **(E,F)** paired *t*-test. * $p < 0.05$, ** $p < 0.01$, *** $p < 0.001$, **** $p < 0.0001$

Effect of PGC-1 β on metabolic phenotype of differentially-activated DCs

We next investigated how PGC-1 β deficiency affects the metabolic phenotypes of differentially-activated DCs. Since stimulation by LPS results in rapid downregulation of *Ppargc1b* expression (Fig. 1F), we hypothesized PGC-1 β deficiency would not have a considerable effect on the metabolism of LPS-activated DCs. IFN- β -treated DCs, in contrast, maintain PGC-1 β expression, and therefore were predicted to be affected by PGC-1 β deficiency. As expected, ATP production rates by LPS-activated DCs were not significantly affected by PGC-1 β deficiency (Fig. 3A). ATP production rates by oxidative metabolism in IFN- β -treated DCs lacking PGC-1 β , however, were impaired at both basal metabolism and maximal respiration (Fig. 3B). Basal ATP production rates by glycolysis were higher in PGC-1 β -deficient DCs treated with IFN- β (Fig. 3B). These data confirm that PGC-1 β is required for optimal bioenergetic output in differentially-activated DCs that use oxidative metabolism.

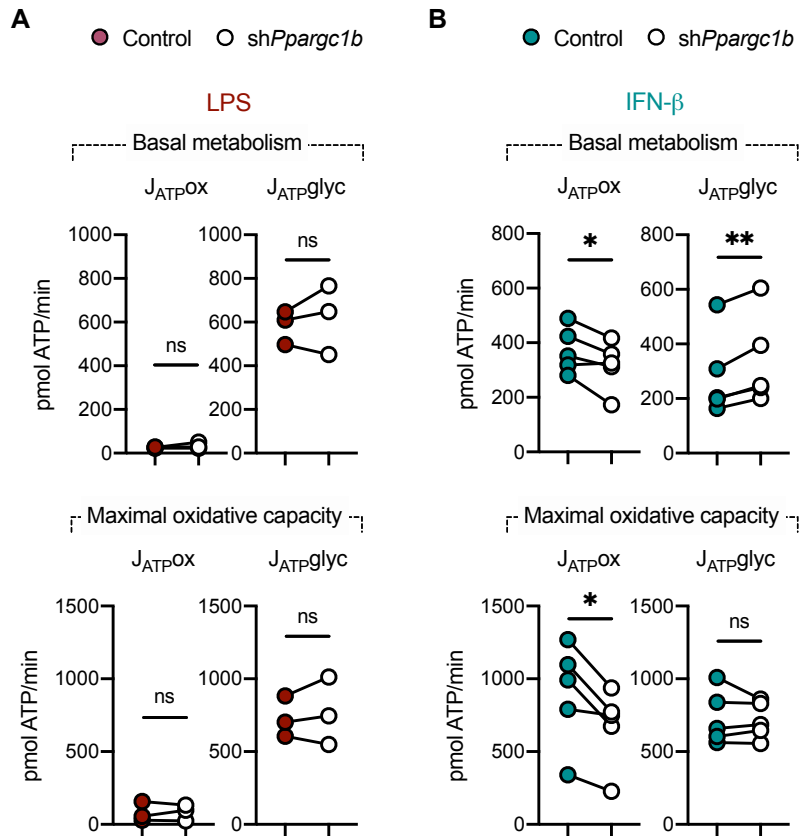


Figure 3 – Effect of PGC-1 β on metabolic phenotype of differentially-activated DCs

DCs that were stimulated with **(A)** LPS (100 ng/mL) or **(B)** IFN- β (1000 U/mL) and ATP production rates by oxidative metabolism ($J_{ATP^{OX}}$) and glycolysis ($J_{ATP^{glyc}}$) were calculated from Seahorse assay measurements at basal metabolism and maximal oxidative capacity. Colored circles are control DCs and open circles are DCs transduced with *Pparg1b* shRNA, and both were stimulated with **(A)** LPS or **(B)** IFN- β . Data in **(A-B)** are of **(A)** three or **(B)** five experiments pooled together, with each individual experiment represented by a circle. Statistical significance was determined by paired *t*-test. * $p < 0.05$, ** $p < 0.01$

PGC-1 β -deficient DCs exhibit reduced FAO but unchanged total mitochondrial mass

Since PGC-1 co-activators are known to be important for mitochondrial biogenesis in many tissues (21), we examined whether the impaired OCR by PGC-1 β -deficient DCs was due to reduced mitochondrial content. By flow cytometry, we determined that the mean fluorescence intensity (MFI) of a dye to measure mitochondrial mass is not reduced in PGC-1 β -deficient DCs (Fig. 4A). The levels of voltage-dependent anion channel (VDAC), typically used as a loading control for mitochondrial content, also remained unchanged (Fig. 4B). Since total mitochondrial content is not affected by PGC-1 β loss, we next explored whether any changes in the levels of ETC components could account for the diminished OCR. However, ETC component levels were also unchanged (Fig. 4B). Processing of different substrates, including fatty acids, can contribute to the OCR. Since PGC-1 β is known to target transcription factors that regulate lipid metabolism (10,22), we examined whether components involved in FAO were affected by PGC-1 β deficiency. We determined that gene expression of *Hadha* and *Cpt1a*, which encode enzymes involved in key steps of FAO, were reduced in PGC-1 β -deficient DCs (Fig. 4C). CPT-1a protein expression was similarly diminished (Fig. 4D, Fig. S3). In addition, control DCs more readily utilize fatty acids as fuel after nutrient starvation compared to PGC-1 β -deficient DCs, as determined by OCR when the cells are in the presence of BSA-conjugated palmitate (Fig. 4E). Together, these data suggest that the reduced oxidative metabolism by PGC-1 β -deficient DCs is likely in part due to impaired FAO, and not due to diminished mitochondrial biosynthesis.

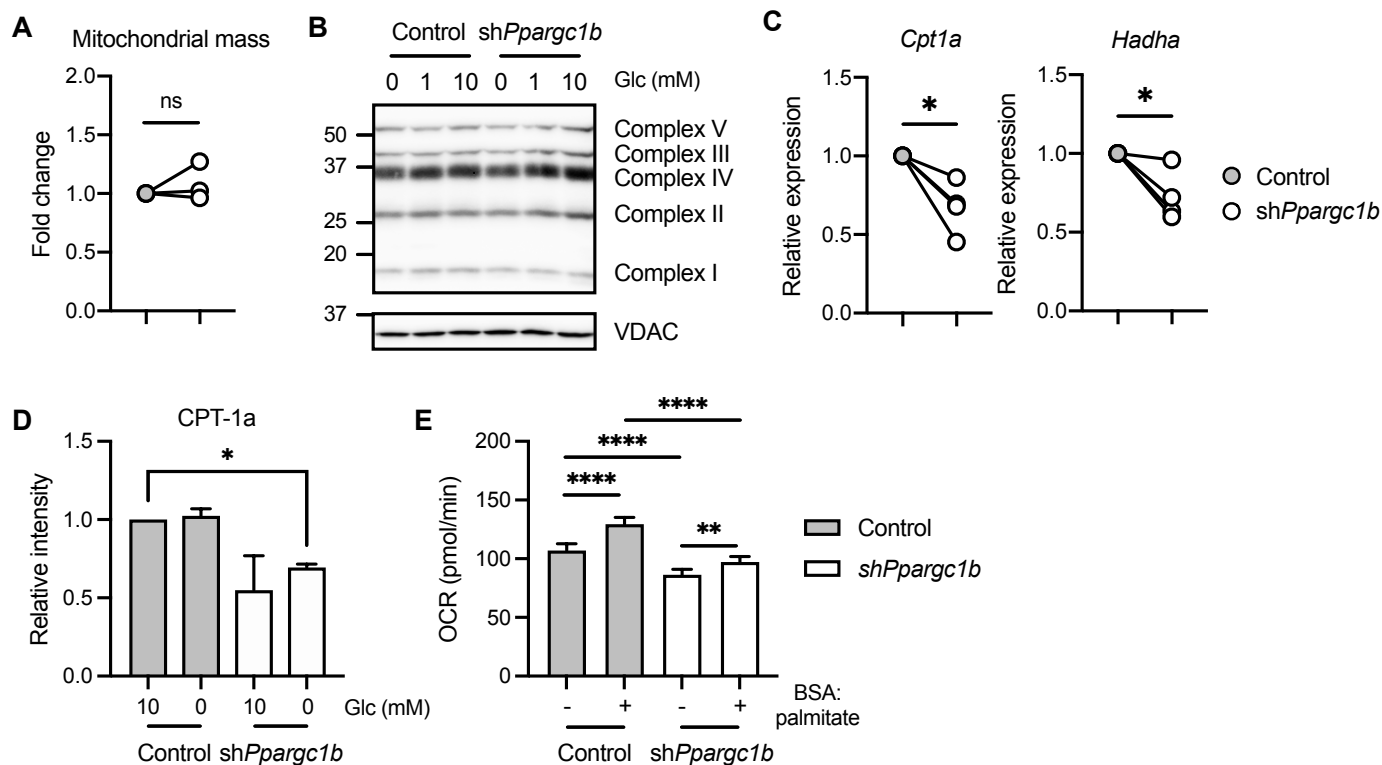


Figure 4 – PGC-1 β -deficient DCs exhibit reduced fatty acid oxidation, but unchanged total mitochondrial mass

DCs were transduced with control shRNA or *Ppargc1b* shRNA. **(A)** Mitochondrial mass of DCs stained with MitoSpy Green or MitoTracker Deep Red, with geometric MFIs represented as fold changes relative to the control condition. **(B)** Protein expression of complexes I-V of the ETC and VDAC of control or PGC-1 β -deficient DCs cultured with 0, 1, or 10 mM glucose for 6 hours. **(C)** Gene expression fold changes of *Cpt1a* (left) and *Hadha* (right) relative to *Hprt*. **(D)** Relative intensity of bands representing CPT-1a visualized by Western blot shown in Fig. S3. **(E)** DCs were cultured in nutrient-limiting media for 6 hours and OCR was measured immediately following addition of either BSA or BSA-conjugated palmitate. Data from **(A,C)** are of **(A)** three and **(C)** four experiments pooled together, with each individual experiment represented by a circle. Data from **(B)** is one experiment representative of three. Data from **(D)** is the average of two experiments. Data from **(E)** is of one experiment. Statistical significance was determined by **(A,C)** paired *t*-test or **(D,E)** two-way ANOVA. * $p < 0.05$, ** $p < 0.01$, **** $p < 0.0001$

PGC-1 β -deficient DCs have reduced mitophagy and increased autophagic flux

Recent reports suggest PGC-1 α regulates autophagy (23,24); therefore, we examined whether PGC-1 β also controls autophagy in DCs. BNIP3 is a protein that can promote cell death or survival by stimulating apoptosis or autophagy of mitochondria (mitophagy), respectively, depending on the stress signals the cell receives (25). Cells were cultured in either full glucose conditions or in the absence of glucose to induce nutrient stress. In addition, chloroquine treatment blocks the fusion of the autophagosome and lysosome, resulting in accumulation of autophagosome proteins. In control cells, glucose deprivation results in increased levels of BNIP3, which is further elevated with chloroquine treatment (Fig. 5A). In PGC-1 β -deficient cells, BNIP3 levels do not increase to an equivalent extent with glucose deprivation or with chloroquine treatment (Fig. 5A), suggesting that upregulation of BNIP3 expression is impaired in these cells. To address whether the pro-apoptotic function of BNIP3 was affected, we used flow cytometry to detect apoptotic cells and found there was no significant difference between control and PGC-1 β -deficient cells (Fig. S4). In contrast to BNIP3 expression, the expression of autophagy-related proteins sequestosome 1 (SQSTM1) and microtubule-associated protein 1 light chain 3 (LC3) was elevated in PGC-1 β -deficient DCs. Gene expression of SQSTM1 is also elevated with glucose deprivation (Fig. 5B). LC3 is involved in autophagosome formation, with LC3-I as the cytoplasmic form and LC3-II as the modified form that associates with autophagosomes. The relative intensity of LC3-II normalized to β -actin levels shows that LC3-II increases with chloroquine treatment to a greater extent in PGC-1 β -deficient cells (Fig. 5C). Autophagic flux, measured by determining the difference in intensity of LC3-II in the presence or absence of chloroquine for a given condition, is elevated in PGC-1 β -deficient cells as well (Fig. 5D, right).

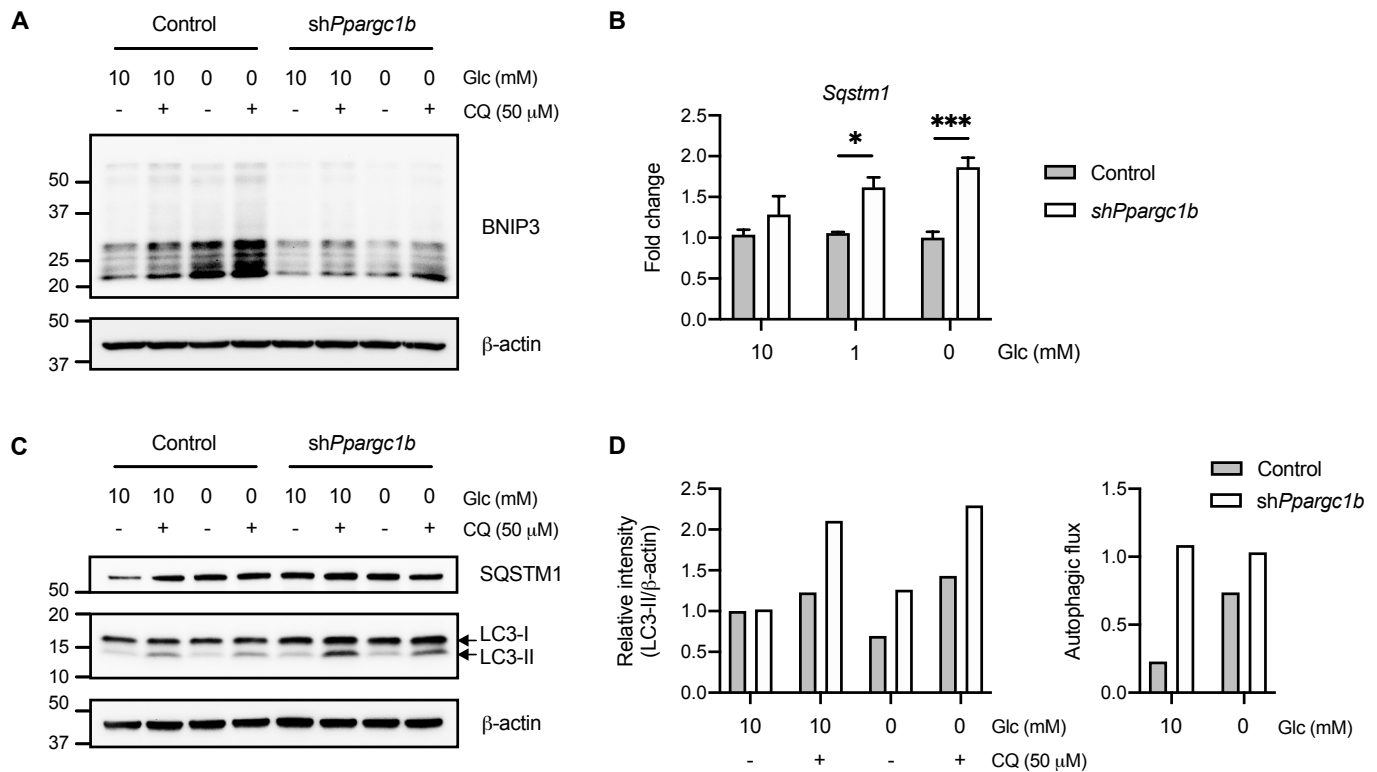


Figure 5 – PGC-1 β -deficient DCs have reduced mitophagy and enhanced autophagic flux

DCs were transduced with control shRNA or *Ppargc1b* shRNA, and then cultured in 0 or 10 mM glucose for 6 hours and 50 μ M chloroquine (CQ) was added for the last 2 hours of culture. (A) BNIP3, (B) SQSTM1/p62, and (C) LC3I/II (left) were visualized by Western blots. (D) Ratio of relative intensity of LC3II to β -actin from blot in (C) (left). Autophagic flux was calculated by determining the difference between the intensity of LC3-II normalized to β -actin in the presence and absence of chloroquine (right). Data are one experiment representative of (A-D) two experiments. Statistical significance in (B) was determined by two-way ANOVA. * $p < 0.05$, *** $p < 0.001$

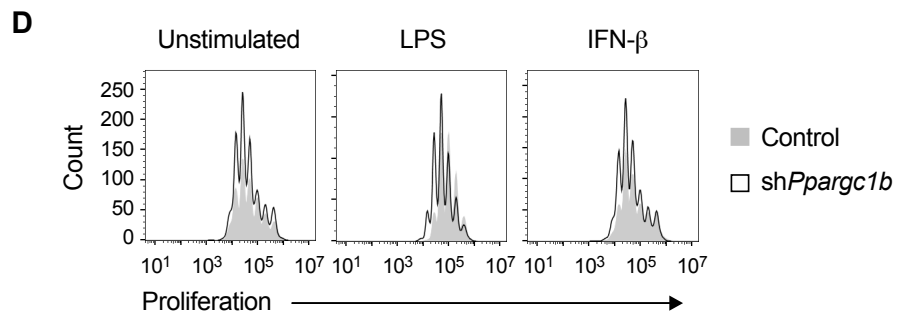
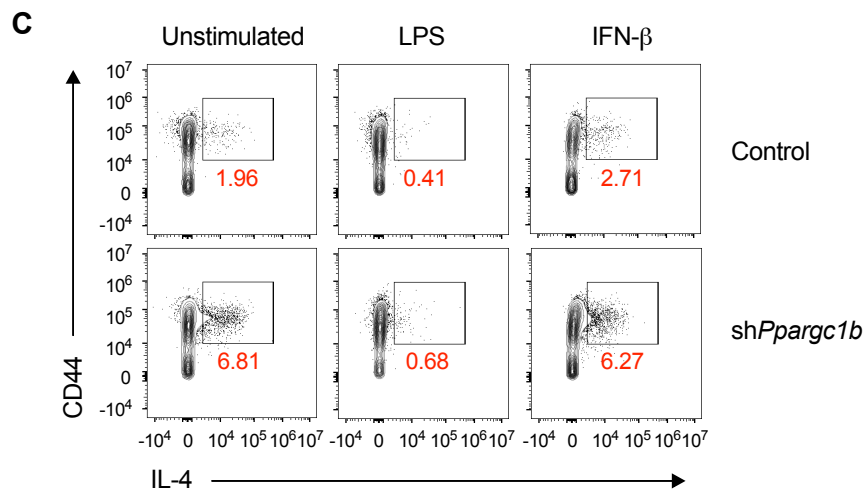
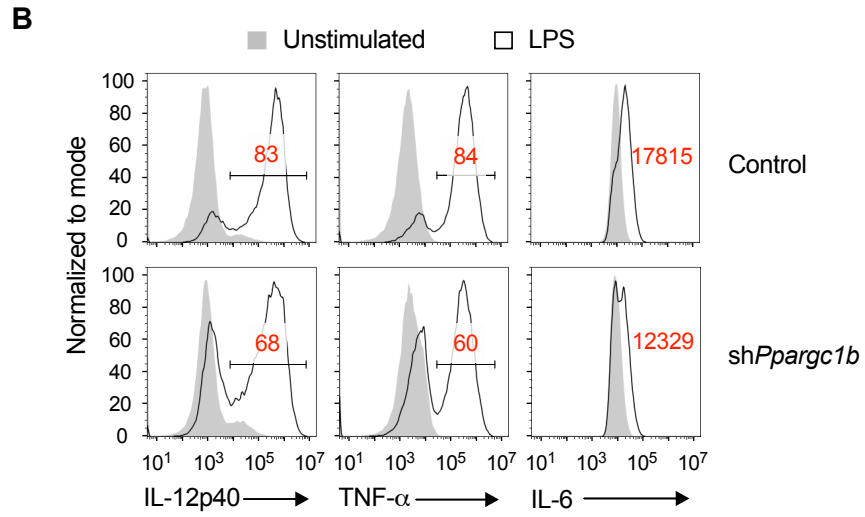
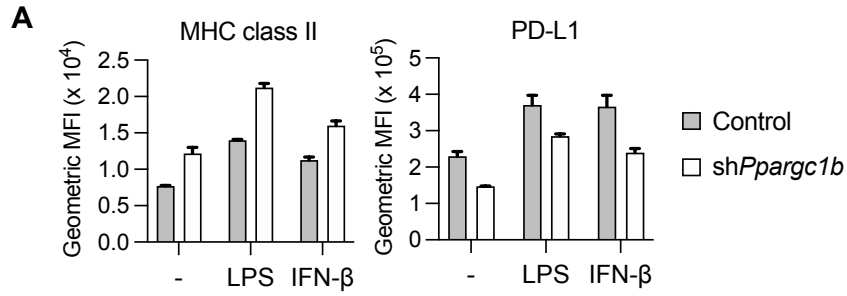
PGC-1 β -deficient DCs have reduced pro-inflammatory cytokine production and promote T cell expansion and Th2 differentiation

We examined how PGC-1 β deficiency affects the immune functions of DCs. First, we determined that PGC-1 β -deficient DCs, whether unstimulated or treated with LPS or IFN- β ,

express higher levels of MHC class II, a molecule for antigen presentation, and reduced levels of PD-L1, an immunomodulatory ligand, compared to control DCs (Fig. 6A, S6A). In addition, PGC-1 β -deficient DCs produce lower levels of pro-inflammatory cytokines IL-12/23p40, TNF- α , and IL-6 (Fig. 6B, S6B). We co-cultured ovalbumin-specific CD4⁺ T cells with DCs pulsed with whole ovalbumin protein and found that PGC-1 β -deficient DCs that were unstimulated or IFN- β -treated induced greater IL-4 production by CD4⁺ T cells (Fig. 6C, S6C), suggesting PGC-1 β -deficient DCs promote Th2 differentiation. Since LPS promotes a strong Th1 response, LPS-activated DCs induced minimal IL-4 production as expected. Other cytokines, including TNF- α , IL-2, and Th1-associated IFN- γ , were not significantly different between T cells primed by control DCs or DCs lacking PGC-1 β (Fig. S6D). PGC-1 β -deficient DCs also promote CD4⁺ T cell expansion, regardless of the inflammatory phenotype of the DCs (Fig. 6D, S6E).

Discussion

Previous studies have demonstrated that cellular metabolism is crucial for the regulation of immune cell function and activation (2,3). In this study, we aimed to investigate the role of the transcriptional co-activator PGC-1 β , a major regulator of mitochondrial metabolism, in DCs. To compare contrasting metabolic profiles, we selected LPS and IFN- β to treat DCs. We have shown that unstimulated DCs deficient in PGC-1 β expression have impaired oxidative metabolism, but elevated glycolytic activity. PGC-1 β deficiency similarly affects the metabolism of IFN- β -treated DCs, which normally maintain their mitochondrial metabolism, while the metabolism of LPS-activated DCs is unaffected. The increase in glycolytic rates is likely a compensatory mechanism by the PGC-1 β -deficient DCs to maintain intracellular ATP levels in



(legend on next page)

Figure 6 – PGC-1 β -deficient DCs promote T cell expansion and Th2 differentiation

DCs were transduced with control shRNA or *Ppargc1b* shRNA, (A) stimulated with LPS (100 ng/mL) or IFN- β (1000 U/mL) for 18 hours, and MHC class II and PD-L1 surface expression were measured by flow cytometry and represented as geometric MFI. (B) DCs were stimulated with or without LPS for 4 hours, and intracellular levels of cytokines IL-12/23p40, TNF- α , and IL-6 were determined by flow cytometry. Numbers in red represent percentage of cells positive for IL-12/23p40 and TNF- α , or geometric MFI for IL-6. DCs stimulated with LPS (5 ng/mL) or IFN- β (50 U/mL) for 6 hours in the presence of whole ovalbumin protein (9 μ g/mL for cytokine production and 3 μ g/mL for proliferation) were co-cultured with OT-II CD4⁺ T cells, and (C) IL-4 production after 4 days and (D) proliferation by the T cells after 3 days were measured. Data are from one experiment representative of (A) > three experiments (mean and s.d. of triplicates), (B-D) three experiments.

response to the drop in ATP production by the mitochondria. While gene expression of glucose transporter *Slc2a1* in PGC-1 β -deficient DCs is comparable to that of control DCs in full glucose conditions, glucose deprivation results in a greater fold change in *Slc2a1* expression. This result suggests that the DCs cannot sufficiently shift their metabolic activity to mitochondrial metabolism due to the loss of PGC-1 β and increased reliance on glycolysis.

To determine how PGC-1 β deficiency leads to impaired oxidative metabolism, we first examined mitochondrial content since PGC-1 proteins are known to be important for mitochondrial biogenesis in certain contexts. However, mitochondrial mass was not consistently different between control and PGC-1 β -deficient DCs, nor were the levels of ETC components (Fig. 4A,B). PGC-1 proteins also have a role in FAO by co-activating transcription factors, such as PPAR α , to promote transcription of FAO enzymes (22,26). The gene expression of the enzymes CPT-1a and HADHA and the protein levels of CPT-1a were decreased in PGC-1 β -deficient DCs, suggesting that impaired FAO contributes to the lowered oxidative metabolism in these cells.

Another potential contributor to the diminished oxidative metabolic rates may be the accumulation of dysfunctional mitochondria. BNIP3, a protein involved in mitophagy, is reduced in expression in PGC-1 β -deficient DCs (Fig. 5A). This may lead to impaired recycling of mitochondria, which can promote the accumulation of dysfunctional mitochondria (27). Further, this may mask any change in total mitochondrial mass that results from diminished mitochondrial biosynthesis due to PGC-1 β deficiency. A clear link has been established in previous studies between mitochondrial dysfunction and impairment of immune cell function. For example, T cells in the tumor microenvironment or in chronic viral infection have dysfunctional mitochondria and impaired effector functions; overexpression of PGC-1 α helps restore these defects (13,28).

While mitophagy may be impaired, our data suggests autophagy is elevated in PGC-1 β -deficient DCs. This result is in contrast with a few studies showing positive regulation by PGC-1 α and PGC-1 β in muscle cells: PGC-1 α deficiency results in a reduction in autophagy, and PGC-1 β overexpression upregulates autophagy-related genes (23,29). Similarly, another study describes that the upregulation of autophagy-related genes induced in skeletal muscle cells by exercise is attenuated in PGC-1 α -deficient mice (24). Potential explanations for these conflicting findings may be that PGC-1 β -deficient DCs either do not impair autophagy or the nutrient requirements that result from metabolic defects of PGC-1 β -deficient DCs exceed any inhibitory effects of autophagy. Further study is required to determine whether stress signals are present due to bioenergetic or nutrient insufficiencies in DCs lacking PGC-1 β . The activation of the energy-sensing kinase AMPK, for example, can upregulate glycolysis as well as autophagy (30)—processes we observed in PGC-1 β -deficient DCs.

We examined whether PGC-1 β -deficiency in DCs resulted in functional defects. We found that PGC-1 β -deficient DCs had reduced pro-inflammatory cytokine production, but elevated MHC II expression. Surprisingly, PGC-1 β -deficient DCs that were unstimulated or IFN- β -treated—both maintaining their mitochondrial metabolism—induce IL-4 production in antigen-specific CD4⁺ T cells. This was an unexpected result since PGC-1 β deficiency in macrophages is known to promote type 1 immunity (15) and IL-4 is a type 2 cytokine. Elevated autophagic flux is known to promote antigen presentation on MHC class II molecules in innate immune cells (31), which is in line with our findings that PGC-1 β -deficient DCs display greater autophagic activity and higher MHC class II surface expression. This likely contributes to the enhanced expansion of T cells by PGC-1 β -deficient DCs as well.

There are other reported cases of DCs with mitochondrial dysfunction promoting Th2 differentiation. DCs that are infected with the intracellular pathogen *Chlamydia muridarum* and deficient in enolase 1 (ENO1), a glycolytic enzyme that converts 2-phosphoglycerate to phosphoenolpyruvate, display reduced pyruvate production, fragmented mitochondria, and increased capacity to promote Th2 immunity (32). ENO1-deficient DCs differ from PGC-1 β -deficient DCs in that ENO1-deficient DCs have lower MHC II expression compared to control DCs (32). Accordingly, the T cells they stimulate have reduced proliferation. Moreover, DCs deficient in sirtuin 1 (SIRT1), an NAD⁺-dependent deacetylase, and infected with respiratory syncytial virus (RSV), have dysfunctional mitochondria compared to RSV-infected wild-type DCs, exhibiting increased depolarization, greater mitochondrial ROS production, and decreased mitochondrial respiration (33). RSV-infected DCs normally induce an anti-viral Th1 response, but SIRT1 deficiency skews this response to Th2 and Th17 immunity (33). These studies suggest

that mitochondrial dysfunction in DCs impacts T cell polarization by favoring Th2 differentiation, although the exact mechanism by which this occurs requires further investigation.

In all, our findings highlight the importance of PGC-1 β in maintaining an oxidative metabolic program in DCs, and its effect on DC activation and function. This knowledge provides further insight into how the regulation of cellular metabolism can affect immunity.

Experimental procedures

Mice

Nos2^{-/-} mice and OT-II mice were obtained from Jackson Laboratory. *Ppargc1b*^{*fl/fl*} mice were kindly provided by the lab of Jennifer Estall (Institut de recherches cliniques de Montréal) and generated by the lab of Daniel Kelly (University of Pennsylvania). *Ppargc1b*^{*fl/fl*} mice were crossed with *CD11c*^{*cre*} mice. C57BL/6 were bred and maintained at the Van Andel Research Institute in a specific pathogen-free environment. All animal studies were carried out in compliance with Animal Use Protocol 18-09-026 approved by the Van Andel Research Institute Institutional Animal Care and Use Committee and used at 8 to 20 weeks of age.

In vitro differentiation and retroviral transduction of dendritic cells

Bone marrow from the tibia and femur of C57BL/6 mice was extracted and seeded at day 0 in 6-well non-tissue culture-treated plates at 7.5×10^5 non-erythrocytes/well or at 1×10^6 non-erythrocytes/well if the cells were to undergo retroviral transduction. The cells were cultured in the presence of 20 ng/mL of granulocyte-macrophage colony-stimulating factor (GM-CSF; from Peprotech) in complete DC medium (CDCM): RPMI-1640 medium (Corning) containing 100 U/mL penicillin-streptomycin (Gibco), 2 mM L-glutamine (Gibco), 55 μ M β -mercaptoethanol

(Gibco), and 10% heat-inactivated Nu-Serum (Corning), with media changes at days 3 and 6. For retroviral transductions, the sequence for the *Ppargc1b* short hairpin RNA (shRNA) was obtained from RNAi Codex and cloned into the LMP retroviral vector expressing a human CD8 reporter (16). Retrovirus containing a control shRNA (firefly luciferase) or the *Ppargc1b* shRNA were produced by 293T cells transfected using Lipofectamine 2000 (Invitrogen). After 48 hours, supernatant containing retrovirus was collected and applied to day 2 DC culture and spun at 2500 rpm 30°C for 90 minutes. At day 8 or 9, DCs were harvested and sorted on either CD11c (for DCs differentiated from bone marrow of *Ppargc1b^{fl/fl} CD11c^{cre}* mice) or human CD8 (for retrovirally transduced DCs) using anti-biotin microbeads (Miltenyi). Sorted cells were seeded at a final density of 1×10^6 cells/mL and were left unstimulated or stimulated with 100 ng/mL LPS (*Escherichia coli* O111:B4; Invivogen) or 1000 U/mL IFN- β (PBL Interferon Source) unless otherwise stated for the indicated length of time.

Metabolic assay

DCs were analyzed by Seahorse XFe96 Analyzer (Agilent) to measure ECAR and OCR in real-time. DCs were seeded at 7×10^4 cells/well in CDCM and stimulated for the indicated length of time. For the XF Cell Mito Stress Test (Agilent), the cell medium was replaced with XF RPMI base medium containing 10 mM glucose, 2 mM glutamine, and 5% FBS, with pH adjusted to 7.4. The DCs were sequentially treated with oligomycin (1.5 μ M), FCCP (1.5 μ M), and antimycin/rotenone (both 1 μ M). For the XF Glycolysis Stress Test (Agilent), the cell medium was replaced with XF RPMI base medium containing 2 mM glutamine and 5% FBS, but no glucose. The DCs were sequentially treated with glucose (10 mM), oligomycin (1.5 μ M), and 2-deoxyglucose (50 mM). For the XF Palmitate Oxidation Stress Test (Agilent), DCs were

cultured for 6 hours in nutrient-limiting media (RPMI-1640 containing 0.5 mM glucose, 1 mM L-glutamine, 1% FBS, 55 μ M β -mercaptoethanol, 100 U/mL penicillin-streptomycin, and 0.5 mM carnitine), followed by replacing this with XF RPMI base medium containing 2 mM glucose and 0.5 mM carnitine. BSA or BSA-conjugated palmitate was added immediately prior to starting the run. For all assays, cells were placed at 37°C in the absence of CO₂ for approximately 1 hour prior to the start of each run. After each run, cells were stained with 20 μ M of Hoescht stain (ThermoFisher Scientific) for 15 minutes at 37°C and imaged using a Cytation imaging reader (BioTek). Measurements from the assay were then normalized by cell number. Bioenergetic rates were calculated based on protocols developed by Mookerjee *et al.*, and adapted by Ma *et al* (17,18). J_{ATP} rates by glycolysis (J_{ATPglyc}) and oxidative metabolism (J_{ATPOX}) were calculated by ECAR or OCR, respectively, before any drug treatment for basal metabolism, and after FCCP treatment for maximal respiration. J_{ATPtotal} rates represent the sum of J_{ATPglyc} and J_{ATPOX}.

Quantitative RT-PCR

RNA was isolated using TRIzol (ThermoFisher Scientific) according to manufacturer's instructions. cDNA was obtained using RT MasterMix (Applied Biological Materials) and used to perform a SYBR-based real-time PCR (BioLine) with primers (Table 1) from Integrated DNA Technologies. Data were generated using the $\Delta\Delta$ Cq method. Relative gene expression was normalized to that of hypoxanthine-guanine phosphoribosyltransferase (HPRT).

Table 1 – List of primers used for qPCR

| Gene name | Forward primer | Reverse primer |
|-----------------|------------------------------------|--|
| <i>Ppargc1b</i> | GGC AGG TTC AAC CCC GA | CTT GCT AAC ATC ACA GAG GAT ATC TTG |
| <i>Slca21</i> | CTG GAC CTC AAA CTT CAT TGT GGG | GGG TGT CTT GTC ACT TTG GCT GG |
| <i>Sqstm1</i> | CCT CAG CCC TCT AGG CAT TG | TTC TGG GGT AGT GGG TGT CA |
| <i>Hadha</i> | AGT GGA AAG CGT GAC TCC AG | ACA TCC ACA CCC ACT TCG TC |
| <i>Cpt1a</i> | GGA CTC CGC TCG CTC ATT | ACC TTG ACC ATA GCC ATC CAG |
| <i>Hprt</i> | AGG ACC TCT CGA AGT GTT GG | GGC TTT GTA TTT GGC TTT TCC |

T cell co-culture

DCs were pulsed with ovalbumin (Worthington) and left unstimulated or stimulated with 5 ng/mL LPS or 50 U/mL IFN- β for 6 hours before co-culture with isolated CD4⁺ T cells from OT-II mice expressing transgenic T cell receptors specific for ovalbumin. T cells were isolated using EasySep Mouse CD4⁺ T cell Isolation Kit (StemCell). To examine T cell proliferation, OT-II T cells were stained with Cell Proliferation Dye eFluor 450 (Invitrogen) according to manufacturer's instructions prior to co-culture with DCs. At day 3, T cells were collected and stained with antibodies for flow cytometry. To examine intracellular cytokine production, at day 4, T cells were treated with PMA (50 ng/mL) and ionomycin (500 ng/mL) for 4 hours, with brefeldin A for the last 2 hours, and then stained with antibodies for flow cytometry.

Flow cytometry

Cells were washed with wash buffer (PBS containing 1% FBS, 1 mM EDTA, and 0.05% sodium azide) and stained with eFluor 506 Fixable Viability Dye (Invitrogen) and Fc block (anti-CD16/CD32) prior to staining with cell surface markers, which include human CD8 (OKT-8), CD11c (N418), MHC-II (M5/144.15.2), PD-L1 (10F.9G2) for DCs and CD44 (IM7) for T cells.

To examine intracellular cytokines, which include IL-12p40 (C17.8), TNF- α (MP6-XT22), and IL-6 (MP5-20F3) for DCs, and IFN- γ (XMG1.2), IL-4 (11B11), IL-2 (JES6-5H4), and TNF- α (MP6-XT22) for T cells, cells were fixed with IC Fixation Buffer (Invitrogen) for 30 minutes, followed by cell permeabilization using Permeabilization Buffer (Invitrogen), and > 1 hour of intracellular cytokine staining. For mitochondrial staining, cells were stained with 50 nM MitoSpy Green (BioLegend) or 50 nM MitoTracker Deep Red (ThermoFisher Scientific) in HBSS at 37°C for 20 minutes. Apotracker Green (BioLegend) was used at 400 nM according to manufacturer's instructions to detect apoptotic cells. Samples were acquired on the Cytotflex (Beckman Coulter) or Aurora (Cytek) and analyzed using FlowJo software.

Western blot

Protein lysates were prepared in RIPA lysis buffer with protease inhibitor and phosphatase inhibitor, then quantified by detergent compatible protein assay (Bio-Rad). Samples were run on 10% or 12.5% gels using SDS-polyacrylamide gel electrophoresis, and proteins were transferred by Turbo transfer system (Bio-Rad) onto methanol-activated polyvinylidene fluoride membranes. After blocking for 1 hour with 5% milk, membranes were incubated overnight at 4°C with antibodies against β -actin (13E5), LC3I/II, SQSTM1 (D1Q5S), and BNIP3 (all from Cell Signaling Technology), and CPT-1a (8F6AE9) and Total OXPHOS Rodent WB Antibody Cocktail (both from Abcam), all at 1:1000 in 4% BSA. The Total OXPHOS Rodent WB Antibody Cocktail contains antibodies against complex I subunit NDUFB8, complex II iron-sulfur protein subunit, complex III core protein 2, complex IV subunit I, and complex V alpha subunit. Following washes with Tris-buffered saline (TBS) containing 0.1% Tween-20 (TBS-T), membranes were incubated with horseradish peroxidase-linked antibody to rabbit or mouse IgG

in 5% milk for 45 minutes. Enhanced chemiluminescence using SuperSignal substrate (ThermoFisher Scientific) and ChemiDoc (Bio-Rad) were used to develop blots.

Statistical analysis

Data were analyzed using GraphPad Prism software (version 9). An unpaired or paired Student's *t*-test was performed as indicated to determine statistical significance between two conditions. A two-way analysis of variance was performed to determine statistical significance between multiple groups. Differences between conditions were considered significant when *P* values were below 0.05.

Supplementary Figures

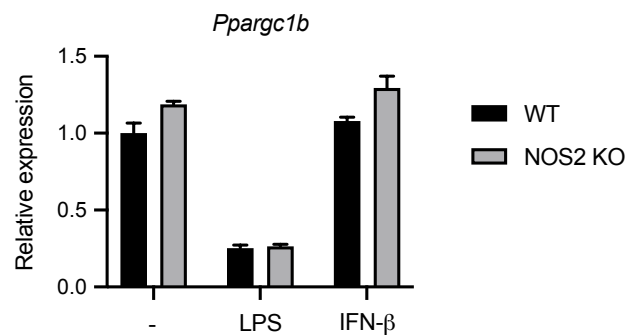


Figure S1 – NOS2 expression does not affect *Ppargc1b* expression

DCs derived from wild-type (WT) or *Nos2*^{-/-} (KO) mice were left unstimulated or stimulated with LPS (100 ng/mL) or IFN- β (1000 U/mL) for 18 hours. Fold changes of *Ppargc1b* expression was made relative to *Hprt*. Data are from one experiment representative of two experiments.

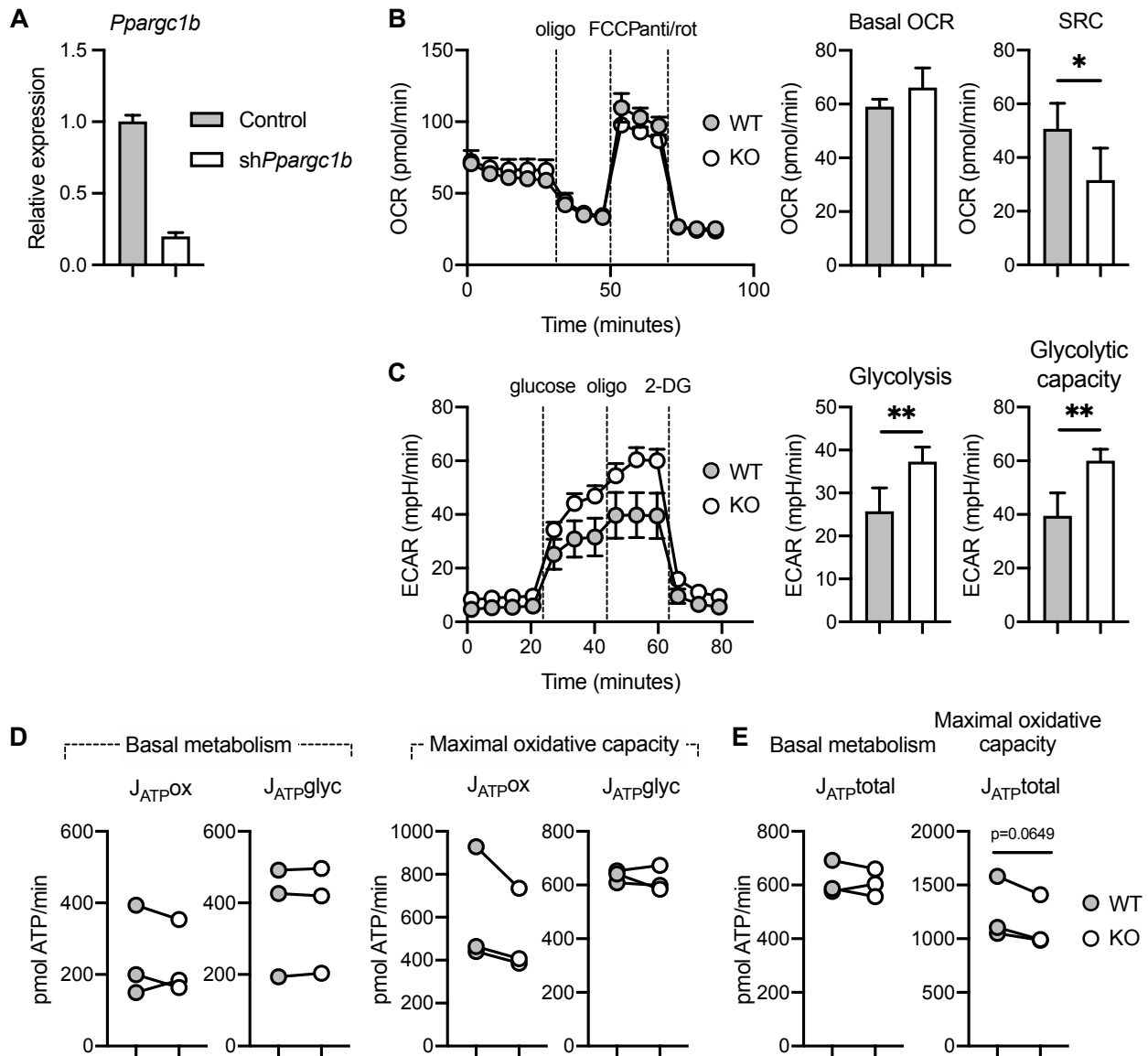


Figure S2 – PGC-1 β knockdown efficiency and bioenergetic phenotype of PGC-1 β KO DCs

(A) Gene expression of *Ppargc1b* in DCs transduced with control shRNA or *Ppargc1b* shRNA to confirm knockdown. (B-E) Bone marrow-derived CD11c⁺ DCs from wild-type (WT) or *Ppargc1b*^{fl/fl} *CD11c-cre* (KO) mice were examined by Seahorse bioanalyzer, measuring (B) OCR over time with sequential treatments with oligomycin (oligo), FCCP, and antimycin and rotenone (anti/rot). Basal oxygen consumption rate (OCR) and spare respiratory capacity (SRC) were determined from these measurements (right). (C) ECAR was measured over time with sequential treatments with glucose, oligomycin, and 2-deoxyglucose (2-DG). From this graph (left), glycolysis (difference between ECAR after glucose addition and non-glycolytic ECAR before glucose addition) and glycolytic capacity (maximal ECAR after oligomycin treatment) were

determined. **(D)** ATP production rates by oxidative metabolism ($J_{ATP_{OX}}$) and glycolysis ($J_{ATP_{glyc}}$) calculated from Seahorse assay measurements (see Methods) at basal (left) and maximal (right) respiratory rates. **(E)** Total ATP production rates ($J_{ATP_{total}}$) at basal metabolism and maximal respiration determined by adding $J_{ATP_{OX}}$ and $J_{ATP_{glyc}}$ from **(D)**. Data in **(A-C)** are one experiment representative of **(A)** > three experiments, **(B)** three experiments, and **(C)** two experiments. Experiments in **(B-C)** have six replicates per condition. Data in **(D,E)** are three experiments pooled together, with each individual experiment represented by a circle. Statistical significance was determined by **(B,C)** unpaired *t*-test or **(D,E)** paired *t*-test. * $p < 0.05$, ** $p < 0.01$

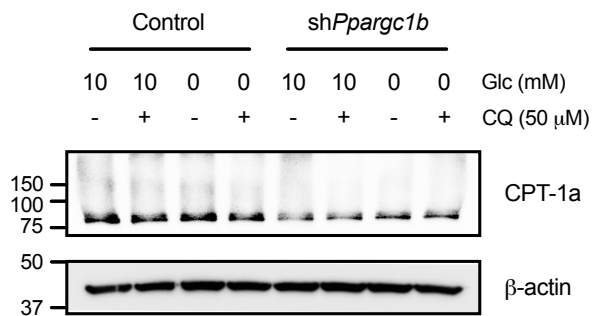


Figure S3 – CPT-1a protein levels are reduced in PGC-1 β -deficient DCs

DCs were transduced with control shRNA or *Ppargc1b* shRNA and incubated with or without 10 mM of glucose for 6 hours in the presence or absence of chloroquine (50 μ M) for the last 2 hours. CPT-1a and β -actin were visualized by Western blot. Data are one experiment representative of two experiments.

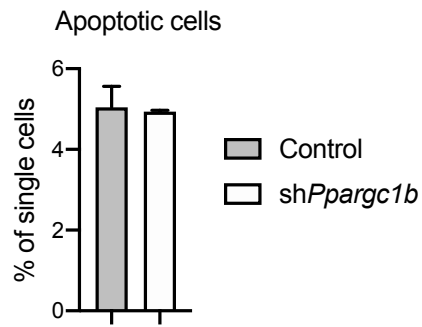


Figure S4 – Frequency of apoptotic cells are not affected by PGC-1 β deficiency

DCs that were transduced with control shRNA or sh*Ppargc1b* were examined for apoptosis, represented by the frequency of cells that were positive for both ApoTracker Green and efluor 506 Fixable Viability Dye. Data are of one experiment (mean and s.d. of triplicates).

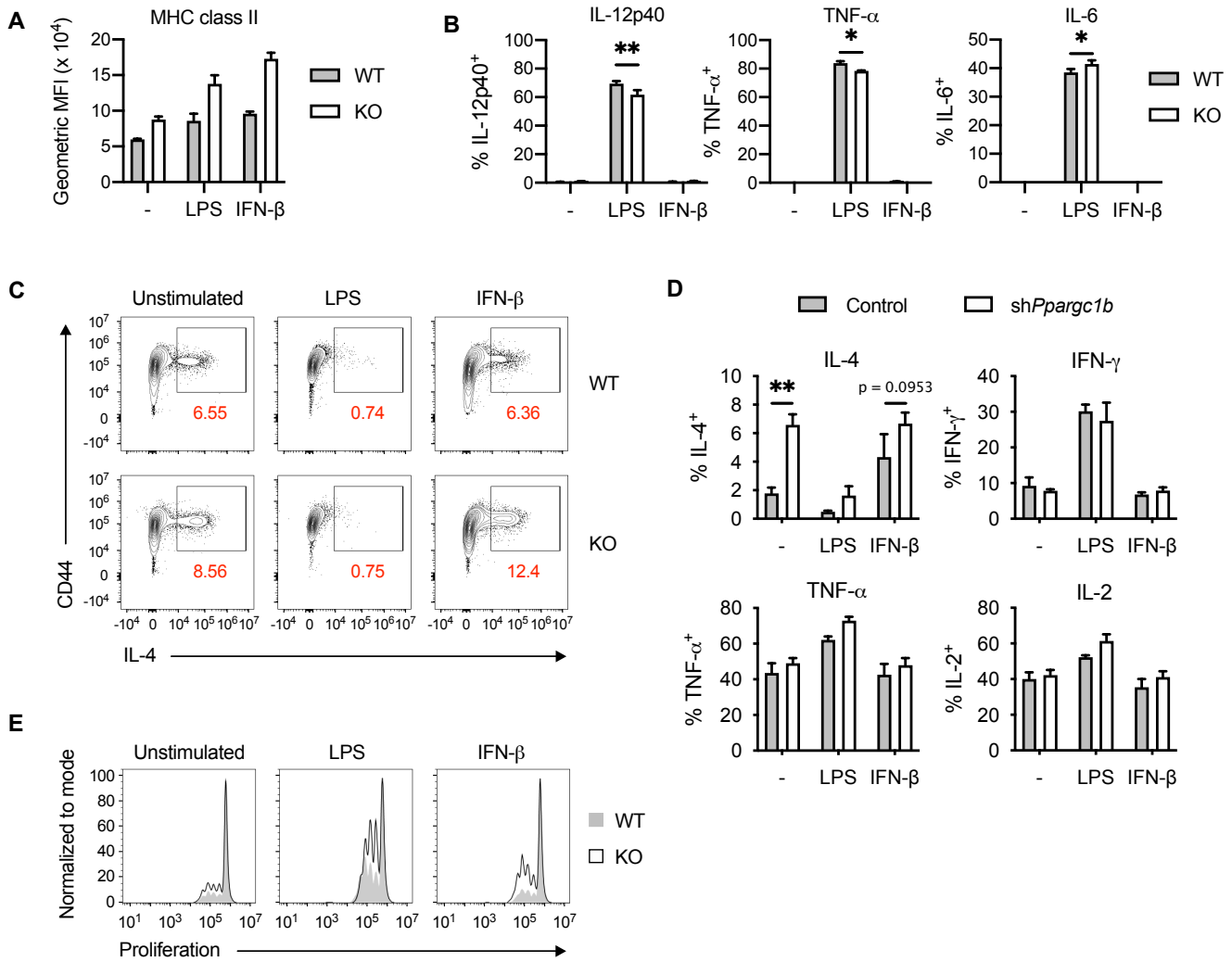


Figure S5 – Immune phenotype of PGC-1 β KO DCs

Bone marrow-derived CD11c⁺ DCs from wild-type (WT) or *Ppargc1b*^{fl/fl} *CD11c-cre* (KO) mice were left unstimulated or stimulated with LPS or IFN- β for **(A)** 18 hours and MHC-II expression measured, **(B)** 4 hours and intracellular cytokine production of IL-12p40, TNF- α , and IL-6 were measured by flow cytometry. **(C)** WT and KO DCs left unstimulated or stimulated with LPS (5 ng/mL) or IFN- β (50 U/mL) and pulsed with whole ovalbumin protein (12 μ g/mL for cytokine production and 4 μ g/mL for proliferation) for 6 hours, were subsequently co-cultured with OT-II CD4⁺ T cells, and **(D)** intracellular production of IL-4, IFN- γ , TNF- α , and IL-2 after 4 days and **(E)** proliferation after 3 days were measured by flow cytometry. **(D)** DCs transduced with control shRNA or sh*Ppargc1b* co-cultured with OT-II CD4⁺ T cells, with graphs corresponding to the experiment in Fig. 6C. Data are from one experiment representative of **(A,D)** three experiments (mean and s.d. of **(A)** triplicates, **(D)** duplicates), **(B,C,E)** one experiment (mean and s.d. of duplicates). * $p < 0.05$, ** $p < 0.01$

References

1. Krawczyk CM, Holowka T, Sun J, Blagih J, Amiel E, DeBerardinis RJ, et al. Toll-like receptor–induced changes in glycolytic metabolism regulate dendritic cell activation. *Blood*. 2010 Jun 10;115(23):4742–9.
2. O’Neill LAJ, Kishton RJ, Rathmell J. A guide to immunometabolism for immunologists. *Nat Rev Immunol*. 2016 Sep;16(9):553–65.
3. Buck MD, Sowell RT, Kaech SM, Pearce EL. Metabolic Instruction of Immunity. *Cell*. 2017 May 4;169(4):570–86.
4. Everts B, Amiel E, Huang SC-C, Smith AM, Chang C-H, Lam WY, et al. TLR-driven early glycolytic reprogramming via the kinases TBK1-IKK ϵ supports the anabolic demands of dendritic cell activation. *Nat Immunol*. 2014 Apr;15(4):323–32.
5. Zhao F, Xiao C, Evans KS, Theivanthiran T, DeVito N, Holtzhausen A, et al. Paracrine Wnt5a- β -Catenin Signaling Triggers a Metabolic Program that Drives Dendritic Cell Tolerization. *Immunity*. 2018 Jan 16;48(1):147-160.e7.
6. Malinarich F, Duan K, Hamid RA, Bijin A, Lin WX, Poidinger M, et al. High Mitochondrial Respiration and Glycolytic Capacity Represent a Metabolic Phenotype of Human Tolerogenic Dendritic Cells. *J Immunol*. 2015 Jun 1;194(11):5174–86.
7. Pantel A, Teixeira A, Haddad E, Wood EG, Steinman RM, Longhi MP. Direct Type I IFN but Not MDA5/TLR3 Activation of Dendritic Cells Is Required for Maturation and Metabolic Shift to Glycolysis after Poly IC Stimulation. *PLOS Biol*. 2014 Jan 7;12(1):e1001759.
8. Lin J, Handschin C, Spiegelman BM. Metabolic control through the PGC-1 family of transcription coactivators. *Cell Metab*. 2005 Jun 1;1(6):361–70.
9. Rhee J, Inoue Y, Yoon JC, Puigserver P, Fan M, Gonzalez FJ, et al. Regulation of hepatic fasting response by PPAR γ coactivator-1 α (PGC-1): Requirement for hepatocyte nuclear factor 4 α in gluconeogenesis. *Proc Natl Acad Sci U S A*. 2003 Apr 1;100(7):4012–7.
10. Lin J, Yang R, Tarr PT, Wu P-H, Handschin C, Li S, et al. Hyperlipidemic Effects of Dietary Saturated Fats Mediated through PGC-1 β Coactivation of SREBP. *Cell*. 2005 Jan 28;120(2):261–73.
11. St-Pierre J, Lin J, Krauss S, Tarr PT, Yang R, Newgard CB, et al. Bioenergetic Analysis of Peroxisome Proliferator-activated Receptor γ Coactivators 1 α and 1 β (PGC-1 α and PGC-1 β) in Muscle Cells. *J Biol Chem*. 2003 Jul 18;278(29):26597–603.
12. Dumauthioz N, Tschumi B, Wenes M, Marti B, Wang H, Franco F, et al. Enforced PGC-1 α expression promotes CD8 T cell fitness, memory formation and antitumor immunity. *Cell Mol Immunol*. 2020 Feb 13;1–11.

13. Scharping NE, Menk AV, Moreci RS, Whetstone RD, Dadey RE, Watkins SC, et al. The Tumor Microenvironment Represses T Cell Mitochondrial Biogenesis to Drive Intratumoral T Cell Metabolic Insufficiency and Dysfunction. *Immunity*. 2016 Aug 16;45(2):374–88.
14. Zaccagnino P, Saltarella M, Maiorano S, Gaballo A, Santoro G, Nico B, et al. An active mitochondrial biogenesis occurs during dendritic cell differentiation. *Int J Biochem Cell Biol*. 2012 Nov 1;44(11):1962–9.
15. Vats D, Mukundan L, Odegaard JI, Zhang L, Smith KL, Morel CR, et al. Oxidative metabolism and PGC-1 β attenuate macrophage-mediated inflammation. *Cell Metab*. 2006 Jul;4(1):13–24.
16. Paddison PJ, Cleary M, Silva JM, Chang K, Sheth N, Sachidanandam R, et al. Cloning of short hairpin RNAs for gene knockdown in mammalian cells. *Nat Methods*. 2004 Nov;1(2):163–7.
17. Mookerjee SA, Gerencser AA, Nicholls DG, Brand MD. Quantifying intracellular rates of glycolytic and oxidative ATP production and consumption using extracellular flux measurements. *J Biol Chem*. 2017 Apr 28;292(17):7189–207.
18. Ma EH, Verway MJ, Johnson RM, Roy DG, Steadman M, Hayes S, et al. Metabolic Profiling Using Stable Isotope Tracing Reveals Distinct Patterns of Glucose Utilization by Physiologically Activated CD8⁺ T Cells. *Immunity*. 2019 Nov 19;51(5):856–870.e5.
19. Everts B, Amiel E, Windt GJW van der, Freitas TC, Chott R, Yarasheski KE, et al. Commitment to glycolysis sustains survival of NO-producing inflammatory dendritic cells. *Blood*. 2012 Aug 16;120(7):1422.
20. Wu D, Sanin DE, Everts B, Chen Q, Qiu J, Buck MD, et al. Type 1 interferons induce changes in core metabolism that are critical for immune function. *Immunity*. 2016 Jun 21;44(6):1325–36.
21. Jornayvaz FR, Shulman GI. Regulation of mitochondrial biogenesis. Brown GC, Murphy MP, editors. *Essays Biochem*. 2010 Jun 14;47:69–84.
22. Wolfrum C, Stoffel M. Coactivation of Foxa2 through Pgc-1 β promotes liver fatty acid oxidation and triglyceride/VLDL secretion. *Cell Metab*. 2006 Feb 1;3(2):99–110.
23. Salazar G, Cullen A, Huang J, Zhao Y, Serino A, Hilenski L, et al. SQSTM1/p62 and PPARGC1A/PGC-1 α at the interface of autophagy and vascular senescence. *Autophagy*. 16(6):1092–110.
24. Vainshtein A, Tryon LD, Pauly M, Hood DA. Role of PGC-1 α during acute exercise-induced autophagy and mitophagy in skeletal muscle. *Am J Physiol-Cell Physiol*. 2015 Feb 11;308(9):C710–9.

25. Kubli DA, Gustafsson ÅB. Mitochondria and Mitophagy: The Yin and Yang of Cell Death Control. *Circ Res.* 2012 Oct 12;111(9):1208–21.
26. Vega RB, Huss JM, Kelly DP. The Coactivator PGC-1 Cooperates with Peroxisome Proliferator-Activated Receptor α in Transcriptional Control of Nuclear Genes Encoding Mitochondrial Fatty Acid Oxidation Enzymes. *Mol Cell Biol.* 2000 Mar;20(5):1868–76.
27. Gottlieb RA, Bernstein D. Mitochondrial Remodeling: Rearranging, Recycling, and Reprogramming. *Cell Calcium.* 2016 Aug;60(2):88–101.
28. Bengsch B, Johnson AL, Kurachi M, Odorizzi PM, Pauken KE, Attanasio J, et al. Bioenergetic Insufficiencies Due to Metabolic Alterations Regulated by the Inhibitory Receptor PD-1 Are an Early Driver of CD8⁺ T Cell Exhaustion. *Immunity.* 2016 Aug 16;45(2):358–73.
29. Sopariwala DH, Yadav V, Badin P-M, Likhite N, Sheth M, Lorca S, et al. Long-term PGC1 β overexpression leads to apoptosis, autophagy and muscle wasting. *Sci Rep.* 2017 Aug 31;7(1):10237.
30. Hardie DG. AMP-activated/SNF1 protein kinases: conserved guardians of cellular energy. *Nat Rev Mol Cell Biol.* 2007 Oct;8(10):774–85.
31. Schmid D, Pypaert M, Münz C. MHC class II antigen loading compartments continuously receive input from autophagosomes. *Immunity.* 2007 Jan;26(1):79–92.
32. Ryans K, Omosun Y, McKeithen DN, Simoneaux T, Mills CC, Bowen N, et al. The immunoregulatory role of alpha enolase in dendritic cell function during Chlamydia infection. *BMC Immunol.* 2017 May 19;18(1):27.
33. Elesela S, Morris SB, Narayanan S, Kumar S, Lombard DB, Lukacs NW. Sirtuin 1 regulates mitochondrial function and immune homeostasis in respiratory syncytial virus infected dendritic cells. *PLOS Pathog.* 2020 Feb 27;16(2):e1008319.

CHAPTER 4 – Characterization of conventional dendritic cell subsets at homeostasis and in high fat-diet induced obesity

Abstract

The conventional dendritic cell (cDC) subsets *in vivo*, which include cDC1, cDC2A, and cDC2B, have shared and distinct immune functions and metabolic profiles in lymphoid tissues. How these profiles compare in other tissues is not well-studied. Here, we characterize and compare the proportions and activation as well as the mitochondrial and lipid content of cDC subsets in several tissues and how these metabolic features are altered by a high fat diet (HFD) challenge. We found that the frequencies of all cDC subsets in white adipose tissue are elevated during HFD-induced obesity, and that cDC2A and cDC2B increase to a proportionally greater extent than do cDC1. In addition, mitochondrial mass drops considerably, while intracellular lipid content increases in all adipose tissue-associated cDCs. The differences in metabolic features of cDC subsets across tissues at steady state and HFD-induced obesity indicate that they are regulated, in part, by their environment. Weight loss after discontinuation of HFD feeding does not completely restore the levels of mitochondrial mass, suggesting that some metabolic damage due to HFD-induced obesity persists in cDCs.

Introduction

Dendritic cells (DCs) are innate immune cells that possess an exceptional capacity for responding to changes in their environment. DCs comprise conventional DCs (cDCs) and plasmacytoid DCs (pDCs). cDCs, the primary focus of our study, are known for their superior antigen presenting abilities, while pDCs are characterized by their capacity to produce mass quantities of type I interferons during antiviral immunity (1). cDC can be further divided into subsets referred to as cDC1 and cDC2, defined by the expression of the transcription factors interferon regulatory factor 8 (IRF8) and IRF4, respectively (1,2). cDC2s can be further divided into cDC2A and cDC2B subsets, based on mutually exclusive expression of the transcription factors TBET and ROR γ t, respectively (3,4). They possess differing inflammatory properties in lymphoid tissues, with cDC2A being considered more anti-inflammatory and cDC2B more stimulatory (3). cDCs originate from hematopoietic stem cells in the bone marrow, which develop into pre-cDCs before exiting and seeding tissues throughout the body, where they mature into cDCs. While there is evidence that pre-cDCs have pre-determined fates to develop into cDC1 or cDC2 (5), the study by Brown *et al.* suggests that further differentiation into cDC2A and cDC2B subsets are directed by cues from the microenvironment of the tissues that the pre-cDCs seed (3).

The cDC subsets share several functions, including sensing of foreign material, migration to the lymph node, and stimulation of T cells. However, these subsets are also distinct from each other based on the range of materials they are stimulated by and the T cell subsets they preferentially activate. cDC1s are superior at cross-presenting antigen, and they therefore play an important role in immune responses involving CD8⁺ T cell responses, such as responses against tumors and intracellular pathogens (6). cDC2s are more involved in antigen presentation on

MHC class II to CD4⁺ T cells, inducing, for example, T helper 2 (Th2) differentiation during an allergic response, or Th17 during autoimmune disease (7,8). Further, cDC subsets are precisely positioned within the lymph node to favor interactions with specific T cell subsets; cDC1 and cDC2 primarily interact with CD8⁺ and CD4⁺ T cells, respectively, although cDC1 can activate CD4⁺ T cells as well during a type 1 response (9). cDC subsets also exhibit different metabolic phenotypes that have been shown to be important for their distinct functions; splenic cDC1 possess more mitochondria and exhibit greater oxidative metabolism than cDC2 (10).

Transcriptional signatures reveal that cDC2A are enriched for pathways related to glucose metabolism, while cDC2B are characterized by pathways related to lipid metabolism, although the functional effects of these signatures were not examined (3). Currently, there are few studies comparing the metabolic differences between cDC subsets outside of the spleen.

The immune cell composition of adipose tissue differs between lean and obese conditions. During high-fat diet-induced obesity, the number of immune cells in the adipose tissue increases and shifts in the proportions of regulatory immune cells such as Treg cells and M2-like macrophages, to more inflammatory cells such as neutrophils, Th1 and Th17 cells, and M1-like macrophages, with macrophages being the most abundant immune cell type (11). While the role of macrophages in obesity is well-established, the importance of adipose tissue-associated DCs in homeostasis or inflammation is only beginning to be understood. One study demonstrates that the accumulation of DCs in adipose tissue during high-fat diet (HFD) challenge significantly contributes to inflammation and insulin resistance (12). In mice, CD11c⁺ cells found in adipose tissue of HFD-fed mice promotes Th17 differentiation *in vitro* (13). In humans with obesity, a positive correlation has been established between body mass index and Th17 cell frequency (14). DCs also play an important role in maintaining immune homeostasis

of visceral adipose tissue, with the cDC1s and cDC2s suppressing inflammation via the Wnt/ β -catenin and PPAR- γ pathways, respectively (15). Impairment of these pathways exacerbates inflammation promoted by diet-induced obesity (15). Despite these recent advances in knowledge, not all studies on adipose tissue-associated DCs adequately discern cDCs from macrophages, as markers defining their distinct lineages have been established relatively recently (3,16).

In this study, we characterize cDC subsets and their composition, activation, and metabolic properties between several tissues and during a metabolic perturbation by HFD challenge of mice. We show that the differences in metabolic properties such as mitochondrial and lipid content that have been described in cDC subsets of the spleen are not necessarily identical in other tissues, highlighting the importance of tissue environment in influencing the metabolism of cDC subsets. In addition, perturbing the environment with HFD feeding results in an impaired mitochondrial phenotype in all cDC subsets. Removal of the HFD, however, does not completely restore this mitochondrial impairment in cDC2s, suggesting long-term reprogramming is caused by the HFD feeding.

Results

Comparison of metabolic phenotypes of cDC subsets in lymphoid and non-lymphoid tissues

To characterize the differences in mitochondrial phenotype between cDC subsets across select tissues in mice, we examined cDCs in the spleen, inguinal and brachial lymph nodes (LN), and the epididymal white adipose tissue (eWAT) (Fig. S1A). Mitochondrial mass and mitochondrial membrane potential were both measured by staining with mitochondrial dyes and

assessed by flow cytometry. Mitochondrial mass reflects the amount of mitochondria in the cell, while the membrane potential represents the functional state and energy storage of the mitochondria. Splenic cDC have lower mitochondrial mass than cDC in the LN and eWAT (Fig. 1A). Comparing subsets reveals that splenic cDC1 contain more mitochondria than splenic cDC2, but cDC2B are closer to cDC1 in mitochondrial content than cDC2A (Fig. 1A). Similar results are seen with mitochondrial membrane potential of splenic cDC (Fig. 1B). cDC subsets in the LN and eWAT, however, are not significantly different from each other in mitochondrial content (Fig. 1A), although eWAT cDC2B do have higher mitochondrial membrane potential than eWAT cDC1 and cDC2A. (Fig. 1C). Staining of neutral lipids in cDC reveals a similar pattern in splenic cDC as mitochondrial mass, with splenic cDC1 and cDC2B containing more intracellular lipid than cDC2A (Fig. 1D). Both eWAT cDC2A and cDC2B, however, contain more lipid than eWAT cDC1, and LN cDC do not show significant differences in lipid content (Fig. 1D). The difference in lipid content between subsets is not solely due to cell size (Fig. S1B). Together, these data demonstrate that cDC metabolism varies between subsets and tissues, suggesting that the specific tissue environment influences their metabolic phenotype.

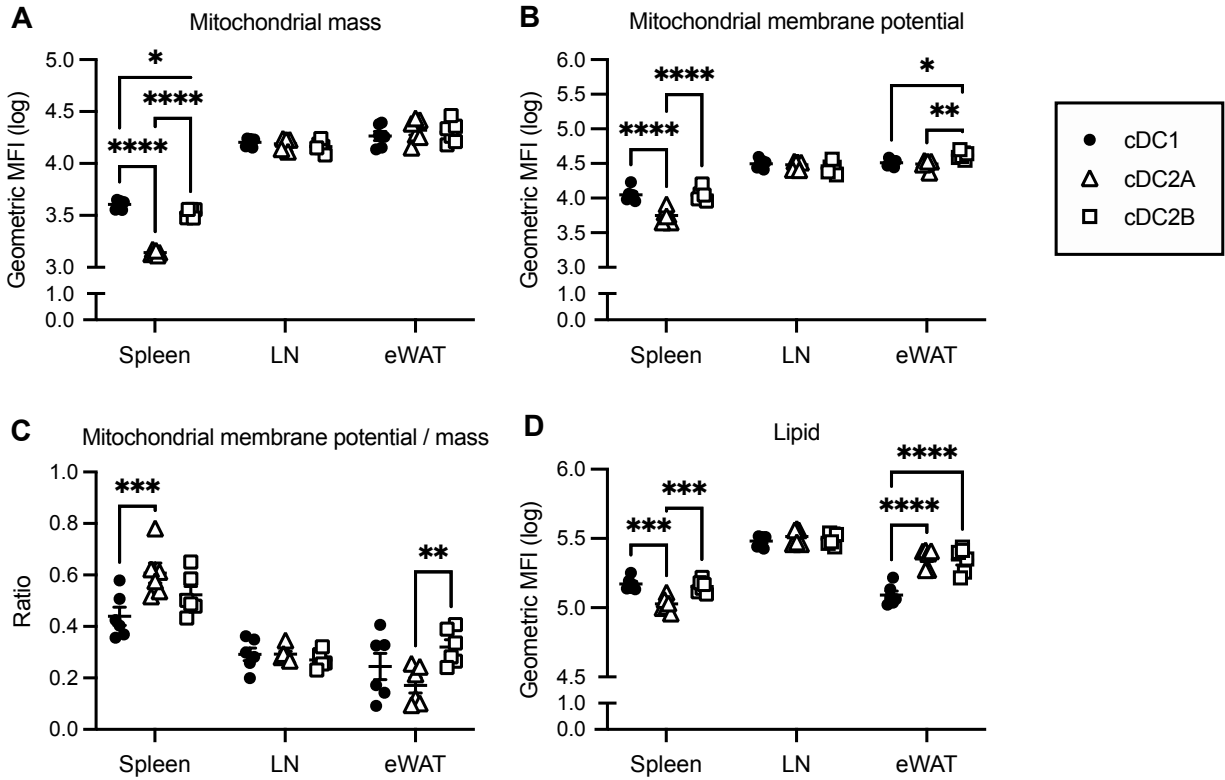


Figure 1 – Comparison of mitochondrial and lipid content in cDC subsets across tissues

cDCs from the spleen, inguinal and brachial lymph nodes (LN), and epididymal white adipose tissue (eWAT) were examined by flow cytometry and represented as geometric mean fluorescence intensity (MFI). (A) Mitochondrial mass by MitoSpy Green staining. (B) Mitochondrial membrane potential by TMRM staining. C) Ratio of TMRM to MitoSpy Green geometric MFI from (A) and (B). (D) Neutral lipids staining by BODIPY. Data are of one experiment representative of three experiments for spleen and eWAT, and two experiments for LN. * $p < 0.05$, ** $p < 0.01$, *** $p < 0.001$, **** $p < 0.0001$

Comparison of metabolic phenotypes of migratory and tissue-resident cDC subsets in the lymph node

To further examine the LN cDC populations, we separated the MHC class II (MHC-II)⁺Lin⁻ cells into migratory and resident cDC based on positive CD11c and MHC II expression, with migratory cDC expressing higher levels of MHC-II and resident cDC expressing

intermediate levels (Fig. S2A) (19). There are no significant differences in MHCII levels between cDC subsets within the same group (Fig. S2B). While there is no significant difference in mitochondrial staining between cDC1 and cDC2 subsets when examining total MHC II⁺CD11c⁺ cells (Fig. 1A), dividing this population into migratory and resident cDC reveals that mitochondrial mass and mitochondrial membrane potential are greater overall in migratory cDC compared to resident cDC (Fig. 2A, B). This result suggests that migratory cDC require greater metabolic activity. Within the migratory cDC subsets, cDC1 have the highest mitochondrial mass compared to both cDC2 subsets. Similar to splenic cDC, lymph node-resident cDC1 and cDC2B have comparable mitochondrial mass levels that are greater than that of cDC2A (Fig. 2A). Mitochondrial membrane potential normalized to mass is higher in cDC2 subsets compared to cDC1 in migratory subsets, while in resident cDCs, this value is higher in cDC1s compared to cDC2B (Fig. 2C).

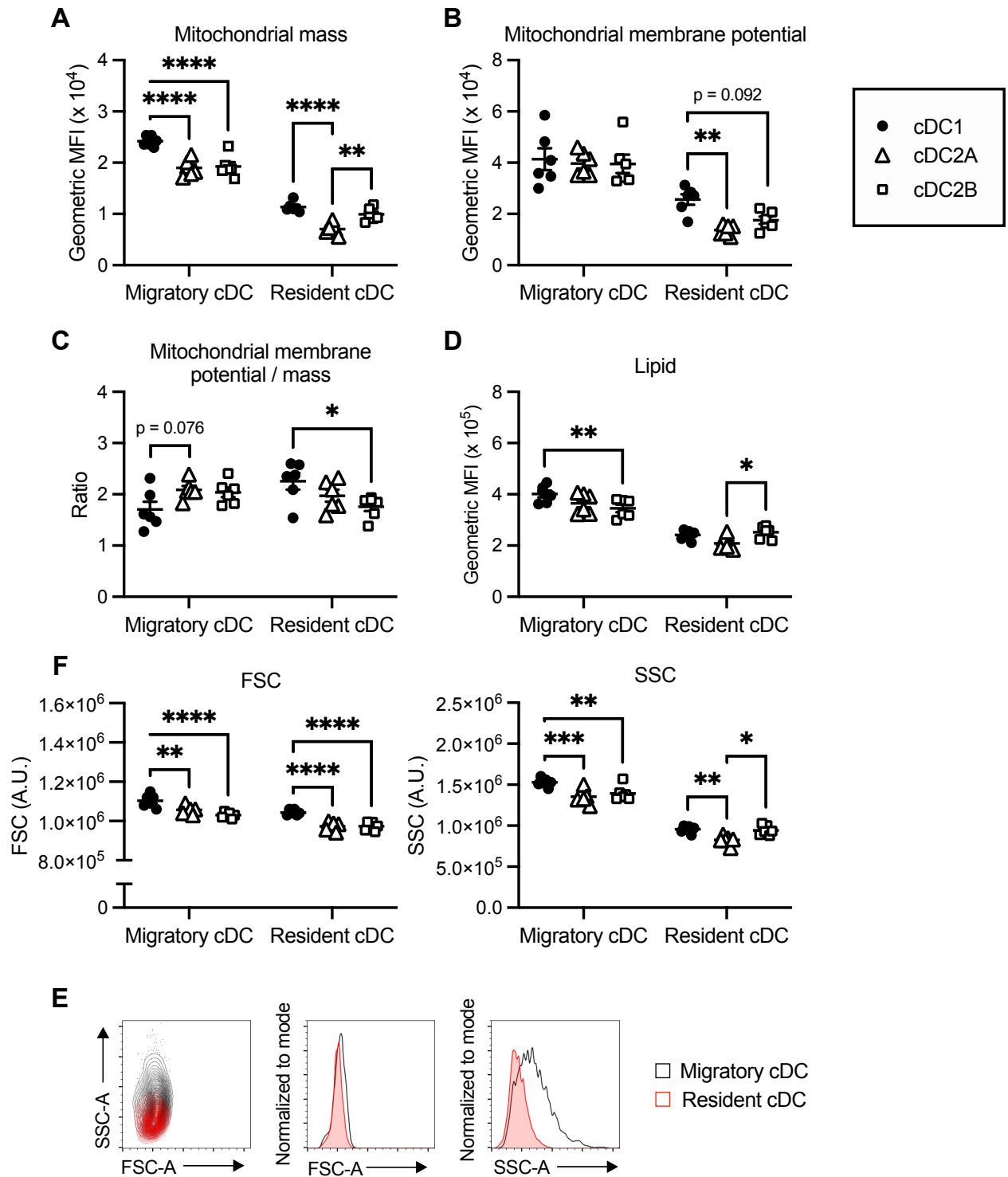
Staining of intracellular neutral lipids shows that migratory cDC have greater lipid content compared to resident cDC (Fig. 2D). Migratory cDC1 have more lipid content than cDC2 subsets, while LN-resident cDC2B have similar lipid levels as cDC1 and slightly more than cDC2A (Fig. 2D).

Since cell size could affect the total mitochondrial and lipid content of each cell, we compared the forward scatter (FSC), which is a measure of cell size, between migratory and resident cDC. The FSC had minimal shifts between the migratory and resident cDC (Fig. 2E). Side scatter (SSC), which is a measure of cellular granularity and internal complexity, was considerably greater in migratory cDC compared to resident cDC (Fig. 2E). Since cellular organelles can affect the SSC (20), this suggests the greater mitochondrial mass in migratory cDC is not an outcome of increased cell size. Comparing FSC between cDC subsets within the

migratory and LN-resident populations shows that cDC1 are larger in cell size than both cDC2A and cDC2B (Fig. 2F). In the migratory population, cDC2A are slightly larger than cDC2B, but they are not significantly different in the LN-resident population (Fig. 2F). In regard to SSC, migratory cDC1 exhibit greater SSC than cDC2A and cDC2B, and resident cDC1 and cDC2B have greater SSC than resident cDC2A (Fig. 2F). In summary, migratory cDC are slightly larger in size and possess considerably more internal complexity than LN-resident cDC. Within these populations, cDC1 are larger than both cDC2 subsets. cDC1 have more internal complexity than both cDC2 subsets in the migratory population and just cDC2A in the LN-resident population.

Changes in cDC proportion and activation over time in high fat diet-fed mice

Since we see that the metabolic phenotypes of cDC subsets are influenced by their tissue environment, we sought to introduce a metabolic perturbation to the mice with high-fat diet (HFD) feeding. To determine how early changes in DC composition and activation occur, we fed mice HFD and examined the cDC in the spleen and eWAT over several timepoints between one and twelve weeks of feeding. The percentage of body fat expands early and steadily increases over time (Fig. 3A). The percentage of cDC1 and cDC2 in the eWAT SVF also increases within one week of HFD feeding (Fig. 3B). In addition, the ratio of cDC2 to cDC1 increases within two weeks of HFD feeding and this ratio starts to decrease and approach control conditions after week 8 (Fig. 3C). MHC II expression, which can shift when cDC are stimulated, is also affected by HFD (Fig. 3D). MHC II expression by both cDC1 and cDC2 is negatively correlated with eWAT mass across all examined weeks (Fig. 3D; cDC1 $p = 0.0245$, cDC2 $p = 0.0304$), suggesting that HFD or the consequent gain of body fat reduces the capacity of DCs to present antigen on MHC II. In the spleen, however, MHC II expression of cDCs is not correlated to eWAT mass (Fig. S3).



(legend on next page)

Figure 2 – Comparison of mitochondrial and lipid content in migratory and lymphoid-resident cDC subsets

Migratory and tissue-resident cDC subsets cDC1, cDC2A, and cDC2B were examined in pooled inguinal and brachial lymph nodes by flow cytometry. (A) Mitochondrial mass by MitoSpy Green staining. (B) Mitochondrial membrane potential by TMRM staining. (C) Ratio of TMRM to MitoSpy Green geometric MFI from A and B. (D) Neutral lipid staining by BODIPY. (E) Representative plot and histograms of overlaid migratory and resident cDC. (F) Forward scatter (FSC) and side scatter (SSC) represented by arbitrary units. Data are of one experiment representative of two experiments. Mean and s.e.m. of six mice per condition. * $p < 0.05$, ** $p < 0.01$, *** $p < 0.001$, **** $p < 0.0001$

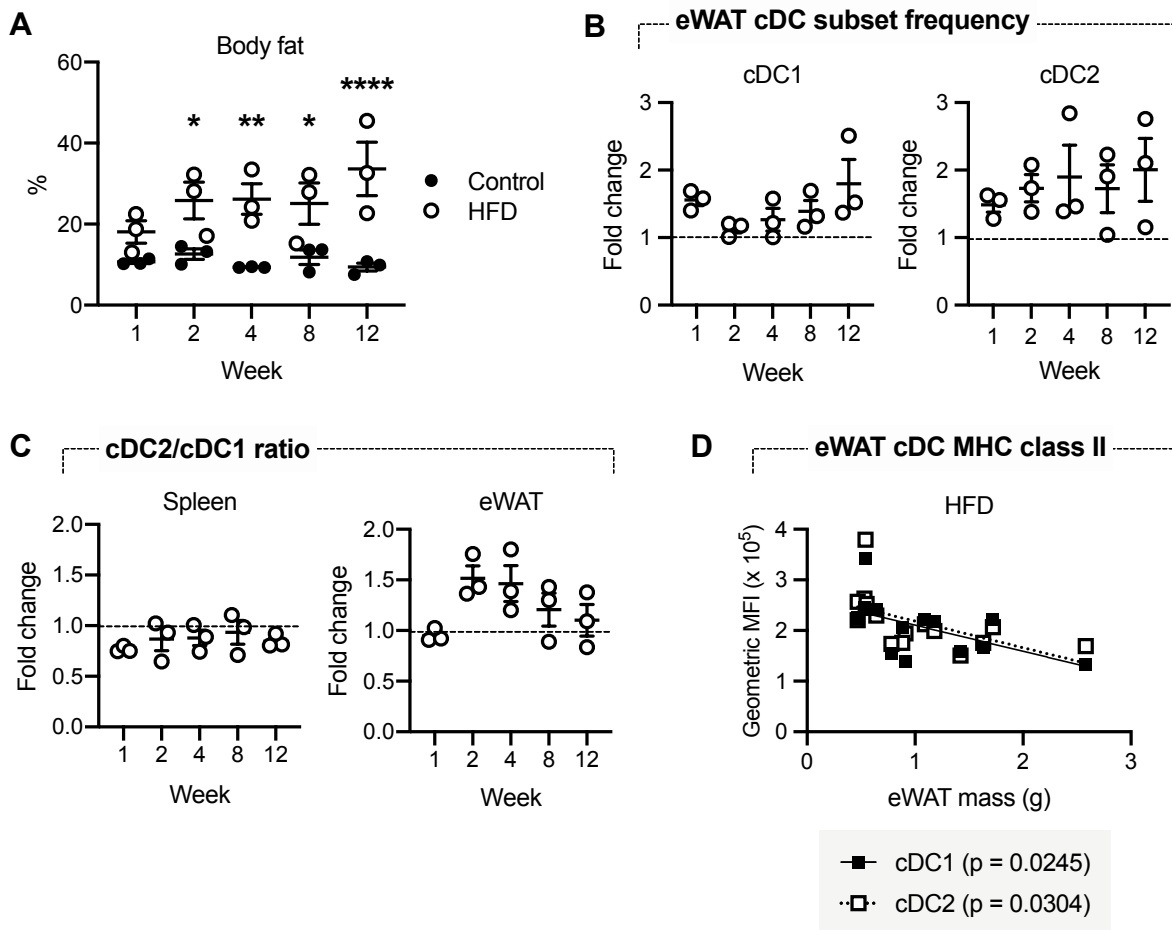


Figure 3 – HFD-induced changes to cDC proportions and activation over time

Mice were fed control diet or HFD and cDCs were examined in the spleen and eWAT at 1, 2, 4, 8, and 12 week(s) of feeding. (A) Percentage of body fat as determined by EchoMRI measurements. (B) Proportion of cDC1 and cDC2 of the stromal vascular fraction (SVF) of the

eWAT in HFD-fed mice relative to control diet-fed mice. **(C)** Ratio of cDC2 to cDC1 frequency of eWAT SVF in HFD-fed mice relative to control diet-fed mice. **(D)** Simple linear regression of expression of MHC class II by cDC1 and cDC2 of eWAT versus eWAT mass for mice fed HFD across all weeks, with significance for each subset expressed by p value. Data are of one experiment. Mean and s.e.m. of three mice per condition. * $p < 0.05$, ** $p < 0.01$, *** $p < 0.001$, **** $p < 0.0001$

Changes in cDC proportion, activation, and metabolic phenotype in high fat diet-fed mice

Next, we investigated the changes in mitochondrial and lipid content in cDC subsets that are caused by HFD feeding by examining cDCs from mice fed either control diet or HFD for six weeks. This is a relatively short feeding period where weight gain occurs without extensive pathologies of organs (21). After six weeks, mice fed HFD gained approximately four-fold more body fat percentage over control mice and did not significantly increase their lean mass (Fig. 4A). The mass of eWAT and the cell count of the isolated stromal vascular fraction (SVF) was similarly increased in the HFD-fed mice (Fig. 4B-C, S4A-B). The frequency of all cDC subsets also increased with HFD feeding (Fig. 4D), with the proportion of both cDC2A and cDC2B increasing to a greater extent than cDC1 (Fig. 4E). In the spleen, the total cellularity does not change based on diet, although there is a small but significant increase in frequency of cDC1 and decrease in cDC2A to cDC1 ratio (Fig. 4F-H, S4D). Also notable is that at steady state, the frequency of each cDC subset differs when comparing cDCs of the adipose tissue and those of lymphoid tissue, with cDC2B have the greatest frequency in adipose tissue but lowest in the spleen (Fig. 4D,G). Mitochondrial staining reveals drastically diminished mitochondrial mass and mitochondrial membrane potential in cDC found in the eWAT of HFD-fed mice (Fig. 4I-K). The intracellular lipid content of these cells is also greatly elevated (Fig. 4L). Building on the results from Fig. 3, here MHC II expression after a six-week HFD challenge is confirmed to be decreased for all eWAT cDC subsets (Fig. S4C). Splenic cDC, however, do not have

significantly different mitochondrial mass, membrane potential, or lipid content, except for a small decrease in cDC2B mitochondrial mass in HFD-fed mice (Fig. S4E-H). Overall, this data demonstrates that after six weeks of HFD feeding, eWAT cDC have greatly reduced mitochondria mass, while splenic cDC have minimal changes.

Mitochondrial changes in cDC subsets after weight loss following HFD challenge

We next examined whether changes in mitochondrial metabolic phenotype and proportions of cDCs in response to HFD persist once mice are no longer on HFD. We fed mice with either a control diet or HFD for eight weeks, then placed all mice on the control diet for an additional eight weeks (Fig. 5A). The body fat percentage of the mice that had been on HFD decreased once the HFD was removed but plateaued after four weeks (Fig. 5A). While the cell count of isolated SVF from the eWAT of the fatter mice is still greater than that of control mice, the percentage of cDC subsets returns to levels of the control mice that were never fed HFD (Fig. 5B-D). The ratio of cDC2 to cDC1 is no longer greater in the fatter mice; in fact, the ratio of cDC2A to cDC1 is reduced, while cDC2B to cDC1 is no longer significantly different from the control mice (Fig. 5E). There were no changes in the frequency of cDC subsets in the spleen as well (Fig. S5A,B). Despite the proportions of eWAT cDC subsets returning to control values, the mitochondria of the cDC2 subsets continue to exhibit an impaired phenotype (Fig. 5F-H). While the mitochondrial mass and membrane potential of eWAT cDC1 are now equivalent in both diet conditions, these measurements are reduced in both cDC2A and cDC2B from mice formerly fed HFD (Fig. 5D). In the spleen of these mice, the mitochondrial mass is also lower in the cDC2 subsets compared to the control condition, while the mitochondrial membrane potential is largely unchanged (Fig. 5I-K). We examined whether this reduced mitochondrial mass is due to the higher body fat percentage of the mice that were formerly fed HFD, and there is no correlation

(Fig. S5C). These data suggest that cDC2, unlike cDC1, do not recover from the mitochondrial impairment resulting from HFD feeding within eight weeks of weight loss.

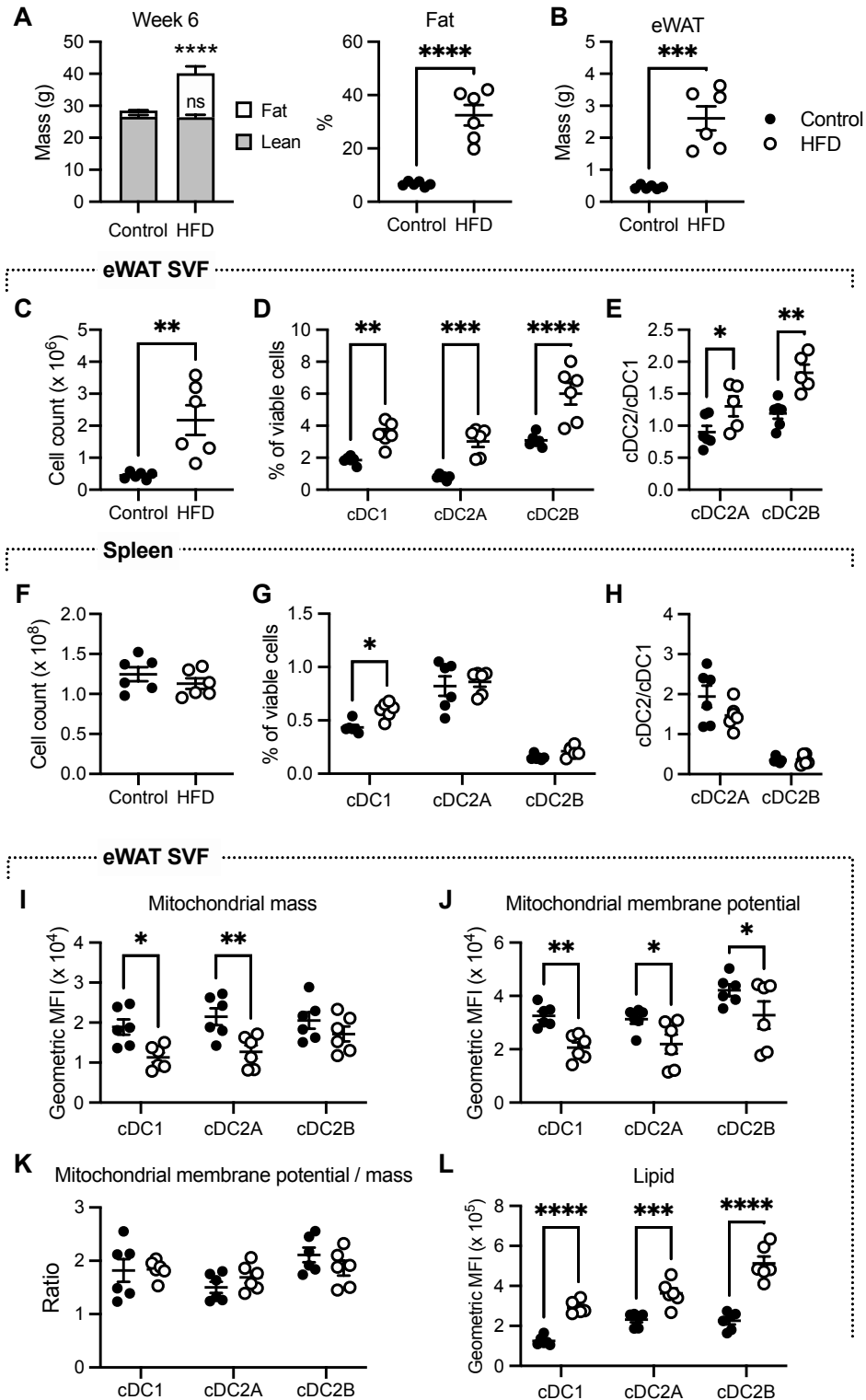


Figure 4 – HFD-induced changes to mitochondrial and lipid content in cDC subsets of the spleen and adipose tissue

Mice were fed control diet or HFD for six weeks and cDC1, cDC2A, and cDC2B were examined in spleen and eWAT by flow cytometry. **(A)** Fat and lean mass at six weeks of feeding as measured by EchoMRI. **(B)** eWAT mass. **(C)** Cell count of viable SVF isolated from eWAT. **(D)** Percentage of each cDC subset of viable SVF. **(E)** Ratio of the frequency of cDC2A or cDC2B from D to cDC1. **(F)** Viable splenocyte cell count. **(G)** Percentage of each cDC subset of viable splenocytes. **(H)** Ratio of the frequency of cDC2A or cDC2B from G to cDC1. **(I)** Mitochondrial mass by MitoSpy Green staining. **(J)** Mitochondrial membrane potential by TMRM staining. **(K)** Ratio of TMRM to MitoSpy Green geometric MFI from **(I)** and **(J)**. **(L)** Lipid content by BODIPY staining. Data are of one experiment representative of **(A-J, L)** three experiments or **(K)** one experiment. Mean and s.e.m. of six mice per condition. * $p < 0.05$, ** $p < 0.01$, *** $p < 0.001$, **** $p < 0.0001$

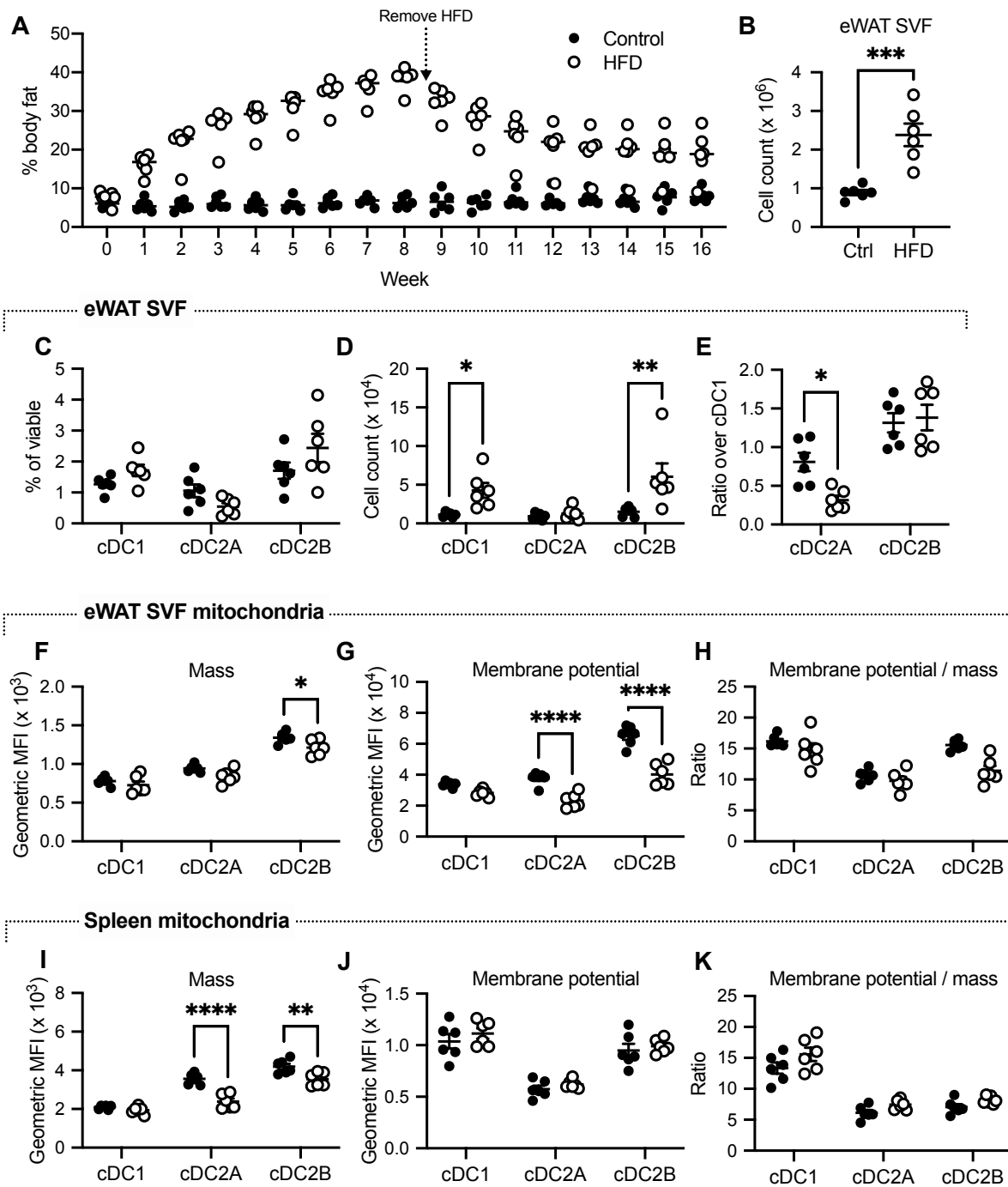


Figure 5 – Mitochondrial changes in cDC subsets of the spleen and adipose tissue after weight loss following HFD challenge

Mice were fed control diet or HFD for eight weeks and all mice were fed control diet for an additional eight weeks. (A) Percentage of body fat over time as measured by EchoMRI. (B) Cell count of viable SVF isolated from eWAT. (C) Percentage and (D) cell count of each cDC subset

of viable eWAT SVF. **(E)** Ratio of the frequency of cDC2A or cDC2B of eWAT SVF to cDC1. Of eWAT SVF, **(F)** mitochondrial mass by MitoSpy Green staining, **(G)** mitochondrial membrane potential by TMRM staining, and **(H)** ratio of TMRM to MitoSpy Green geometric MFI from **(F)** and **(G)**. Of splenocytes, **(I)** mitochondrial mass by MitoSpy Green staining, **(J)** mitochondrial membrane potential by TMRM staining, and **(K)** ratio of TMRM to MitoSpy Green geometric MFI from **(I)** and **(J)**. Data are of one experiment. Mean and s.e.m. of six mice per condition. * $p < 0.05$, ** $p < 0.01$, *** $p < 0.001$, **** $p < 0.0001$

Discussion

The recently described roles of DCs in both maintaining visceral adipose tissue homeostasis and promoting inflammation establish their significance in diet-induced obesity and the associated pathophysiology (12,15). In this study, we have characterized the differences in mitochondrial and lipid content in cDC subsets across tissues and upon metabolic perturbation with HFD challenge. HFD-induced changes include increased numbers of all cDC subsets, with proportionally greater expansion of cDC2s, decrease in mitochondrial content, and increase in lipid content. We have also found that weight loss after HFD challenge does not completely restore this decrease in mitochondria in cDCs.

Due to several surface markers overlapping between cDCs and macrophages, such as CD11c, MHC II, and CD11b, many studies on adipose tissue-associated cDCs have likely included macrophages in their analysis. We therefore used analysis to more reliably distinguish cDC1, cDC2A, and cDC2B across different tissues while excluding macrophages (3,16). We have confirmed that splenic cDC1s contain more mitochondria than splenic cDC2s (10), and have further characterized the cDC2A and cDC2B subsets. While cDC2s on average have less mitochondria, cDC2B are closer in mitochondrial content to cDC1 and have more mitochondria than cDC2A. In the LN, tissue-resident cDCs exhibit the same pattern of mitochondrial content between subsets, while in migratory cDCs, there are no significant differences between cDC2A

and cDC2B. Overall, migratory cDCs in the LN have greater mitochondrial mass and intracellular lipids, likely to fulfil the high bioenergetic demand and coordination required by cellular migration (22).

Unlike lymphoid-resident cDCs, eWAT cDCs lack significant differences in mitochondrial mass between subsets. However, both eWAT cDC2 subsets have more lipid content than cDC1s, which is not attributed to cell size (Fig. S1C). These results are also in contrast to the patterns seen in lymphoid tissue-resident cDCs, where cDC2 subsets have either comparable or lower lipid content than cDC1s. The metabolic contribution to immune function of the cDC2A and cDC2B subsets has not been examined in great detail, although the established link between mitochondrial function and functions of splenic cDC1s and cDC2s (10) suggests there is a likely role. Thus, the differing pattern of mitochondrial and lipid content of cDC2A and cDC2B between tissues raises the question of how much the subsets differ in function in the eWAT, and remains to be examined.

We observed that intracellular lipid content is higher in cDC1 and cDC2B of lymphoid tissues compared to cDC2A. Lipid bodies in splenic cDC1 have been reported to serve as scaffolds for antigen cross-presentation machinery (23). Although cDC1s are the predominant subset that cross-presents, inflammatory cDC2s have also been shown to present antigen to both CD4⁺ and CD8⁺ T cells during respiratory virus infection (24). In the liver, two distinct populations of DCs were identified based on intracellular lipid levels and the population with higher lipid content was found to have greater immunogenicity, displaying enhanced cytokine production and T cell activation (25). Their pro-inflammatory functions were directly related to their lipid levels, as inhibiting fatty acid synthesis impaired these functions as well (25). This characteristic is in line with splenic cDC2B being reported as having greater pro-inflammatory

characteristics compared to cDC2A (3). In regards to their metabolism, lipids can serve as a fuel source used by the relatively high abundance of mitochondria in cDC2B, generating energy and metabolic intermediates required for their functions. Whether the increased lipids serve solely as metabolic support or to mediate their inflammatory function in other ways remains to be determined.

With HFD challenge, the lipid content of all cDC subsets in the eWAT increase substantially, likely through uptake and storage of the excess free fatty acids in the tissue microenvironment. During HFD challenge, expanding adipose tissue mass contributes to inflammation by releasing increased levels of free fatty acids as well as pro-inflammatory cytokines such as TNF- α and IL-1 β (26). Typically, polyunsaturated fatty acids (PUFAs) have anti-inflammatory effects, while saturated fatty acids (SFAs) are pro-inflammatory (27). Accordingly, PUFAs have been shown to lead to decreased expression of MHC II and co-stimulatory molecules in bone marrow-derived DCs, while SFAs like lauric acid upregulate co-stimulatory marker expression in monocyte-derived DCs (27–29).

Our results show that MHC II expression is consistently reduced in cDCs with HFD challenge. After removal of HFD challenge, MHC II expression for eWAT cDC2s largely returns to control levels. Since MHC II expression is also correlated with eWAT mass, together these results suggest that MHC II suppression may be due to the elevated FFAs from HFD-induced expansion of adipose tissue mass. However, this conflicts with findings that adipose tissue-associated DCs have increased MHC II expression after HFD feeding, although the HFD in this particular study was administered for considerably longer (up to 20 weeks), which could account for a different inflammatory profile as a result of extensive metabolic pathologies (12). With a long HFD challenge, the increased MHC II expression may be due to the enhanced

inflammatory signals resulting from chronic inflammation. Another study shows that adipocytes themselves increase MHC II expression within two weeks of HFD feeding, activating adipose tissue-resident T cells (30). MHC II expression in macrophages was not affected within this time frame and DCs were not examined. In intestinal stem cells, however, HFD suppresses MHC II expression by perturbing PRR and IFN- γ signaling, which are pathways that promote MHC II expression (31). Thus, the effects of HFD on MHC II expression may be cell-specific and dependent on the length of the HFD challenge. The suppressive effects of PUFAs on MHC II expression may also play a role. In addition, fatty acid synthesis has been shown to be essential for DC maturation, and blocking this process reduces MHC II expression (32). Therefore, the effects of HFD on MHC II expression may be due to overloading of the DCs with fatty acids released from diet-induced adipose tissue expansion and the consequent inhibition of fatty acid synthesis. However, the exact mechanism regulating HFD-induced suppression of MHC II expression remains to be determined.

We have found that six weeks of HFD challenge also results in the reduction of mitochondrial mass and membrane potential in all eWAT cDC subsets. Mitochondrial dysfunction due to over-nutrition is commonly observed in several tissues, including skeletal muscle, liver, and central nervous system (33–35), although this has not been previously examined in DCs. Multiple factors have been implicated in mitochondrial dysfunction due to over-nutrition, both as drivers and as consequences of diet-induced metabolic perturbations. In skeletal muscle of diabetic mice, increased oxidative stress and ROS production results in reduced mitochondrial biogenesis and function (36). Treatment of these mice with antioxidants helps restore mitochondrial integrity (36). In the central nervous system, chronic HFD consumption leads to oxidative stress as well, with myelin-producing oligodendrocytes being

particularly susceptible (35,37). Some studies show that insulin signaling in cardiomyocytes promotes mitochondrial fusion and oxidative metabolism, and that defective insulin signaling due to insulin resistance leads to diabetic cardiomyopathy (38,39). These studies suggest that mitochondrial dysfunction is a result of other metabolic perturbations of chronic HFD feeding, including oxidative stress or insulin resistance.

However, development of diabetes in mice typically requires multiple weeks of HFD feeding (21,40), and the reduction of OXPHOS-related genes in skeletal muscle takes place as early as three days of feeding (41), suggesting that mitochondrial dysfunction can arise before insulin resistance is established. In line with these findings, overloading of mitochondria with lipids occurs due to diet-induced obesity and leads to insulin resistance in skeletal muscle (33). Mitochondrial stress results from excessive but incomplete FAO activity and consequent toxic accumulation of partially degraded fatty acids (33). Further, mice lacking malonyl-CoA decarboxylase, an enzyme that promotes FAO, resist diet-induced glucose intolerance, indicating that the elevated FAO helps drive obesity-related insulin resistance (33). Treatment of HFD-fed mice with resveratrol, a polyphenol found in grape skin, increases mitochondrial biogenesis and function (42). Despite comparable body weight, these mice exhibit improved insulin sensitivity and general health (42). Together, these studies indicate multiple mechanisms are involved in inducing mitochondrial dysfunction caused by HFD feeding, both preceding and following pathological changes. Although we did not measure insulin resistance in our study, six weeks of HFD feeding (Fig. 4) is typically considered shorter than chronic feeding (> 8 weeks) and before insulin resistance is established (21,40). Therefore, at six weeks of HFD feeding, lipid toxicity is the more likely mechanism by which mitochondrial dysfunction in DCs occurs rather than

insulin insensitivity. However, further study is required to determine the exact mechanisms by which HFD feeding induces mitochondrial dysfunction in DCs.

After changing to a control diet following eight weeks of HFD challenge, mitochondrial content of eWAT cDC1s during HFD feeding returns to control levels, while mitochondria of eWAT cDC2A and cDC2B remain impaired. This observation coupled with our finding that cDC2 subsets expand to a greater extent than cDC1s do suggests that cDC2s are more sensitive to the effects of HFD-induced obesity. Macrophages in adipose tissue of mice that undergo weight loss after 12 weeks of HFD feeding retain a pro-inflammatory profile (43), which is in line with our findings that the phenotype of adipose tissue-associated DCs is not restored despite weight loss.

In all, to further our understanding about these cells, we have characterized metabolic differences between cDCs of different tissues, demonstrating that these features are influenced by their microenvironment. Our results also provide further insight into some of the metabolic changes cDCs undergo during a diet-related metabolic perturbation.

Experimental procedures

Mice

C57BL/6 were bred and maintained at the Van Andel Research Institute in a specific pathogen-free environment. At 8 weeks of age, mice were placed on a control diet (13% fat; rodent diet 5010) or a rodent diet containing 60 % fat (D12492; Research Diets, Inc.) for the indicated length of time. Lean and fat mass of mice were measured weekly using an EchoMRI instrument. Male mice were used in all experiments except for the experiment in Fig. 3 in which female mice were used. All animal studies were carried out in compliance with Animal Use

Protocol 18-09-026 approved by the Van Andel Research Institute's Institutional Animal Care and Use Committee.

Spleen and lymph node digestion

Spleens were injected with digestion buffer, which is HBSS with Ca^{2+} and Mg^{2+} containing 1 mg/mL collagenase D (Roche) and 10 $\mu\text{g}/\text{mL}$ DNase I (Roche), and incubated for 20 minutes at 37°C. The spleens were then mashed and incubated for an additional 20 minutes at 37°C. The digested spleen suspension was filtered through a 70 μm cell strainer, followed by red blood cell lysis for 2 minutes, and cell resuspension in wash buffer (PBS with 1% FBS, 1 mM EDTA, 0.05% sodium azide). LNs were placed in digestion buffer and cut up with dissection scissors, followed by shaking at 200 rpm for a 30-minute incubation at 37°C. The digested LN suspension was filtered through a 70 μm cell strainer, and resuspended in wash buffer. Viable cells in the single cell suspension were counted using an Accuri flow cytometer (BD Biosciences) and excluding 7-AAD⁺ cells.

Isolation of the stromal vascular fraction of eWAT

Digestion of epididymal white adipose tissue (eWAT) is adapted from previously established protocols (17,18). Digestion buffer containing 3% BSA, 1.2 mM CaCl_2 , 1.0 mM MgCl_2 , 0.8 mM ZnCl_2 , and 0.8 mg/mL collagenase II (Worthington Biochemical) in HBSS was used to digest adipose tissue, using 10 mL of digestion buffer if less than 0.8 g of adipose tissue or 20 mL of digestion buffer if more. Adipose tissue was minced and transferred to digestion buffer and incubated at 37°C with 200 rpm agitation, vortexing tubes every 10 minutes until tissue chunks were no longer present. Samples were spun at 300 x g for 10 minutes, supernatant (containing adipocytes) discarded, and cell pellet washed with RPMI-1640 containing 10% FBS.

The cell suspension was transferred to a 70 μ m cell strainer, then centrifuged at 300 x g for 5 minutes, followed by RBC lysis for 2 minutes, and quenching the reaction with RPMI containing 10% FBS. This cell suspension was transferred to a 40 μ m cell strainer, centrifuged again at 300 x g for 5 minutes, and resuspended in wash buffer for cell counting and staining for flow cytometry.

Flow cytometry

For mitochondrial or lipid dyes, cells were stained with 25 nM MitoSpy Green (BioLegend), 25 nM TMRM (ThermoFisher Scientific), or 250 nM BODIPY 493/503 (ThermoFisher Scientific) in HBSS for 20 minutes at 37°C. Cells were then washed and stained with eFluor 506 fixable viability dye in PBS and blocked with Fc block (anti-CD16/CD32; ThermoFisher Scientific), followed by staining for surface molecules using antibodies against CD11c (N418), MHC II (M5/144.15.2), PD-L1 (10F.9G2), F4/80 (BM8), CD64 (X54-5/7.1), XCR1 (ZET), CD172a (P84), CLEC12A (5D3/CLEC12A), and markers for “lineage” (Lin) CD3 (17A2), CD19 (1D3), B220 (RA3-6B2), Ly6G (IAB-Ly6G), and NK1.1 (PK136) (purchased from BioLegend or ThermoFisher Scientific). After staining, cells were washed and fixed with IC Fixation Buffer (ThermoFisher Scientific) prior to sample acquisition on the Aurora spectral cytometer (Cytex) and data analysis using FlowJo software.

Statistical analysis

Data were analyzed using GraphPad Prism software (version 9). A two-way analysis of variance was performed to determine statistical significance between multiple groups. Differences between conditions were considered significant when *P* values were below 0.05.

Supplementary figures

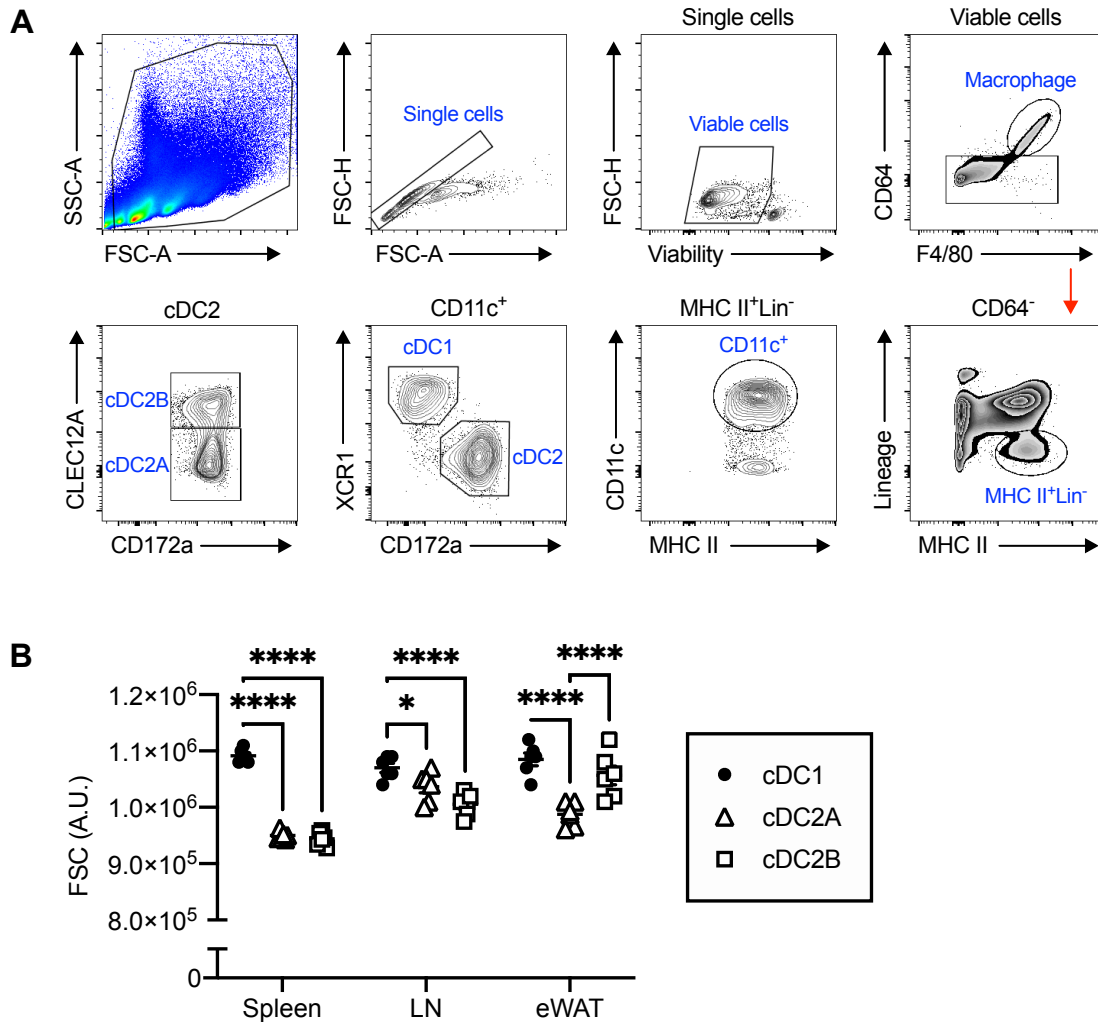


Figure S1

(A) Gating strategy of cDC subsets on a representative spleen sample based on Guilliams *et al* (16). Viable single cells are gated on CD64⁻ cells, and then MHC II⁺Lineage⁻(CD3, CD19, NK1.1, B220, Ly6G)⁻CD11c⁺ cells. cDC1 and cDC2 subsets are defined by XCR1 and CD172a expression, respectively. cDC2 are further divided into CLEC12A⁺ (cDC2B) and CLEC12A⁻ (cDC2A), based on Brown *et al* (3). (B) Cell size as represented by FSC of cDCs from the spleen, inguinal and brachial LNs, and eWAT. Data are of one experiment representative of three experiments. * p < 0.05, ** p < 0.01, *** p < 0.001, **** p < 0.0001

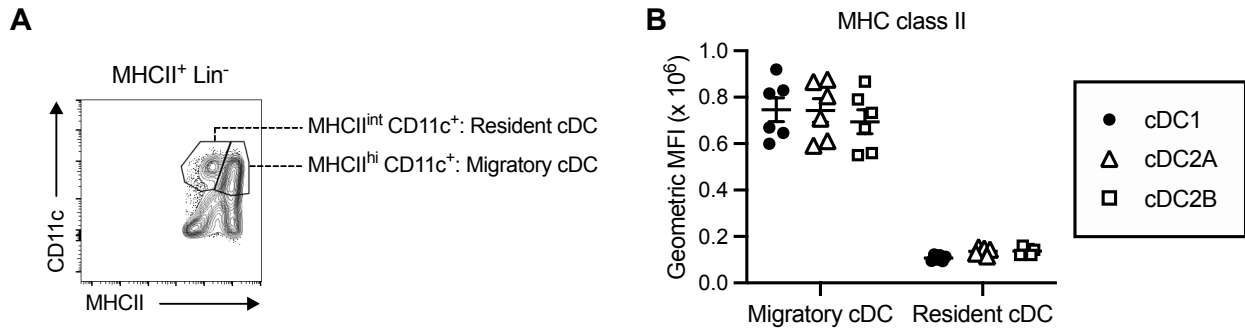


Figure S2

(A) Migratory and resident cDC of the LN are defined by CD11c⁺ and MHC II^{hi} (migratory) and MHC II^{int} (resident) expression (19). (B) MHC II expression of migratory and resident cDC subsets in LNs. Data are of one experiment representative of three experiments. *** p < 0.001, **** p < 0.0001

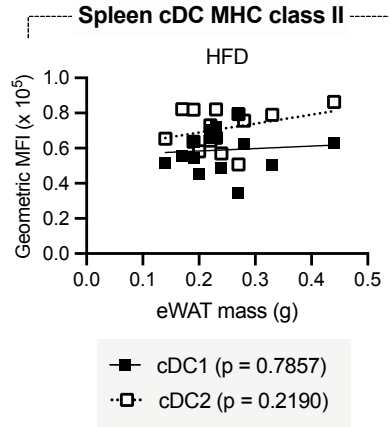


Figure S3

Simple linear regression of expression of MHC class II by cDC1 and cDC2 of spleen versus eWAT mass for mice fed HFD across all weeks, with significance for each subset expressed by p value.

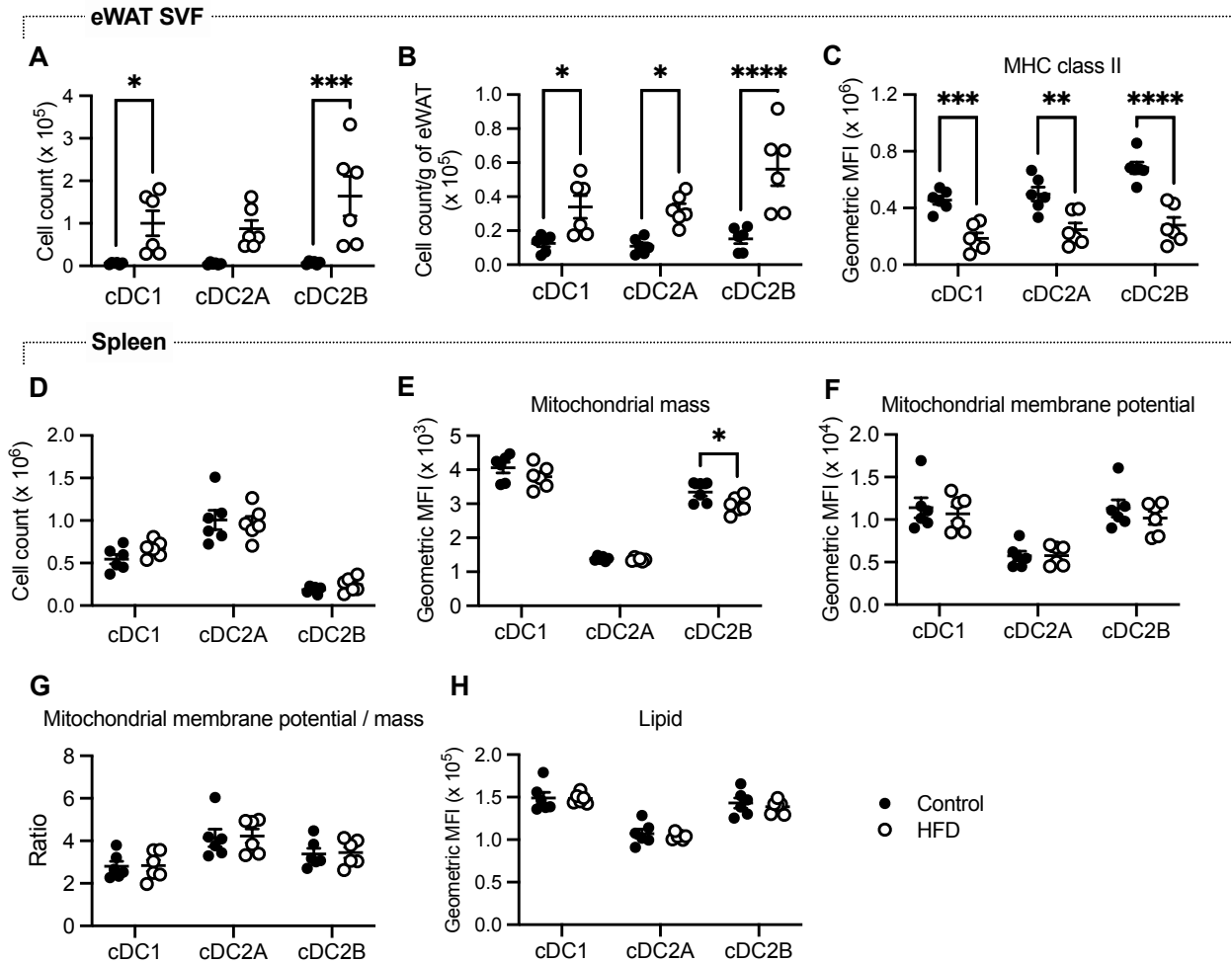


Figure S4

Mice were fed control diet or HFD for six weeks and cDC1, cDC2A, and cDC2B were examined in spleen and eWAT by flow cytometry. In isolated SVF from the eWAT, (A) viable cell count (B) cell count per gram of eWAT, and (C) MHC II expression of each cDC subset were measured. In the spleen, (D) viable cell count, (E) mitochondrial mass by MitoSpy Green staining, (F) mitochondrial membrane potential by TMRM staining, (G) TMRM to MitoSpy Green geometric MFI ratio, and (H) neutral lipids by BODIPY staining were measured. Data are one experiment representative of three experiments. ** $p < 0.01$, *** $p < 0.001$, **** $p < 0.0001$

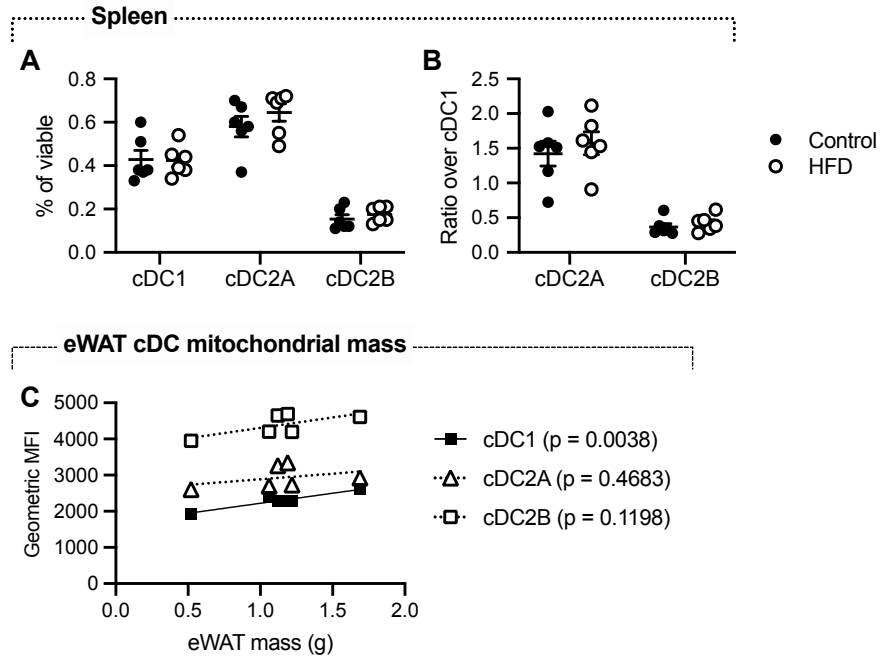


Figure S5

Mice were fed control diet or HFD for eight weeks and all mice were fed control diet for an additional eight weeks. In the spleen, (A) frequency of each cDC subset of viable cells and (B) ratio of cDC2A or cDC2B to cDC1 frequency were determined. (C) Simple linear regression of mitochondrial mass as measured by MitoSpy Green staining of eWAT cDC subsets versus eWAT mass for mice formerly fed HFD. Data are of one experiment.

References

1. Merad M, Sathe P, Helft J, Miller J, Mortha A. The Dendritic Cell Lineage: Ontogeny and Function of Dendritic Cells and Their Subsets in the Steady State and the Inflamed Setting. *Annu Rev Immunol*. 2013 Mar 21;31:563-604.
2. Durai V, Murphy KM. Functions of Murine Dendritic Cells. *Immunity*. 2016 Oct 18;45(4):719–36.
3. Brown CC, Gudjonson H, Pritykin Y, Deep D, Lavallée V-P, Mendoza A, et al. Transcriptional Basis of Mouse and Human Dendritic Cell Heterogeneity. *Cell*. 2019 Oct 31;179(4):846-863.e24.
4. Lewis KL, Caton ML, Bogunovic M, Greter M, Grajkowska LT, Ng D, et al. Notch2 Receptor Signaling Controls Functional Differentiation of Dendritic Cells in the Spleen and Intestine. *Immunity*. 2011 Nov 23;35(5):780–91.
5. Schlitzer A, Sivakamasundari V, Chen J, Sumatoh HRB, Schreuder J, Lum J, et al. Identification of cDC1- and cDC2-committed DC progenitors reveals early lineage priming at the common DC progenitor stage in the bone marrow. *Nat Immunol*. 2015 Jul;16(7):718–28.
6. Dudziak D, Kamphorst AO, Heidkamp GF, Buchholz VR, Trumpheller C, Yamazaki S, et al. Differential Antigen Processing by Dendritic Cell Subsets in Vivo. *Science*. 2007 Jan 5;315(5808):107–11.
7. Plantinga M, Guilliams M, Vanheerswynghels M, Deswarte K, Branco-Madeira F, Toussaint W, et al. Conventional and Monocyte-Derived CD11b+ Dendritic Cells Initiate and Maintain T Helper 2 Cell-Mediated Immunity to House Dust Mite Allergen. *Immunity*. 2013 Feb 21;38(2):322–35.
8. Bailey SL, Schreiner B, McMahon EJ, Miller SD. CNS myeloid DCs presenting endogenous myelin peptides “preferentially” polarize CD4+ TH-17 cells in relapsing EAE. *Nat Immunol*. 2007 Feb;8(2):172–80.
9. Eisenbarth SC. Dendritic cell subsets in T cell programming: location dictates function. *Nat Rev Immunol*. 2019 Feb;19(2):89–103.
10. Du X, Wen J, Wang Y, Karmaus P, Khatamian A, Tan H, et al. Hippo/Mst signaling couples metabolic state and immune function of CD8 α + dendritic cells. *Nature*. 2018 Jun;558(7708):141–5.
11. Ferrante AW. The Immune Cells in Adipose Tissue. *Diabetes Obes Metab*. 2013 Sep;15(03):34–8.
12. Cho KW, Zamarron BF, Muir LA, Singer K, Porsche CE, DelProposto JB, et al. Adipose Tissue Dendritic Cells are Independent Contributors to Obesity-Induced Inflammation and Insulin Resistance*. *J Immunol Baltim Md 1950*. 2016 Nov 1;197(9):3650–61.

13. Chen Y, Tian J, Tian X, Tang X, Rui K, Tong J, et al. Adipose tissue dendritic cells enhances inflammation by prompting the generation of Th17 cells. *PLoS One*. 2014;9(3):e92450.
14. Bertola A, Ciucci T, Rousseau D, Bourlier V, Duffaut C, Bonnafous S, et al. Identification of Adipose Tissue Dendritic Cells Correlated With Obesity-Associated Insulin-Resistance and Inducing Th17 Responses in Mice and Patients. *Diabetes*. 2012 Sep;61(9):2238–47.
15. Macdougall CE, Wood EG, Loschko J, Scagliotti V, Cassidy FC, Robinson ME, et al. Visceral Adipose Tissue Immune Homeostasis Is Regulated by the Crosstalk between Adipocytes and Dendritic Cell Subsets. *Cell Metab*. 2018 Mar;27(3):588-601.e4.
16. Guillemins M, Dutertre C-A, Scott CL, McGovern N, Sichien D, Chakarov S, et al. Unsupervised High-Dimensional Analysis Aligns Dendritic Cells across Tissues and Species. *Immunity*. 2016 Sep 20;45(3):669–84.
17. Berry R, Rodeheffer MS. Characterization of the adipocyte cellular lineage in vivo. *Nat Cell Biol*. 2013 Mar;15(3):302–8.
18. Camell CD, Günther P, Lee A, Goldberg EL, Spadaro O, Youm Y-H, et al. Aging induces an Nlrp3 inflammasome-dependent expansion of adipose B cells that impairs metabolic homeostasis. *Cell Metab*. 2019 Dec 3;30(6):1024-1039.e6.
19. Ohl L, Mohaupt M, Czeloth N, Hintzen G, Kiafard Z, Zwirner J, et al. CCR7 Governs Skin Dendritic Cell Migration under Inflammatory and Steady-State Conditions. *Immunity*. 2004 Aug 1;21(2):279–88.
20. Marina OC, Sanders CK, Mourant JR. Correlating light scattering with internal cellular structures. *Biomed Opt Express*. 2012 Jan 13;3(2):296–312.
21. Heydemann A. An Overview of Murine High Fat Diet as a Model for Type 2 Diabetes Mellitus. Vol. 2016, *Journal of Diabetes Research*. Hindawi; 2016 Jul 31. p. e2902351.
22. Guak H, Krawczyk CM. Implications of cellular metabolism for immune cell migration. *Immunology*. 2020;161(3):200–8.
23. Bougnères L, Helft J, Tiwari S, Vargas P, Chang BH-J, Chan L, et al. A Role for Lipid Bodies in the Cross-presentation of Phagocytosed Antigens by MHC Class I in Dendritic Cells. *Immunity*. 2009 Aug 21;31(2):232–44.
24. Bosteels C, Neyt K, Vanheerswynghels M, Helden MJ van, Sichien D, Debeuf N, et al. Inflammatory Type 2 cDCs Acquire Features of cDC1s and Macrophages to Orchestrate Immunity to Respiratory Virus Infection. *Immunity*. 2020 Jun 16;52(6):1039-1056.e9.
25. Ibrahim J, Nguyen AH, Rehman A, Ochi A, Jamal M, Graffeo CS, et al. Dendritic Cell Populations with Different Concentrations of Lipid Regulate Tolerance and Immunity in Mouse and Human Liver. *Gastroenterology*. 2012 Oct;143(4):1061.

26. Boden G. Obesity and Free Fatty Acids (FFA). *Endocrinol Metab Clin North Am*. 2008 Sep;37(3):635–ix.
27. Radzikowska U, Rinaldi AO, Çelebi Sözen Z, Karaguzel D, Wojcik M, Cypryk K, et al. The Influence of Dietary Fatty Acids on Immune Responses. *Nutrients*. 2019 Dec 6;11(12).
28. Kong W, Yen J-H, Vassiliou E, Adhikary S, Toscano MG, Ganea D. Docosahexaenoic acid prevents dendritic cell maturation and in vitro and in vivo expression of the IL-12 cytokine family. *Lipids Health Dis*. 2010 Feb 1;9:12.
29. Weatherill AR, Lee JY, Zhao L, Lemay DG, Youn HS, Hwang DH. Saturated and Polyunsaturated Fatty Acids Reciprocally Modulate Dendritic Cell Functions Mediated through TLR4. *J Immunol*. 2005 May 1;174(9):5390–7.
30. Deng T, Lyon CJ, Minze LJ, Lin J, Zou J, Liu JZ, et al. Class II Major Histocompatibility Complex Plays an Essential Role in Obesity-Induced Adipose Inflammation. *Cell Metab*. 2013 Mar 5;17(3):411–22.
31. Beyaz S, Roper J, Bauer-Rowe KE, Xifaras ME, Ergin I, Dohnalova L, et al. Dietary suppression of MHC-II expression in intestinal stem cells enhances intestinal tumorigenesis. *bioRxiv*. 2020 Sep 8;2020.09.05.284174.
32. Rehman A, Hemmert KC, Ochi A, Jamal M, Henning JR, Barilla R, et al. Role of Fatty-acid Synthesis in Dendritic Cell Generation and Function. *J Immunol Baltim Md 1950*. 2013 May 1;190(9):4640–9.
33. Koves TR, Ussher JR, Noland RC, Slentz D, Mosedale M, Ilkayeva O, et al. Mitochondrial Overload and Incomplete Fatty Acid Oxidation Contribute to Skeletal Muscle Insulin Resistance. *Cell Metab*. 2008 Jan 1;7(1):45–56.
34. García-Ruiz I, Solís-Muñoz P, Fernández-Moreira D, Grau M, Colina F, Muñoz-Yagüe T, et al. High-fat diet decreases activity of the oxidative phosphorylation complexes and causes nonalcoholic steatohepatitis in mice. *Dis Model Mech*. 2014 Nov 1;7(11):1287–96.
35. Langley MR, Yoon H, Kim HN, Choi C-I, Simon W, Kleppe L, et al. High fat diet consumption results in mitochondrial dysfunction, oxidative stress, and oligodendrocyte loss in the central nervous system. *Biochim Biophys Acta BBA - Mol Basis Dis*. 2020 Mar 1;1866(3):165630.
36. Bonnard C, Durand A, Peyrol S, Chansemaume E, Chauvin M-A, Morio B, et al. Mitochondrial dysfunction results from oxidative stress in the skeletal muscle of diet-induced insulin-resistant mice. *J Clin Invest*. 2008 Feb 1;118(2):789–800.
37. Cavaliere G, Trinchese G, Penna E, Cimmino F, Pirozzi C, Lama A, et al. High-Fat Diet Induces Neuroinflammation and Mitochondrial Impairment in Mice Cerebral Cortex and Synaptic Fraction. *Front Cell Neurosci*. 2019 Nov 12;13.

38. Westermeier F, Navarro-Marquez M, López-Crisosto C, Bravo-Sagua R, Quiroga C, Bustamante M, et al. Defective insulin signaling and mitochondrial dynamics in diabetic cardiomyopathy. *Biochim Biophys Acta BBA - Mol Cell Res.* 2015 May 1;1853(5):1113–8.
39. Parra V, Verdejo HE, Iglewski M, Campo A del, Troncoso R, Jones D, et al. Insulin Stimulates Mitochondrial Fusion and Function in Cardiomyocytes via the Akt-mTOR-NFκB-Opa-1 Signaling Pathway. *Diabetes.* 2014 Jan 1;63(1):75–88.
40. Mosser RE, Maulis MF, Moullé VS, Dunn JC, Carboneau BA, Arasi K, et al. High-fat diet-induced β-cell proliferation occurs prior to insulin resistance in C57Bl/6J male mice. *Am J Physiol-Endocrinol Metab.* 2015 Jan 27;308(7):E573–82.
41. Sparks LM, Xie H, Koza RA, Mynatt R, Hulver MW, Bray GA, et al. A High-Fat Diet Coordinately Downregulates Genes Required for Mitochondrial Oxidative Phosphorylation in Skeletal Muscle. *Diabetes.* 2005 Jul 1;54(7):1926–33.
42. Baur JA, Pearson KJ, Price NL, Jamieson HA, Lerin C, Kalra A, et al. Resveratrol improves health and survival of mice on a high-calorie diet. *Nature.* 2006 Nov 16;444(7117):337–42.
43. Zamarron BF, Mergian TA, Cho KW, Martinez-Santibanez G, Luan D, Singer K, et al. Macrophage Proliferation Sustains Adipose Tissue Inflammation in Formerly Obese Mice. *Diabetes.* 2017 Feb;66(2):392–406.

Summary

The regulation of immune cells at all stages—from development to activation—requires extensive changes in metabolic activity. The data presented in this thesis highlight several aspects of metabolism and their roles in regulating DCs. In Chapter 2, the results show the necessity for glycolysis in DC activation and migration, demonstrating that an early increase in glycolysis occurs in activated DCs regardless of the strength of pro-inflammatory phenotype. Long-term glycolytic reprogramming, however, takes place in highly pro-inflammatory DCs and coincides with HIF-1 α and iNOS activity. This glycolytic activity was found to be required for optimal DC motility as well as CCR7 oligomerization for chemokine-induced migration. Next, Chapter 3 focuses on oxidative metabolism and the role of PGC-1 β —a major regulator of mitochondrial and lipid metabolism—in DC function and activation. We found that PGC-1 β gene expression changes dynamically with LPS activation. Examination of PGC-1 β deficiency in DCs reveals an altered bioenergetic profile, with reduced oxidative metabolism and increased glycolysis. Further, the effect PGC-1 β deficiency has on the immune function of DCs includes enhanced MHC II surface expression and promotion of T cell expansion and Th2 differentiation. Finally, Chapter 4 characterizes the differences in mitochondrial and lipid content of cDC subsets in lymphoid and non-lymphoid tissues *in vivo* at both steady state and with a metabolic perturbation. This data shows the effect that changes in whole-body metabolism due to HFD challenge has on cDCs, with increased expansion of all cDC subsets, reduced mitochondrial content, and increased intracellular lipid levels. Together, this work highlights the importance of

multiple facets of metabolism in regulating DC function and activation, further contributing to our understanding of the role of metabolism in immunity.

The relationship between cellular metabolism and the cytoskeleton

Data in Chapter 2 describes the requirement of glycolysis for DC motility. Multiple studies that have investigated the link between glycolysis and the cytoskeleton provide additional insight into the regulatory mechanisms that may be taking place. The dynamic remodeling of the cytoskeleton that occurs during cell motility is energetically demanding, most notably for the use of ATP in actin polymerization and GTP by the Rho family of GTPases and microtubules. Although OXPHOS is more efficient at generating ATP, the requirement of glycolysis for cell motility has been observed in multiple systems for over forty years (129–131). Unlike the enzymes involved in OXPHOS, glycolytic enzymes are not partitioned by membrane-bound organelles. However, coordination of cell movement demands local energy production furnished through compartmentalization of glycolysis. Indeed, it has long been observed that many glycolytic enzymes are associated with the cytoskeleton (132–134). The anchoring of glycolytic enzymes at the cytoskeleton also promotes the efficiency of glycolysis by bringing the enzymes in close proximity (135).

More recently, specific compartmentalization of glycolytic enzymes has been shown to be important for cytoskeletal remodeling required for cell motility. The PI3K-AKT pathway links several types of cell surface receptors—including growth factor receptors, T-cell receptors, B-cell receptors, TLRs and integrins—to metabolic changes, primarily promoting glycolysis (136,137). PI3K signaling substantially colocalizes with F-actin bundles at membrane protrusions and participates in a positive feedback loop of actin polymerization (138). Aldolase,

a glycolytic enzyme that converts fructose-1,6-bisphosphate to glyceraldehyde 3-phosphate and dihydroxyacetone phosphate, is associated with F-actin (139). Upon actin remodeling coordinated by PI3K and RAC1, aldolase is released, activating its function in the glycolytic pathway (139). These studies suggest that PI3K signaling is a mechanism that spatially regulates glycolysis at areas of active cytoskeletal remodeling. Another enzyme that localizes at the cytoskeleton is 6-phosphofructo-2-kinase/fructose-2,6-bisphosphatase 3 (PFKFB3), which converts fructose-6-phosphate to fructose-2,6-bisphosphate and increases glycolytic activity (140). PFKFB3 compartmentalizes at cell protrusions through actin interactions in endothelial cells to promote their migration during vessel formation (140). In Treg cells, glucokinase, a hexokinase isozyme, inducibly associates with the cytoskeleton following PI3K-mTORC2 signaling to generate energy to fuel Treg cell migration (129).

Compartmentalized metabolism may also help direct the flux of metabolites to specific pathways. For example, PKM2 was found to be co-localized with F-actin at cell protrusions in macrophages (141). Under hypoxic conditions, macrophages have enhanced migratory capacity, attributed in part to HIF-1 α -pyruvate dehydrogenase kinase 1 (PDK1) signaling that redirects flux of pyruvate away from the TCA cycle and instead into lactate production, leading to localized energy generation (141). In DCs, NAD⁺ produced by LDHA has been shown to support actin polymerization and thus migration (142). Generation of NAD⁺ can help sustain glycolytic flux, as glycolytic enzyme GAPDH requires NAD⁺ for its enzymatic reaction. Inflammatory macrophages in the encephalomyelitis mouse model of multiple sclerosis likely rely on a similar mechanism, as they also require LDHA as well as lactate transporter MCT-4 for infiltration into the brain (143). Together, these studies suggest a close relationship and reciprocal regulation between glycolytic enzymes and cytoskeletal remodeling.

Cellular metabolism can also be affected by interactions with the extracellular matrix (ECM). Integrins couple the cytoskeleton and the ECM to generate traction along a surface during cell migration. Integrins are also chief mediators of mechanotransduction, a process by which mechanical stimuli such as stiffness are translated to biochemical signals, which impact functions (144–146). Integrin signaling engages signaling cascades that promote cell spreading and survival, and stimulates pathways such as PI3K/AKT known to affect cellular metabolism (147). Although there is a well-established link between cytoskeletal rearrangements, integrin signaling and mechanotransduction in immune cells (146,148), how these processes directly affect cellular metabolism and migratory capacity of immune cells is currently not well understood. However, a number of studies in other cell types suggest that integrin engagement and signaling result in changes in metabolism (149). For example, a recent study establishes a link between integrins, mechanotransduction and glycolysis (150). Cells can sense the stiffness of their environment through engagement of integrins. Under low adhesion and reduced integrin signaling (low stiffness), E3 ubiquitin ligase TRIM21 can be released from the actin cytoskeleton to target rate-limiting enzyme phosphofructokinase (PFK) for degradation, resulting in downregulation glycolysis (150). As integrin engagement is often localized to establish cell polarity in migrating cells, it is likely a mechanism that triggers localized glycolysis at areas of active cytoskeletal rearrangements. Indeed, recent findings reveal that DC metabolism is also regulated by mechanotransduction, with higher environmental stiffness increasing inflammatory function and glycolytic flux in DCs (151). Under chronic inflammatory conditions, stiffness can increase in tissues, potentially influencing DC metabolism, and therefore, their migratory ability.

Subcellular localization of mitochondria also plays an important role in immune cell migration. Mitochondria have been shown to accumulate at the rear (uropod) of migrating T cells

in response to CXCL12 or CCL21 (152). Mitochondrial Rho GTPase-1 (MIRO-1) contributes to mitochondrial redistribution by coupling mitochondria to microtubule dynein motors, thereby facilitating their positioning to the cell uropod (153). This redistribution of mitochondria requires mitochondrial fission, which is regulated by the GTPase dynamin-related protein 1 (DRP1), and DRP1 deficiency results in impaired T-cell transmigration across endothelial cells as well as infiltration into tumors (154). Localized mitochondrial ATP is necessary for the ATP-dependent phosphorylation of myosin light chain (MLC), which activates the ATPase activity of myosin II that is required for contraction of the actin cytoskeleton at the cell rear (152,154). While most mitochondria localize to the cell rear, a smaller portion of mitochondria accumulate near the front of the migrating T cell (155). The mitochondria provide ATP that is released and acts on the cell's purinergic P2X4 receptor, which promotes the formation of actin protrusions (155). Neutrophils, despite generating energy primarily through glycolysis (156), have also been shown to exhibit this differential activation of mitochondria in response to a chemoattractant (157). The minor portion of mitochondria that localizes to the front of the cell displays higher membrane potential and is enhanced by local mTOR signaling (157). In addition, disruption of components of the ETC and antioxidant proteins in neutrophils of zebrafish hampers their migratory abilities, demonstrating the importance of the ETC and redox status, respectively, for neutrophil motility (158). Together these studies provide evidence that mitochondria with contrasting metabolic properties localized to either ends of polarized immune cell, and that both groups significantly support migration. Mitochondrial metabolism in DCs and its maintenance by the transcriptional co-activator PGC-1 β is the focus of Chapter 3. Although we have not yet examined how DC motility or migration may be affected by PGC-1 β , these studies suggest that mitochondrial dysfunction would likely alter the dynamics of DC migration. Despite the fact that PGC-1 β

deficiency results in increased glycolytic activity, there is a slight bioenergetic insufficiency due to impaired oxidative metabolism, thus energy derived from glycolysis is not likely being prioritized for an energetically demanding process like migration. However, whether metabolic regulation by PGC-1 β does affect DC migration remains to be determined.

The influence of diet on immune responses

Nutrient availability in microenvironments—whether in primary or secondary lymphoid tissues or in inflamed peripheral tissues—will impact the metabolic pathways used by cells to support their bioenergetic and biosynthetic needs (159). How local nutrient availability affects immune homeostasis and response to infection adds another dimension to our understanding of host immunity. For example, the increased metabolic demands of both tumor cells and activated immune cells may lead to competition for nutrients in the tumor microenvironment. Anti-tumor immunity can be influenced by nutrient depletion the tumor microenvironment, such as glucose restriction by tumors impairing T cell effector function (160), and glutamine depletion promoting the differentiation of T cells into Treg cells (161). Nutrient competition in the dense lymph node environment likely also occurs, potentially impacting both spatial organization of immune cells and egress to the periphery.

We showed in Chapter 4 some of the effects HFD challenge has on cDCs, including preferential increase in the proportion of cDC2s, and an increase in intracellular lipid levels, but a significant decrease in mitochondrial mass. The model of HFD-induced obesity has been useful for examining other diseases that eventually develop after long-term feeding, such as type 2 diabetes, nonalcoholic fatty liver disease, and cardiomyopathy (162). Importantly, there is also a change in the amount and composition of circulating nutrients, but the effects of the diet itself are not always distinguished from the effects of diet-induced consequences such as obesity on

immune cells. However, studies examining systemic altering of nutrient availability, largely through diet manipulations, are demonstrating profound effects on immune function. ILC2s, for example, take up large amounts of fatty acids from their environment, and pharmacologically inhibiting intestinal absorption of dietary fatty acids impairs their expansion and cytokine production during helminth infection (163). A ketogenic diet, which contains low amounts of carbohydrates and high fat, is protective in mice during an influenza A virus infection by promoting the expansion of $\gamma\delta$ T cells in the lung (164). These $\gamma\delta$ T cells promote lung barrier integrity, although the precise mechanism by which this occurs requires further investigation (164). Dietary amino acids can also be essential for optimal immune responses. Dietary restriction of the essential amino acid methionine, for example, reduces disease severity in the experimental autoimmune encephalomyelitis model of multiple sclerosis by limiting the expansion of Th17 cells (165). Methionine is required for synthesizing the methyl donor S-adenosyl methionine, which in turn provides methyl groups for histone methylation (165). Methionine restriction in effector T cells results in partial reduction of histone methylation marks and downregulation of certain genes, including those involved in cell proliferation and the Th17-defining *Il17a*, thus resulting in an impaired Th17 response (165). In addition, mice fed a diet lacking non-essential amino acids serine and glycine exhibit a reduced number of antigen-specific CD8⁺ T cell when challenged with *Listeria monocytogenes* infection (166). While cytokine production of these T cells is not affected, their proliferative capacity is impaired, as serine metabolism was shown to be necessary for purine nucleotide biosynthesis (166). These studies on how systemic changes in nutrient availability affect immune responses emphasize the importance of diet in health and disease.

Dietary regulation of PGC-1 proteins

In Chapter 4, we found that HFD-induced obesity leads to decreased mitochondrial mass in DCs. This is also observed in other cell types, including skeletal muscle and hepatocytes, and is linked to diet-induced metabolic perturbations (167,168). In line with these observations, mice lacking PGC-1 α in white adipose tissue develop insulin resistance associated with impaired lipid metabolism (169). HFD challenge also reduces the gene expressions of both PGC-1 α and PGC-1 β in skeletal muscle cells (170). In Chapter 3, we showed that PGC-1 β deficiency in DCs results in reduced oxidative metabolism, but unchanged total mitochondrial mass. Certain dietary regulators improve pathological consequences of diet-induced obesity, in part by promoting mitochondrial metabolism and biosynthesis, such as through the induction of PGC-1 proteins (171). Consumption of the long-chain polyunsaturated fatty acids (PUFAs) eicosapentaenoic acid (EPA) and docosahexaenoic acid (DHA), which are found in fish oil, restores PGC-1 α gene expression in white adipose tissue and skeletal muscle of HFD-fed mice (172,173). Although the mice gain a similar amount of weight, those given EPA and DHA exhibit improved insulin sensitivity of skeletal muscle cells (173). PUFAs have also been described to promote anti-inflammatory functions in immune cells, including that of DCs (174).

Butyrate is a short-chain fatty acid that is a fermentation product of dietary fiber by gut bacteria and is also found in certain foods like butter; it improves insulin sensitivity and prevents increase in body fat percentage in HFD-fed mice (175). Dietary butyrate supplementation increases PGC-1 α gene expression and protein levels, and accordingly, the mitochondrial biogenesis and function in both skeletal muscle and brown adipose tissue (175). Butyrate is also known to have anti-inflammatory effects on intestinal DCs by promoting the expression of immunosuppressive enzymes retinaldehyde dehydrogenase and IDO (176,177). These DCs

induce the differentiation of naïve T cells into Treg cells, which is protective against inflammation-associated colitis and colon cancer in mice (176). While the effect of butyrate and PUFAs on adipose tissue-associated DCs has not yet been examined, these studies suggest it is likely these DCs would also upregulate PGC-1 α and possibly PGC-1 β expression and contribute to the overall anti-inflammatory environment.

Although we examined adipose tissue-associated CD11c⁺ cells that lack PGC-1 β , we did not find any significant changes in cell numbers, activation markers, or mitochondrial content. A likely explanation for this is that PGC-1 α may compensate for PGC-1 β deficiency in cDCs *in vivo*. Thus, cDC-specific genetic ablation of both PGC-1 α and PGC-1 β may allow us to better investigate the role of PGC-1 proteins and mitochondrial metabolism of cDCs *in vivo*.

Challenges in studying metabolism in DCs

As mentioned earlier, a caveat of BMDCs differentiated in the presence of GM-CSF is the heterogeneity of the culture (15). Another caveat to these cells is their expression of iNOS upon TLR stimulation, as *in vivo*-derived cDCs do not express iNOS (38). Since nitric oxide inhibits mitochondrial metabolism by binding components of the ETC, the effect of nitric oxide on DC metabolism must be taken into consideration. According to Everts *et al.*, detectable LPS-induced iNOS expression and nitric oxide production occurs at around six hours post-stimulation (64). Thus, the inhibition of the ETC in LPS-activated DCs only occurs past six hours and does not affect the early increase in glycolysis (40,64). Although TLR-activated bone marrow-derived DCs differ from cDCs in their expression of iNOS, they correspond more closely with TNF and iNOS-producing (TIP)-DCs that develop from monocytes in certain inflammatory contexts, such as infection with *Listeria monocytogenes* (178). In addition, other cells such as macrophages and

endothelial cells produce nitric oxide in inflammatory settings in response to cytokines (179). Nitric oxide can easily diffuse across cell membranes, affecting not only pathogens with their antimicrobial activity, but other host cells as well (180). For example, nitric oxide also acts on smooth muscle cells to induce vasodilation, thereby promoting blood flow and immune cell recruitment to the inflammatory site (179). iNOS-deficient BMDCs in the presence of iNOS-expressing wild-type BMDCs still have impaired oxidative metabolism when activated with LPS, suggesting that extrinsic nitric oxide is capable of inhibiting oxidative metabolism (66). Overall, the effects of nitric oxide on metabolic mechanisms regulating DC function are necessary to consider when translating *in vitro* experiments in BMDCs to *in vivo* DCs, whether they are monocyte-derived or conventional, and at steady state or in an inflammatory context with nitric oxide present.

While studying metabolic mechanisms in *in vitro*-differentiated DCs has certain advantages, their metabolism has adapted to the *in vitro* setting which differs from the *in vivo* environment. For example, stable isotope tracing demonstrates that CD8⁺ T cells activated in response to *Listeria monocytogenes* are much more oxidative than CD8⁺ T cells activated *in vitro* (181). However, examining the metabolism of DCs *in vivo* presents another set of challenges. Due to the scarcity of established protocols for culturing cDCs *ex vivo*, the harsh processing that is involved in isolating tissue cDCs, and the relatively low cell numbers, it is difficult to move away from *in vitro* cultures. DCs have been shown to be sensitive to mechanical stimulation, as they respond to mechanical forces by upregulating MHC II and co-stimulatory marker expression, but not cytokine production (182). The process of FACS sorting itself contributes to cell stress. In fact, FACS sorting exerts mechanical stress on cell membranes by activating mechanosensory signaling, which leads to changes in metabolites associated with plasma

membranes (183). FACS-sorted cells also exhibit altered redox states, with large increases in ROS levels as well as in the ratio of oxidized glutathione to reduced glutathione (184). Further, levels of many metabolites, including intermediates of glycolysis, the TCA cycle, and the pentose phosphate pathway, are reduced in FACS-sorted cells (184). Addition of serum to the sorting buffer could partially mitigate some of the changes in redox state and metabolite levels (184). DCs are relatively short-lived, especially after being stressed or activated, and there is currently an absence of protocols for the maintenance of tissue-derived cDCs *ex vivo*. Even following sorting, the relatively low yield of DCs limits their application.

Despite these challenges, recent advances have presented potential methods for investigating the metabolism of cDCs *in vivo*. Single-cell strategies in particular allow for the examination of low numbers of cells. One group presents a flow cytometry-based strategy termed Met-Flow for analyzing metabolic changes in immune populations with a panel of fluorochrome-conjugated antibodies that target key metabolic proteins, including rate-limiting enzymes, as well as lineage-defining and activation markers (185). Applying this strategy to human PBMCs confirms previously established metabolic profiles of different immune cell types (185). Further, by examining ten metabolic proteins, Met-Flow could define immune populations at a comparable resolution to approximately 500 metabolic genes by single cell RNA sequencing (185). Another study describes a method termed single-cell metabolic regulome profiling (scMEP) and expands the number of targets to 41 key proteins across a range of metabolic pathways, including metabolite transporters, enzymes, and transcription factors, along with lineage-specific markers (186). This panel is detected by mass cytometry or cytometry by time of flight (CyTOF), and the metabolic profile alone can predict the identity of the vast majority of immune cells (94% average) in whole human blood (186). Applying this strategy on single-cell

suspensions of colorectal carcinoma, healthy adjacent tissue, and other tissues, reveals diverse metabolic profiles that are cell- and tissue-dependent (186). Albeit with a smaller number of metabolic features that include mitochondrial and lipid content, data in Chapter 4 also confirms that cDC subset phenotypes are shaped by the tissue microenvironment.

These methods do not, however, reveal the spatial organization of different metabolic phenotypes throughout a tissue. By adapting the scMEP approach to multiplexed ion beam imaging by time of flight (MIBI-TOF), metabolic features of immune cells could also be measured from intact tissue sections (186). This method has the additional advantage of evaluating the spatial distribution of metabolic markers. Examination of human tissue sections from patients with colorectal carcinoma reveals that the metabolic features of immune cells along the tumor-immune boundary differ from those that are more distant, identifying a unique metabolic niche at this boundary (186). Indeed, metabolic competition in the tumor microenvironment between immune cells and tumor cells can modulate immune cell function (160). These technological approaches offer promising options to examine cDCs, since they are a relatively rare *in vivo* cell population.

Clinical implications

Cancer immunotherapy

The ability of DCs to initiate antigen-specific immune responses makes them ideal tools to harness and manipulate to generate efficient, targeted immunity. Precision immunotherapy against tumors using DCs has especially been an area of great interest. Of the cDC subsets, cDC1s typically promote anti-tumor immunity by cross-presenting tumor-associated antigens to CD8⁺ T cells and promoting Th1 differentiation of CD4⁺ T cells. Tumors have, however,

developed mechanisms to evade detection and killing by DCs and other immune cells. The tumor microenvironment is often immunosuppressive, preventing optimal development, recruitment, or anti-tumor effector functions of immune cells. Therefore, promising studies have demonstrated that DCs in combination with other immunotherapies that combat these immunosuppressive effects enhance anti-tumor responses. For example, in mouse melanoma models, the anti-tumor response by CD103⁺ cDC1s is greatly enhanced by the combined therapy of PD-L1 blockade, FLT3L to expand DC progenitors, and the TLR3 ligand poly I:C to induce DC maturation and activation (187). While cDC1s have been the main focus in the initiation of anti-tumor immune responses, cDC2s also have the capacity to elicit anti-tumor CD4⁺ T cell responses if the immunosuppressive effects of Treg cells are removed (188). Thus, treatment of mice with anti-CTLA-4 to deplete Treg cells improves cDC2 migration to the tumor-draining lymph node, expression of co-stimulatory molecules, and promotes the expansion of Th1-like cells (188). Moreover, in patients with melanoma, there is a correlation between progression-free survival and more abundant cDC2 but lower Treg cell frequency (188). Another immune evasion strategy is inhibiting the recruitment of DCs to the tumor. Tumor-derived prostaglandin E2 (PGE2) inhibits the function of intratumoral NK cells and chemokine receptor expression by cDC1s (189). Genetic deletion of cyclooxygenases in tumor cells prevents PGE2 production and allows NK cells to produce the chemokines CCL5 and XCL1, which recruit cDC1s to tumors (189). The cDC1s, in turn, subsequently transport tumor-associated antigen to the tumor-draining lymph node in a CCR7-dependent manner and activate T cells (23,189). Targeting of CCR7 expression on DCs by tumor-derived factors therefore greatly impairs anti-tumor immune responses (190). Tumor-derived ligands for the nuclear receptor liver X receptor, for example, inhibit CCR7 expression on DCs (190). In addition, glucose restriction in the tumor environment can occur due

to nutrient competition between immune cells and tumor cells (160). Therefore, in light of our findings in Chapter 2 on the importance of glycolysis for CCR7 oligomerization, impaired CCR7-mediated migration of DCs as a consequence of glucose restriction by tumor cells is another likely mechanism that allows tumor cells to evade the immune system. Using pharmacological agents to manipulate the metabolism of either immune cells or tumor cells can be challenging to target directly due to their reliance on overlapping metabolic pathways. However, many clinical trials using DC-based cancer immunotherapies generate DCs from patient monocytes isolated from peripheral blood, allowing for *in vitro* manipulation (191). In general, promising results from clinical trials using DC-based therapies to treat various cancer types are in combination with other standard therapies (191,192).

Metabolic induction of tolerogenic DCs

In contrast to strategies in cancer immunotherapy to enhance DC immunogenicity, approaches in treating autoimmune diseases require the induction of immune tolerance. Several pharmacological agents induce a tolerogenic phenotype in DCs, including the biologically active form of vitamin D, 1,25-dihydroxyvitamin D₃ (1,25(OH)₂D₃), and the corticosteroid dexamethasone (193). These agents are commonly used separately or together to induce tolerance, primarily on human monocyte-derived DCs *in vitro*. Profiling of 1,25(OH)₂D₃ and dexamethasone reveals they enrich for several of the same anti-inflammatory pathways in DCs (194), but that 1,25(OH)₂D₃ induces more potent changes (195). DCs treated with 1,25(OH)₂D₃ have relatively high rates of glycolysis and oxidative metabolism (196,197). Exposing 1,25(OH)₂D₃-treated DCs to hypoxia does not impair their ability to reduce IFN- γ production by T cells, while inhibiting glycolysis partially restores the ability of the DCs to induce T cell proliferation (196). Inhibiting FAO, however, does not restore the T cell stimulating capacity of

DCs. In line with these findings, the enzyme PFKFB4, which activates the glycolysis rate-limiting enzyme PFK1, is strongly upregulated in 1,25(OH)₂D₃-treated DCs (197). The inhibition of PFKFB4 does not affect the capacity for these cells to induce Treg cell expansion, but does affect the suppressive functions of the Treg cells (197). Together, these reports demonstrate the importance of glycolysis for the tolerogenic functions of 1,25(OH)₂D₃-treated DCs. Another study examines DCs treated with both 1,25(OH)₂D₃ and dexamethasone and find they also display higher oxidative metabolism and glycolytic capacity (198). In this case, however, inhibiting FAO in these cells partially restores T cell activation (198). Inconsistencies across studies are likely a reflection of different experimental conditions, as well as metabolic adaptability and partial reliance on multiple pathways for the functions of tolerogenic DCs. A clinical trial examined the use of tolerogenic DCs generated in the presence of dexamethasone and vitamin D3 to treat rheumatoid arthritis (199). These DCs were also co-cultured with synovial fluid from the inflamed joints of each patient, which allowed them to load the auto-antigens unique to each patient (199). This was followed by direct injection of these cells into inflamed joints (199). The trial deemed the treatment to be safe, and a few patients experienced some improvement of symptoms (199). Completed and ongoing phase I clinical trials based on tolerogenic DCs have also explored the efficacy of these cells in treating other autoimmune diseases, including type 1 diabetes, Crohn's disease, and multiple sclerosis (200). The results of these studies will inform on further design of DC-based immunotherapies going forward.

Final conclusion

DCs have a superior capacity to rapidly sense their microenvironment and stimulate context-specific immune responses. Their role in immunity is regulated in a highly precise manner, which, when dysregulated, can result in an overactive immune system, such as in autoimmune diseases, or poor clearance of pathogens or cancer cells. We aimed to characterize and determine how metabolism regulates this balance in DCs. Our findings highlight the importance of metabolism in regulating crucial DC functions, including the necessity for glycolysis in DC migration, and the role of mitochondrial regulator PGC-1 β in maintaining oxidative metabolism and inducing T cell differentiation. We also characterized specific metabolic features, such as mitochondrial and lipid content, in cDCs *in vivo* across several tissues and with HFD challenge as a metabolic perturbation. Overall, this work contributes to our understanding of DC biology and provides avenues for further study on the metabolic regulation of DC function and activation.

References

1. Abbas AK, Lichtman AH, Pillai S. Cellular and Molecular Immunology. 9th ed. Philadelphia, PA: Elsevier; 2018.
2. Murphy K. Janeway's Immunobiology. 8th ed. New York, USA and Abingdon, UK: Garland Science, Taylor & Francis Group, LLC; 2012.
3. Eisenbarth SC. Dendritic cell subsets in T cell programming: location dictates function. *Nat Rev Immunol*. 2019 Feb;19(2):89–103.
4. Merad M, Sathe P, Helft J, Miller J, Mortha A. The Dendritic Cell Lineage: Ontogeny and Function of Dendritic Cells and Their Subsets in the Steady State and the Inflamed Setting. *Annu Rev Immunol*. 2013 Mar 21;31(1):563–604.
5. Brown CC, Gudjonson H, Pritykin Y, Deep D, Lavallée V-P, Mendoza A, et al. Transcriptional Basis of Mouse and Human Dendritic Cell Heterogeneity. *Cell*. 2019 Oct 31;179(4):846-863.e24.
6. Rodrigues PF, Alberti-Servera L, Eremin A, Grajales-Reyes GE, Ivanek R, Tussiwand R. Distinct progenitor lineages contribute to the heterogeneity of plasmacytoid dendritic cells. *Nature Immunology*. 2018 Jul;19(7):711–22.
7. Dress RJ, Dutertre C-A, Giladi A, Schlitzer A, Low I, Shadan NB, et al. Plasmacytoid dendritic cells develop from Ly6D + lymphoid progenitors distinct from the myeloid lineage. *Nature Immunology*. 2019 Jul;20(7):852–64.
8. Durai V, Murphy KM. Functions of Murine Dendritic Cells. *Immunity*. 2016 Oct 18;45(4):719–36.
9. Schlitzer A, Sivakamasundari V, Chen J, Sumatoh HRB, Schreuder J, Lum J, et al. Identification of cDC1- and cDC2-committed DC progenitors reveals early lineage priming at the common DC progenitor stage in the bone marrow. *Nature Immunology*. 2015 Jul;16(7):718–28.
10. Worbs T, Hammerschmidt SI, Förster R. Dendritic cell migration in health and disease. *Nature Reviews Immunology*. 2017 Jan;17(1):30–48.
11. Williams M, Dutertre C-A, Scott CL, McGovern N, Sichien D, Chakarov S, et al. Unsupervised High-Dimensional Analysis Aligns Dendritic Cells across Tissues and Species. *Immunity*. 2016 Sep 20;45(3):669–84.
12. Miltenyi Biotec. Dendritic cells (mouse) [Internet]. Available from: <https://www.miltenyibiotec.com/US-en/resources/macshandbook/mouse-cells-and-organs/mouse-cell-types/dendritic-cells-mouse.html>

13. Miltenyi Biotec. Dendritic cells (human) [Internet]. Available from: <https://www.miltenyibiotec.com/US-en/resources/macs-handbook/human-cells-and-organs/human-cell-types/dendritic-cells-human.html#gref>
14. Inaba K, Inaba M, Romani N, Aya H, Deguchi M, Ikehara S, et al. Generation of large numbers of dendritic cells from mouse bone marrow cultures supplemented with granulocyte/macrophage colony-stimulating factor. *Journal of Experimental Medicine*. 1992 Dec 1;176(6):1693–702.
15. Helft J, Böttcher J, Chakravarty P, Zelenay S, Huotari J, Schraml BU, et al. GM-CSF Mouse Bone Marrow Cultures Comprise a Heterogeneous Population of CD11c(+)MHCII(+) Macrophages and Dendritic Cells. *Immunity*. 2015 Jun 16;42(6):1197–211.
16. Jin D, Sprent J. GM-CSF Culture Revisited: Preparation of Bulk Populations of Highly Pure Dendritic Cells from Mouse Bone Marrow. *The Journal of Immunology*. 2018 Nov 15;201(10):3129–39.
17. Kirkling ME, Cytlak U, Lau CM, Lewis KL, Resteu A, Khodadadi-Jamayran A, et al. Notch Signaling Facilitates In Vitro Generation of Cross-Presenting Classical Dendritic Cells. *Cell Rep*. 2018 Jun 19;23(12):3658-3672.e6.
18. Takeuchi O, Akira S. Pattern Recognition Receptors and Inflammation. *Cell*. 2010 Mar 19;140(6):805–20.
19. Roh JS, Sohn DH. Damage-Associated Molecular Patterns in Inflammatory Diseases. *Immune Netw*. 2018 Aug 13;18(4).
20. Brown GD, Willment JA, Whitehead L. C-type lectins in immunity and homeostasis. *Nature Reviews Immunology*. 2018 Jun;18(6):374–89.
21. LeibundGut-Landmann S, Groß O, Robinson MJ, Osorio F, Slack EC, Tsoni SV, et al. Syk- and CARD9-dependent coupling of innate immunity to the induction of T helper cells that produce interleukin 17. *Nature Immunology*. 2007 Jun;8(6):630–8.
22. Lubber CA, Cox J, Lauterbach H, Fancke B, Selbach M, Tschopp J, et al. Quantitative Proteomics Reveals Subset-Specific Viral Recognition in Dendritic Cells. *Immunity*. 2010 Feb 26;32(2):279–89.
23. Roberts EW, Broz ML, Binnewies M, Headley MB, Nelson AE, Wolf DM, et al. Critical Role for CD103+/CD141+ Dendritic Cells Bearing CCR7 for Tumor Antigen Trafficking and Priming of T Cell Immunity in Melanoma. *Cancer Cell*. 2016 Aug 8;30(2):324–36.
24. Plantinga M, Guillems M, Vanheerswynghe M, Deswarte K, Branco-Madeira F, Toussaint W, et al. Conventional and Monocyte-Derived CD11b+ Dendritic Cells Initiate and Maintain T Helper 2 Cell-Mediated Immunity to House Dust Mite Allergen. *Immunity*. 2013 Feb 21;38(2):322–35.

25. Idoyaga J, Fiorese C, Zbytnuik L, Lubkin A, Miller J, Malissen B, et al. Specialized role of migratory dendritic cells in peripheral tolerance induction. *J Clin Invest*. 2013 Feb 1;123(2):844–54.
26. Griffith JW, Sokol CL, Luster AD. Chemokines and Chemokine Receptors: Positioning Cells for Host Defense and Immunity. *Annu Rev Immunol*. 2014 Mar 21;32(1):659–702.
27. Lämmermann T, Bader BL, Monkley SJ, Worbs T, Wedlich-Söldner R, Hirsch K, et al. Rapid leukocyte migration by integrin-independent flowing and squeezing. *Nature*. 2008 May;453(7191):51–5.
28. Krishnaswamy JK, Gowthaman U, Zhang B, Mattsson J, Szeponik L, Liu D, et al. Migratory CD11b⁺ conventional dendritic cells induce T follicular helper cell–dependent antibody responses. *Science Immunology*. 2017 Dec 1;2(18).
29. Martínez-López M, Iborra S, Conde-Garrosa R, Sancho D. Batf3-dependent CD103⁺ dendritic cells are major producers of IL-12 that drive local Th1 immunity against *Leishmania major* infection in mice. *Eur J Immunol*. 2015 Jan;45(1):119–29.
30. Ashour D, Arampatzi P, Pavlovic V, Förstner KU, Kaisho T, Beilhack A, et al. IL-12 from endogenous cDC1, and not vaccine DC, is required for Th1 induction. *JCI Insight*. 2020 May 21;5(10).
31. Harpur CM, Kato Y, Dewi ST, Stankovic S, Johnson DN, Bedoui S, et al. Classical Type 1 Dendritic Cells Dominate Priming of Th1 Responses to Herpes Simplex Virus Type 1 Skin Infection. *The Journal of Immunology*. 2019 Feb 1;202(3):653–63.
32. Beier KC, Kallinich T, Hamelmann E. Master switches of T-cell activation and differentiation. *European Respiratory Journal*. 2007 Apr 1;29(4):804–12.
33. Torchinsky MB, Garaude J, Martin AP, Blander JM. Innate immune recognition of infected apoptotic cells directs T H 17 cell differentiation. *Nature*. 2009 Mar;458(7234):78–82.
34. Weichhart T, Hengstschläger M, Linke M. Regulation of innate immune cell function by mTOR. *Nature Reviews Immunology*. 2015 Oct;15(10):599–614.
35. Tan VP, Miyamoto S. Nutrient-sensing mTORC1: integration of metabolic and autophagic signals. *J Mol Cell Cardiol*. 2016 Jun;95:31–41.
36. Powell JD, Pollizzi KN, Heikamp EB, Horton MR. Regulation of Immune Responses by mTOR. *Annu Rev Immunol*. 2012;30:39–68.
37. Lin S-C, Hardie DG. AMPK: Sensing Glucose as well as Cellular Energy Status. *Cell Metabolism*. 2018 Feb 6;27(2):299–313.
38. Pearce EJ, Everts B. Dendritic cell metabolism. *Nat Rev Immunol*. 2015 Jan;15(1):18–29.

39. Krawczyk CM, Holowka T, Sun J, Blagih J, Amiel E, DeBerardinis RJ, et al. Toll-like receptor–induced changes in glycolytic metabolism regulate dendritic cell activation. *Blood*. 2010 Jun 10;115(23):4742–9.
40. Everts B, Amiel E, Huang SC-C, Smith AM, Chang C-H, Lam WY, et al. TLR-driven early glycolytic reprogramming via the kinases TBK1- $\text{IKK}\epsilon$ supports the anabolic demands of dendritic cell activation. *Nat Immunol*. 2014 Apr;15(4):323–32.
41. Tannahill G, Curtis A, Adamik J, Palsson-McDermott E, McGettrick A, Goel G, et al. Succinate is a danger signal that induces IL-1 β via HIF-1 α . *Nature*. 2013 Apr 11;496(7444):238–42.
42. Palsson-McDermott EM, Curtis AM, Goel G, Lauterbach MA, Sheedy FJ, Gleeson LE, et al. Pyruvate Kinase M2 regulates Hif-1 α activity and IL-1 β induction, and is a critical determinant of the Warburg Effect in LPS-activated macrophages. *Cell Metab*. 2015 Jan 6;21(1):65–80.
43. Gubser PM, Bantug GR, Razik L, Fischer M, Dimeloe S, Hoenger G, et al. Rapid effector function of memory CD8 + T cells requires an immediate-early glycolytic switch. *Nature Immunology*. 2013 Oct;14(10):1064–72.
44. Chang C-H, Curtis JD, Maggi LB, Jr, Faubert B, Villarino AV, et al. Posttranscriptional Control of T Cell Effector Function by Aerobic Glycolysis. *Cell*. 2013 Jun 6;153(6):1239.
45. Macintyre AN, Gerriets VA, Nichols AG, Michalek RD, Rudolph MC, Deoliveira D, et al. The Glucose Transporter Glut1 is Selectively Essential for CD4 T Cell Activation and Effector Function. *Cell Metab*. 2014 Jul 1;20(1):61–72.
46. Shi LZ, Wang R, Huang G, Vogel P, Neale G, Green DR, et al. HIF1 α –dependent glycolytic pathway orchestrates a metabolic checkpoint for the differentiation of TH17 and Treg cells. *J Exp Med*. 2011 Jul 4;208(7):1367–76.
47. Lehner R, Quiroga AD. Chapter 5 - Fatty Acid Handling in Mammalian Cells. In: Ridgway ND, McLeod RS, editors. *Biochemistry of Lipids, Lipoproteins and Membranes (Sixth Edition)*. Boston: Elsevier; 2016. p. 149–84.
48. O'Neill LAJ, Kishton RJ, Rathmell J. A guide to immunometabolism for immunologists. *Nature Reviews Immunology*. 2016 Sep;16(9):553–65.
49. Jha AK, Huang SC-C, Sergushichev A, Lampropoulou V, Ivanova Y, Loginicheva E, et al. Network Integration of Parallel Metabolic and Transcriptional Data Reveals Metabolic Modules that Regulate Macrophage Polarization. *Immunity*. 2015 Mar 17;42(3):419–30.
50. Wang F, Zhang S, Vuckovic I, Jeon R, Lerman A, Folmes CD, et al. Glycolytic Stimulation is not a Requirement for M2 Macrophage Differentiation. *Cell Metab*. 2018 Sep 4;28(3):463–475.e4.

51. Rice CM, Davies LC, Subleski JJ, Maio N, Gonzalez-Cotto M, Andrews C, et al. Tumour-elicited neutrophils engage mitochondrial metabolism to circumvent nutrient limitations and maintain immune suppression. *Nature Communications*. 2018 Nov 30;9(1):5099.
52. Siska PJ, Beckermann KE, Mason FM, Andrejeva G, Greenplate AR, Sendor AB, et al. Mitochondrial dysregulation and glycolytic insufficiency functionally impair CD8 T cells infiltrating human renal cell carcinoma. *JCI Insight*. 2017 Jun 15;2(12).
53. O'Sullivan D, van der Windt GJW, Ching-Cheng Huang S, Curtis JD, Chang C-H, Buck MD, et al. Memory CD8⁺ T cells use cell intrinsic lipolysis to support the metabolic programming necessary for development. *Immunity*. 2014 Jul 17;41(1):75–88.
54. Berod L, Friedrich C, Nandan A, Freitag J, Hagemann S, Harmrolfs K, et al. De novo fatty acid synthesis controls the fate between regulatory T and T helper 17 cells. *Nature Medicine*. 2014 Nov;20(11):1327–33.
55. Del Prete A, Zaccagnino P, Di Paola M, Saltarella M, Oliveros Celis C, Nico B, et al. Role of mitochondria and reactive oxygen species in dendritic cell differentiation and functions. *Free Radical Biology and Medicine*. 2008 Apr 1;44(7):1443–51.
56. Zaccagnino P, Saltarella M, Maiorano S, Gaballo A, Santoro G, Nico B, et al. An active mitochondrial biogenesis occurs during dendritic cell differentiation. *The International Journal of Biochemistry & Cell Biology*. 2012 Nov 1;44(11):1962–9.
57. Rehman A, Hemmert KC, Ochi A, Jamal M, Henning JR, Barilla R, et al. Role of Fatty-acid Synthesis in Dendritic Cell Generation and Function. *J Immunol*. 2013 May 1;190(9):4640–9.
58. Sathaliyawala T, O'Gorman WE, Greter M, Bogunovic M, Konjufca V, Hou ZE, et al. Mammalian target of rapamycin controls dendritic cell development downstream of Flt3 ligand signaling. *Immunity*. 2010 Oct 29;33(4):597–606.
59. Haidinger M, Poglitsch M, Geyeregger R, Kasturi S, Zeyda M, Zlabinger GJ, et al. A Versatile Role of Mammalian Target of Rapamycin in Human Dendritic Cell Function and Differentiation. *The Journal of Immunology*. 2010 Oct 1;185(7):3919–31.
60. Kratchmarov R, Viragova S, Kim MJ, Rothman NJ, Liu K, Reizis B, et al. Metabolic control of cell fate bifurcations in a hematopoietic progenitor population. *Immunol Cell Biol*. 2018 Sep;96(8):863–71.
61. Bosteels C, Neyt K, Vanheerswynghels M, Helden MJ van, Sichien D, Debeuf N, et al. Inflammatory Type 2 cDCs Acquire Features of cDC1s and Macrophages to Orchestrate Immunity to Respiratory Virus Infection. *Immunity*. 2020 Jun 16;52(6):1039-1056.e9.
62. Thwe PM, Fritz DI, Snyder JP, Smith PR, Curtis KD, O'Donnell A, et al. Syk-dependent glycolytic reprogramming in dendritic cells regulates IL-1 β production to β -glucan ligands in a TLR-independent manner. *Journal of Leukocyte Biology*. 2019;106(6):1325–35.

63. Thwe P, Pelgrom L, Cooper R, Beauchamp S, Reisz JA, D'Alessandro A, et al. Cell-intrinsic glycogen metabolism supports early glycolytic reprogramming required for dendritic cell immune responses. *Cell metabolism*. 2017 Sep 5;26(3):558.
64. Everts B, Amiel E, Windt GJW van der, Freitas TC, Chott R, Yarasheski KE, et al. Commitment to glycolysis sustains survival of NO-producing inflammatory dendritic cells. *Blood*. 2012 Aug 16;120(7):1422.
65. Pantel A, Teixeira A, Haddad E, Wood EG, Steinman RM, Longhi MP. Direct Type I IFN but Not MDA5/TLR3 Activation of Dendritic Cells Is Required for Maturation and Metabolic Shift to Glycolysis after Poly IC Stimulation. *PLOS Biology*. 2014 Jan 7;12(1):e1001759.
66. Lawless SJ, Kedia-Mehta N, Walls JF, McGarrigle R, Convery O, Sinclair LV, et al. Glucose represses dendritic cell-induced T cell responses. *Nature Communications*. 2017 May 30;8(1):15620.
67. Jantsch J, Chakravorty D, Turza N, Prechtel AT, Buchholz B, Gerlach RG, et al. Hypoxia and Hypoxia-Inducible Factor-1 α Modulate Lipopolysaccharide-Induced Dendritic Cell Activation and Function. *The Journal of Immunology*. 2008 Apr 1;180(7):4697–705.
68. Jantsch J, Wiese M, Schödel J, Castiglione K, Gläsner J, Kolbe S, et al. Toll-like receptor activation and hypoxia use distinct signaling pathways to stabilize hypoxia-inducible factor 1 α (HIF1A) and result in differential HIF1A-dependent gene expression. *Journal of Leukocyte Biology*. 2011;90(3):551–62.
69. Domogalla MP, Rostan PV, Raker VK, Steinbrink K. Tolerance through Education: How Tolerogenic Dendritic Cells Shape Immunity. *Front Immunol*. 2017 Dec 11;8.
70. Zhao F, Xiao C, Evans KS, Theivanthiran T, DeVito N, Holtzhausen A, et al. Paracrine Wnt5a- β -Catenin Signaling Triggers a Metabolic Program that Drives Dendritic Cell Tolerization. *Immunity*. 2018 Jan 16;48(1):147-160.e7.
71. Mondanelli G, Bianchi R, Pallotta MT, Orabona C, Albini E, Iacono A, et al. A Relay Pathway between Arginine and Tryptophan Metabolism Confers Immunosuppressive Properties on Dendritic Cells. *Immunity*. 2017 Feb 21;46(2):233–44.
72. Gabrilovich DI. Myeloid-derived suppressor cells. *Cancer Immunol Res*. 2017 Jan;5(1):3–8.
73. Norian LA, Rodriguez PC, O'Mara LA, Zabaleta J, Ochoa AC, Cella M, et al. Tumor-infiltrating regulatory dendritic cells inhibit CD8⁺ T cell function via L-arginine metabolism. *Cancer Res*. 2009 Apr 1;69(7):3086–94.
74. Ugele I, Cárdenas-Conejo ZE, Hammon K, Wehrstein M, Bruss C, Peter K, et al. D-2-Hydroxyglutarate and L-2-Hydroxyglutarate Inhibit IL-12 Secretion by Human Monocyte-Derived Dendritic Cells. *International Journal of Molecular Sciences*. 2019 Jan;20(3):742.

75. Colegio OR, Chu N-Q, Szabo AL, Chu T, Rhebergen AM, Jairam V, et al. Functional polarization of tumour-associated macrophages by tumour-derived lactic acid. *Nature*. 2014 Sep 25;513(7519):559–63.
76. Brand A, Singer K, Koehl GE, Kolitzus M, Schoenhammer G, Thiel A, et al. LDHA-Associated Lactic Acid Production Blunts Tumor Immunosurveillance by T and NK Cells. *Cell Metabolism*. 2016 Nov 8;24(5):657–71.
77. Gottfried E, Kunz-Schughart LA, Ebner S, Mueller-Klieser W, Hoves S, Andreesen R, et al. Tumor-derived lactic acid modulates dendritic cell activation and antigen expression. *Blood*. 2006 Mar 1;107(5):2013–21.
78. Caronni N, Simoncello F, Stafetta F, Guarnaccia C, Ruiz-Moreno JS, Opitz B, et al. Downregulation of Membrane Trafficking Proteins and Lactate Conditioning Determine Loss of Dendritic Cell Function in Lung Cancer. *Cancer Res*. 2018 Apr 1;78(7):1685–99.
79. Nasi A, Fekete T, Krishnamurthy A, Snowden S, Rajnavölgyi E, Catrina AI, et al. Dendritic Cell Reprogramming by Endogenously Produced Lactic Acid. *The Journal of Immunology*. 2013 Sep 15;191(6):3090–9.
80. Marin E, Bouchet-Delbos L, Renoult O, Louvet C, Nerriere-Daguin V, Managh AJ, et al. Human Tolerogenic Dendritic Cells Regulate Immune Responses through Lactate Synthesis. *Cell Metabolism*. 2019 Dec 3;30(6):1075-1090.e8.
81. Ibrahim J, Nguyen AH, Rehman A, Ochi A, Jamal M, Graffeo CS, et al. Dendritic Cell Populations with Different Concentrations of Lipid Regulate Tolerance and Immunity in Mouse and Human Liver. *Gastroenterology*. 2012 Oct;143(4):1061.
82. Bougnères L, Helft J, Tiwari S, Vargas P, Chang BH-J, Chan L, et al. A Role for Lipid Bodies in the Cross-presentation of Phagocytosed Antigens by MHC Class I in Dendritic Cells. *Immunity*. 2009 Aug 21;31(2):232–44.
83. Herber DL, Cao W, Nefedova Y, Novitskiy SV, Nagaraj S, Tyurin VA, et al. Lipid accumulation and dendritic cell dysfunction in cancer. *Nat Med*. 2010 Aug;16(8):880–6.
84. Veglia F, Tyurin VA, Mohammadyani D, Blasi M, Duperret EK, Donthireddy L, et al. Lipid bodies containing oxidatively truncated lipids block antigen cross-presentation by dendritic cells in cancer. *Nat Communications*. 2017 Dec 14;8.
85. Cao W, Ramakrishnan R, Tyurin VA, Veglia F, Condamine T, Amoscato A, et al. Oxidized lipids block antigen cross-presentation by dendritic cells in cancer Oxidized lipids and DCs in cancer. *J Immunol*. 2014 Mar 15;192(6):2920–31.
86. Cubillos-Ruiz JR, Silberman PC, Rutkowski MR, Chopra S, Perales-Puchalt A, Song M, et al. ER Stress Sensor XBP1 Controls Anti-tumor Immunity by Disrupting Dendritic Cell Homeostasis. *Cell*. 2015 Jun 18;161(7):1527–38.

87. Lin J, Handschin C, Spiegelman BM. Metabolic control through the PGC-1 family of transcription coactivators. *Cell Metabolism*. 2005 Jun 1;1(6):361–70.
88. Puigserver P, Wu Z, Park CW, Graves R, Wright M, Spiegelman BM. A Cold-Inducible Coactivator of Nuclear Receptors Linked to Adaptive Thermogenesis. *Cell*. 1998 Mar 20;92(6):829–39.
89. Lin J, Puigserver P, Donovan J, Tarr P, Spiegelman BM. Peroxisome Proliferator-activated Receptor γ Coactivator 1 β (PGC-1 β), A Novel PGC-1-related Transcription Coactivator Associated with Host Cell Factor *. *Journal of Biological Chemistry*. 2002 Jan 18;277(3):1645–8.
90. Lin J, Yang R, Tarr PT, Wu P-H, Handschin C, Li S, et al. Hyperlipidemic Effects of Dietary Saturated Fats Mediated through PGC-1 β Coactivation of SREBP. *Cell*. 2005 Jan 28;120(2):261–73.
91. Russell AP, Hesselink MKC, Lo SK, Schrauwen P. Regulation of metabolic transcriptional co-activators and transcription factors with acute exercise. *The FASEB Journal*. 2005;19(8):986–8.
92. Rowe GC, Patten IS, Zsengeller ZK, El-Khoury R, Okutsu M, Bampoh S, et al. Disconnecting mitochondrial content from respiratory chain capacity in PGC-1 deficient skeletal muscle. *Cell Rep*. 2013 May 30;3(5):1449–56.
93. Villena JA. New insights into PGC-1 coactivators: redefining their role in the regulation of mitochondrial function and beyond. *The FEBS Journal*. 2015;282(4):647–72.
94. Jones AWE, Yao Z, Vicencio JM, Karkucinska-Wieckowska A, Szabadkai G. PGC-1 family coactivators and cell fate: Roles in cancer, neurodegeneration, cardiovascular disease and retrograde mitochondria–nucleus signalling. *Mitochondrion*. 2012 Jan 1;12(1):86–99.
95. Jäger S, Handschin C, St.-Pierre J, Spiegelman BM. AMP-activated protein kinase (AMPK) action in skeletal muscle via direct phosphorylation of PGC-1 α . *Proc Natl Acad Sci U S A*. 2007 Jul 17;104(29):12017–22.
96. Zong H, Ren JM, Young LH, Pypaert M, Mu J, Birnbaum MJ, et al. AMP kinase is required for mitochondrial biogenesis in skeletal muscle in response to chronic energy deprivation. *Proc Natl Acad Sci U S A*. 2002 Dec 10;99(25):15983–7.
97. Olson BL, Hock MB, Ekholm-Reed S, Wohlschlegel JA, Dev KK, Kralli A, et al. SCFCdc4 acts antagonistically to the PGC-1 α transcriptional coactivator by targeting it for ubiquitin-mediated proteolysis. *Genes Dev*. 2008 Jan 15;22(2):252–64.
98. Rodgers JT, Lerin C, Haas W, Gygi SP, Spiegelman BM, Puigserver P. Nutrient control of glucose homeostasis through a complex of PGC-1 α and SIRT1. *Nature*. 2005 Mar;434(7029):113–8.

99. Cao W, Daniel KW, Robidoux J, Puigserver P, Medvedev AV, Bai X, et al. p38 Mitogen-Activated Protein Kinase Is the Central Regulator of Cyclic AMP-Dependent Transcription of the Brown Fat Uncoupling Protein 1 Gene. *Molecular and Cellular Biology*. 2004 Apr 1;24(7):3057–67.
100. Fernandez-Marcos PJ, Auwerx J. Regulation of PGC-1 α , a nodal regulator of mitochondrial biogenesis. *Am J Clin Nutr*. 2011 Apr;93(4):884S-890S.
101. Tan H, Yang K, Li Y, Shaw TI, Wang Y, Blanco DB, et al. Integrative Proteomics and Phosphoproteomics Profiling Reveals Dynamic Signaling Networks and Bioenergetics Pathways Underlying T Cell Activation. *Immunity*. 2017 Mar 21;46(3):488–503.
102. van Bruggen JAC, Martens AWJ, Fraietta JA, Hofland T, Tonino SH, Eldering E, et al. Chronic lymphocytic leukemia cells impair mitochondrial fitness in CD8⁺ T cells and impede CAR T-cell efficacy. *Blood*. 2019 Jul 4;134(1):44–58.
103. Scharping NE, Menk AV, Moreci RS, Whetstone RD, Dadey RE, Watkins SC, et al. The Tumor Microenvironment Represses T Cell Mitochondrial Biogenesis to Drive Intratumoral T Cell Metabolic Insufficiency and Dysfunction. *Immunity*. 2016 Aug 16;45(2):374–88.
104. Dumauthioz N, Tschumi B, Wenes M, Marti B, Wang H, Franco F, et al. Enforced PGC-1 α expression promotes CD8 T cell fitness, memory formation and antitumor immunity. *Cellular & Molecular Immunology*. 2020 Feb 13;1–11.
105. Bengsch B, Johnson AL, Kurachi M, Odorizzi PM, Pauken KE, Attanasio J, et al. Bioenergetic Insufficiencies Due to Metabolic Alterations Regulated by the Inhibitory Receptor PD-1 Are an Early Driver of CD8⁺ T Cell Exhaustion. *Immunity*. 2016 Aug 16;45(2):358–73.
106. Vats D, Mukundan L, Odegaard JI, Zhang L, Smith KL, Morel CR, et al. Oxidative metabolism and PGC-1 β attenuate macrophage-mediated inflammation. *Cell Metab*. 2006 Jul;4(1):13–24.
107. Eisele PS, Salatino S, Sobek J, Hottiger MO, Handschin C. The Peroxisome Proliferator-activated Receptor γ Coactivator 1 α/β (PGC-1) Coactivators Repress the Transcriptional Activity of NF- κ B in Skeletal Muscle Cells. *J Biol Chem*. 2013 Jan 25;288(4):2246–60.
108. Eisele PS, Furrer R, Beer M, Handschin C. The PGC-1 coactivators promote an anti-inflammatory environment in skeletal muscle in vivo. *Biochem Biophys Res Commun*. 2015 Aug 28;464(3):692–7.
109. Schilling Joel, Lai Ling, Sambandam Nandakumar, Dey Courtney E., Leone Teresa C., Kelly Daniel P. Toll-Like Receptor-Mediated Inflammatory Signaling Reprograms Cardiac Energy Metabolism by Repressing Peroxisome Proliferator-Activated Receptor γ Coactivator-1 Signaling. *Circulation: Heart Failure*. 2011 Jul 1;4(4):474–82.

110. Ishida Y, Fujita H, Aratani S, Chijiwa M, Taniguchi N, Yokota M, et al. The NRF2-PGC-1 β pathway activates kynurenine aminotransferase 4 via attenuation of an E3 ubiquitin ligase, synoviolin, in a cecal ligation/perforation-induced septic mouse model. *Molecular Medicine Reports*. 2018 Aug 1;18(2):2467–75.
111. Chang W-C, Jan Wu Y-J, Chung W-H, Lee Y-S, Chin S-W, Chen T-J, et al. Genetic variants of PPAR-gamma coactivator 1B augment NLRP3-mediated inflammation in gouty arthritis. *Rheumatology*. 2017 Mar 1;56(3):457–66.
112. Cildir G, Akıncılar SC, Tergaonkar V. Chronic adipose tissue inflammation: all immune cells on the stage. *Trends in Molecular Medicine*. 2013 Aug 1;19(8):487–500.
113. Russo L, Lumeng CN. Properties and functions of adipose tissue macrophages in obesity. *Immunology*. 2018;155(4):407–17.
114. Cinti S, Mitchell G, Barbatelli G, Murano I, Ceresi E, Faloia E, et al. Adipocyte death defines macrophage localization and function in adipose tissue of obese mice and humans. *Journal of Lipid Research*. 2005 Nov 1;46(11):2347–55.
115. Kratz M, Coats BR, Hisert KB, Hagman D, Mutskov V, Peris E, et al. Metabolic dysfunction drives a mechanistically distinct pro-inflammatory phenotype in adipose tissue macrophages. *Cell Metab*. 2014 Oct 7;20(4):614–25.
116. Mauer J, Chaurasia B, Plum L, Quast T, Hampel B, Blüher M, et al. Myeloid Cell-Restricted Insulin Receptor Deficiency Protects Against Obesity-Induced Inflammation and Systemic Insulin Resistance. *PLoS Genet*. 2010 May 6;6(5).
117. Weisberg SP, McCann D, Desai M, Rosenbaum M, Leibel RL, Ferrante AW. Obesity is associated with macrophage accumulation in adipose tissue. *J Clin Invest*. 2003 Dec 15;112(12):1796–808.
118. Ferrante AW. The Immune Cells in Adipose Tissue. *Diabetes Obes Metab*. 2013 Sep;15(03):34–8.
119. Han S-J, Zaretsky AG, Andrade-Oliveira V, Collins N, Dzutsev A, Shaik J, et al. The white adipose tissue is a reservoir for memory T cells that promotes protective memory responses to infection. *Immunity*. 2017 Dec 19;47(6):1154-1168.e6.
120. Wang Q, Wu H. T Cells in Adipose Tissue: Critical Players in Immunometabolism. *Front Immunol*. 2018 Oct 30;9.
121. Nishimura S, Manabe I, Nagasaki M, Eto K, Yamashita H, Ohsugi M, et al. CD8 + effector T cells contribute to macrophage recruitment and adipose tissue inflammation in obesity. *Nature Medicine*. 2009 Aug;15(8):914–20.
122. Feuerer M, Herrero L, Cipolletta D, Naaz A, Wong J, Nayer A, et al. Fat Treg cells: a liaison between the immune and metabolic systems. *Nat Med*. 2009 Aug;15(8):930–9.

123. Cho KW, Zamarron BF, Muir LA, Singer K, Porsche CE, DelProposto JB, et al. Adipose Tissue Dendritic Cells are Independent Contributors to Obesity-Induced Inflammation and Insulin Resistance*. *J Immunol*. 2016 Nov 1;197(9):3650–61.
124. Bertola A, Ciucci T, Rousseau D, Bourlier V, Duffaut C, Bonnafous S, et al. Identification of Adipose Tissue Dendritic Cells Correlated With Obesity-Associated Insulin-Resistance and Inducing Th17 Responses in Mice and Patients. *Diabetes*. 2012 Sep;61(9):2238–47.
125. Stefanovic-Racic M, Yang X, Turner MS, Mantell BS, Stolz DB, Sumpter TL, et al. Dendritic Cells Promote Macrophage Infiltration and Comprise a Substantial Proportion of Obesity-Associated Increases in CD11c+ Cells in Adipose Tissue and Liver. *Diabetes*. 2012 Sep;61(9):2330.
126. Macdougall CE, Wood EG, Loschko J, Scagliotti V, Cassidy FC, Robinson ME, et al. Visceral Adipose Tissue Immune Homeostasis Is Regulated by the Crosstalk between Adipocytes and Dendritic Cell Subsets. *Cell Metabolism*. 2018 Mar;27(3):588-601.e4.
127. Zlotnikov-Klionsky Y, Nathansohn-Levi B, Shezen E, Rosen C, Kagan S, Bar-On L, et al. Perforin-Positive Dendritic Cells Exhibit an Immuno-regulatory Role in Metabolic Syndrome and Autoimmunity. *Immunity*. 2015 Oct 20;43(4):776–87.
128. Zangi L, Zlotnikov Klionsky Y, Yarimi L, Bachar-Lustig E, Eidelstein Y, Shezen E, et al. Deletion of cognate CD8 T cells by immature dendritic cells: a novel role for perforin, granzyme A, TREM-1, and TLR7. *Blood*. 2012 Aug 23;120(8):1647–57.
129. Kishore M, Cheung KCP, Fu H, Bonacina F, Wang G, Coe D, et al. Regulatory T Cell Migration Is Dependent on Glucokinase-Mediated Glycolysis. *Immunity*. 2017 Nov 21;47(5):875.
130. Shiraishi T, Verdone JE, Huang J, Kahlert UD, Hernandez JR, Torga G, et al. Glycolysis is the primary bioenergetic pathway for cell motility and cytoskeletal remodeling in human prostate and breast cancer cells. *Oncotarget*. 2015;6(1):130–43.
131. D’Silva H, Gothoskar BP, Jain VK, Advani SH. Cell migration and energy generating metabolic activities. *European Journal of Cancer* (1965). 1978 Nov 1;14(11):1243–8.
132. Masters C. Interactions between glycolytic enzymes and components of the cytomatrix. *J Cell Biol*. 1984 Jul 1;99(1 Pt 2):222s–5s.
133. Arnold H, Pette D. Binding of Glycolytic Enzymes to Structure Proteins of the Muscle. *European Journal of Biochemistry*. 1968;6(2):163–71.
134. Sreere PA. Complexes of sequential metabolic enzymes. *Annu Rev Biochem*. 1987 Jun 1;56(1):89–124.
135. Zala D, Schlattner U, Desvignes T, Bobe J, Roux A, Chavrier P, et al. The advantage of channeling nucleotides for very processive functions. *F1000Res*. 2017 Jul 18;6.

136. Hoxhaj G, Manning BD. The PI3K–AKT network at the interface of oncogenic signalling and cancer metabolism. *Nature Reviews Cancer*. 2020 Feb;20(2):74–88.
137. So L, Fruman DA. PI3K Signaling in B and T Lymphocytes: New Developments and Therapeutic Advances. *The Biochemical journal*. 2012 Mar 15;442(3):465.
138. Johnson HE, King SJ, Asokan SB, Rotty JD, Bear JE, Haugh JM. F-actin bundles direct the initiation and orientation of lamellipodia through adhesion-based signaling. *J Cell Biol*. 2015 Feb 16;208(4):443–55.
139. Hu H, Juvekar A, Lyssiotis CA, Lien EC, Albeck JG, Oh D, et al. Phosphoinositide 3-Kinase Regulates Glycolysis through Mobilization of Aldolase from the Actin cytoskeleton. *Cell*. 2016 Jan 28;164(3):433–46.
140. De Bock K, Georgiadou M, Schoors S, Kuchnio A, Wong BW, Cantelmo AR, et al. Role of PFKFB3-Driven Glycolysis in Vessel Sprouting. *Cell*. 2013 Aug 1;154(3):651–63.
141. Semba H, Takeda N, Isagawa T, Sugiura Y, Honda K, Wake M, et al. HIF-1 α -PDK1 axis-induced active glycolysis plays an essential role in macrophage migratory capacity. *Nature Communications*. 2016 May 18;7(1):11635.
142. Liu J, Zhang X, Chen K, Cheng Y, Liu S, Xia M, et al. CCR7 Chemokine Receptor-Inducible Inc-Dpf3 Restrains Dendritic Cell Migration by Inhibiting HIF-1 α -Mediated Glycolysis. *Immunity*. 2019 Mar 19;50(3):600-615.e15.
143. Kaushik DK, Bhattacharya A, Mirzaei R, Rawji KS, Ahn Y, Rho JM, et al. Enhanced glycolytic metabolism supports transmigration of brain-infiltrating macrophages in multiple sclerosis. *J Clin Invest*. 129(8):3277–92.
144. Doyle AD, Carvajal N, Jin A, Matsumoto K, Yamada KM. Local 3D matrix microenvironment regulates cell migration through spatiotemporal dynamics of contractility-dependent adhesions. *Nature Communications*. 2015 Nov 9;6(1):8720.
145. Jaalouk DE, Lammerding J. Mechanotransduction gone awry. *Nat Rev Mol Cell Biol*. 2009 Jan;10(1):63–73.
146. Rossy J, Laufer JM, Legler DF. Role of Mechanotransduction and Tension in T Cell Function. *Front Immunol*. 2018 Nov 15;9.
147. Geiger B, Bershadsky A, Pankov R, Yamada KM. Transmembrane crosstalk between the extracellular matrix and the cytoskeleton. *Nature Reviews Molecular Cell Biology*. 2001 Nov;2(11):793–805.
148. Upadhyaya A. Mechanosensing in the immune response. *Semin Cell Dev Biol*. 2017 Nov;71:137–45.
149. Ata R, Antonescu CN. Integrins and Cell Metabolism: An Intimate Relationship Impacting Cancer. *Int J Mol Sci*. 2017 Jan 18;18(1).

150. Park JS, Burckhardt CJ, Lazcano R, Solis LM, Isogai T, Li L, et al. Mechanical regulation of glycolysis via cytoskeleton architecture. *Nature*. 2020 Feb;578(7796):621–6.
151. Chakraborty M, Chu K, Shrestha A, Revelo XS, Zhang X, Gold MJ, et al. Mechanical Stiffness Controls Dendritic Cell Metabolism and Function. *Cell Rep*. 2021 Jan 12;34(2):108609.
152. Campello S, Lacalle RA, Bettella M, Mañes S, Scorrano L, Viola A. Orchestration of lymphocyte chemotaxis by mitochondrial dynamics. *J Exp Med*. 2006 Dec 25;203(13):2879–86.
153. Morlino G, Barreiro O, Baixauli F, Robles-Valero J, González-Granado JM, Villa-Bellosta R, et al. Miro-1 Links Mitochondria and Microtubule Dynein Motors To Control Lymphocyte Migration and Polarity. *Mol Cell Biol*. 2014 Apr;34(8):1412–26.
154. Simula L, Pacella I, Colamatteo A, Procaccini C, Cancila V, Bordi M, et al. Drp1 Controls Effective T Cell Immune-Surveillance by Regulating T Cell Migration, Proliferation, and cMyc-Dependent Metabolic Reprogramming. *Cell Reports*. 2018 Dec 11;25(11):3059-3073.e10.
155. Ledderose C, Liu K, Kondo Y, Slubowski CJ, Dertnig T, Denicoló S, et al. Purinergic P2X4 receptors and mitochondrial ATP production regulate T cell migration. *J Clin Invest*. 128(8):3583–94.
156. Maianski NA, Geissler J, Srinivasula SM, Alnemri ES, Roos D, Kuijpers TW. Functional characterization of mitochondria in neutrophils: a role restricted to apoptosis. *Cell Death & Differentiation*. 2004 Feb;11(2):143–53.
157. Bao Y, Ledderose C, Graf AF, Brix B, Birsak T, Lee A, et al. mTOR and differential activation of mitochondria orchestrate neutrophil chemotaxis. *J Cell Biol*. 2015 Sep 28;210(7):1153–64.
158. Zhou W, Cao L, Jeffries J, Zhu X, Staiger CJ, Deng Q. Neutrophil-specific knockout demonstrates a role for mitochondria in regulating neutrophil motility in zebrafish. *Disease Models & Mechanisms*. 2018 Mar 1;11(3).
159. Kedia-Mehta N, Finlay DK. Competition for nutrients and its role in controlling immune responses. *Nature Communications*. 2019 May 9;10(1):2123.
160. Chang C-H, Qiu J, O’Sullivan D, Buck MD, Noguchi T, Curtis JD, et al. Metabolic competition in the tumor microenvironment is a driver of cancer progression. *Cell*. 2015 Sep 10;162(6):1229–41.
161. Klysz D, Tai X, Robert PA, Craveiro M, Cretenet G, Oburoglu L, et al. Glutamine-dependent α -ketoglutarate production regulates the balance between T helper 1 cell and regulatory T cell generation. *Sci Signal*. 2015 Sep 29;8(396):ra97–ra97.

162. Heydemann A. An Overview of Murine High Fat Diet as a Model for Type 2 Diabetes Mellitus. Vol. 2016, Journal of Diabetes Research. Hindawi; 2016 Jul 31. p. e2902351.
163. Wilhelm C, Harrison OJ, Schmitt V, Pelletier M, Spencer SP, Urban JF Jr, et al. Critical role of fatty acid metabolism in ILC2-mediated barrier protection during malnutrition and helminth infection. *Journal of Experimental Medicine*. 2016 Jul 18;213(8):1409–18.
164. Goldberg EL, Molony RD, Kudo E, Sidorov S, Kong Y, Dixit VD, et al. Ketogenic diet activates protective $\gamma\delta$ T cell responses against influenza virus infection. *Sci Immunol*. 2019 Nov 15;4(41).
165. Roy DG, Chen J, Mamane V, Ma EH, Muhire BM, Sheldon RD, et al. Methionine Metabolism Shapes T Helper Cell Responses through Regulation of Epigenetic Reprogramming. *Cell Metabolism*. 2020 Feb 4;31(2):250-266.e9.
166. Ma EH, Bantug G, Griss T, Condotta S, Johnson RM, Samborska B, et al. Serine Is an Essential Metabolite for Effector T Cell Expansion. *Cell Metabolism*. 2017 Feb 7;25(2):345–57.
167. Koves TR, Ussher JR, Noland RC, Slentz D, Mosedale M, Ilkayeva O, et al. Mitochondrial Overload and Incomplete Fatty Acid Oxidation Contribute to Skeletal Muscle Insulin Resistance. *Cell Metabolism*. 2008 Jan 1;7(1):45–56.
168. García-Ruiz I, Solís-Muñoz P, Fernández-Moreira D, Grau M, Colina F, Muñoz-Yagüe T, et al. High-fat diet decreases activity of the oxidative phosphorylation complexes and causes nonalcoholic steatohepatitis in mice. *Disease Models & Mechanisms*. 2014 Nov 1;7(11):1287–96.
169. Kleiner S, Mepani RJ, Laznik D, Ye L, Jurczak MJ, Jornayvaz FR, et al. Development of insulin resistance in mice lacking PGC-1 α in adipose tissues. *PNAS*. 2012 Jun 12;109(24):9635–40.
170. Sparks LM, Xie H, Koza RA, Mynatt R, Hulver MW, Bray GA, et al. A High-Fat Diet Coordinately Downregulates Genes Required for Mitochondrial Oxidative Phosphorylation in Skeletal Muscle. *Diabetes*. 2005 Jul 1;54(7):1926–33.
171. Vaughan RA, Mermier CM, Bisoffi M, Trujillo KA, Conn CA. Dietary stimulators of the PGC-1 superfamily and mitochondrial biosynthesis in skeletal muscle. A mini-review. *J Physiol Biochem*. 2014 Mar 1;70(1):271–84.
172. Flachs P, Horakova O, Brauner P, Rossmeisl M, Pecina P, Franssen-van Hal N, et al. Polyunsaturated fatty acids of marine origin upregulate mitochondrial biogenesis and induce β -oxidation in white fat. *Diabetologia*. 2005 Nov 1;48(11):2365–75.
173. Lanza IR, Blachnio-Zabielska A, Johnson ML, Schimke JM, Jakaitis DR, Lebrasseur NK, et al. Influence of fish oil on skeletal muscle mitochondrial energetics and lipid metabolites during high-fat diet. *Am J Physiol Endocrinol Metab*. 2013 Jun 15;304(12):E1391–403.

174. Zeyda M, Säemann MD, Stuhlmeier KM, Mascher DG, Nowotny PN, Zlabinger GJ, et al. Polyunsaturated Fatty Acids Block Dendritic Cell Activation and Function Independently of NF- κ B Activation *. *Journal of Biological Chemistry*. 2005 Apr 8;280(14):14293–301.
175. Gao Z, Yin J, Zhang J, Ward RE, Martin RJ, Lefevre M, et al. Butyrate Improves Insulin Sensitivity and Increases Energy Expenditure in Mice. *Diabetes*. 2009 Jul;58(7):1509–17.
176. Gurav A, Sivaprakasam S, Bhutia YD, Boettger T, Singh N, Ganapathy V. Slc5a8, a Na⁺-coupled high-affinity transporter for short-chain fatty acids, is a conditional tumor suppressor in colon that protects against colitis and colon cancer under low-fiber dietary conditions. *Biochem J*. 2015 Jul 15;469(2):267–78.
177. Kaisar MMM, Pelgrom LR, van der Ham AJ, Yazdanbakhsh M, Everts B. Butyrate Conditions Human Dendritic Cells to Prime Type 1 Regulatory T Cells via both Histone Deacetylase Inhibition and G Protein-Coupled Receptor 109A Signaling. *Front Immunol*. 2017 Oct 30;8.
178. Serbina NV, Salazar-Mather TP, Biron CA, Kuziel WA, Pamer EG. TNF/iNOS-Producing Dendritic Cells Mediate Innate Immune Defense against Bacterial Infection. *Immunity*. 2003 Jul 1;19(1):59–70.
179. Laskin JD, Heck DE, Laskin DL. Multifunctional role of nitric oxide in inflammation. *Trends in Endocrinology & Metabolism*. 1994 Nov 1;5(9):377–82.
180. Olekhnovitch R, Ryffel B, Müller AJ, Bousso P. Collective nitric oxide production provides tissue-wide immunity during *Leishmania* infection. *J Clin Invest*. 2014 Apr 1;124(4):1711–22.
181. Ma EH, Verway MJ, Johnson RM, Roy DG, Steadman M, Hayes S, et al. Metabolic Profiling Using Stable Isotope Tracing Reveals Distinct Patterns of Glucose Utilization by Physiologically Activated CD8⁺ T Cells. *Immunity*. 2019 Nov 19;51(5):856-870.e5.
182. Lewis JS, Dolgova N, Chancellor TJ, Acharya AP, Karpiak JV, Lele TP, et al. Dendritic cell activation is influenced by cyclic mechanical strain when cultured on adhesive substrates. *Biomaterials*. 2013 Dec;34(36):9063–70.
183. Binek A, Rojo D, Godzien J, Rupérez FJ, Nuñez V, Jorge I, et al. Flow Cytometry Has a Significant Impact on the Cellular Metabolome. *J Proteome Res*. 2019 Jan 4;18(1):169–81.
184. Llufrío EM, Wang L, Naser FJ, Patti GJ. Sorting cells alters their redox state and cellular metabolome. *Redox Biol*. 2018 Mar 9;16:381–7.
185. Ahl PJ, Hopkins RA, Xiang WW, Au B, Kaliaperumal N, Fairhurst A-M, et al. Met-Flow, a strategy for single-cell metabolic analysis highlights dynamic changes in immune subpopulations. *Communications Biology*. 2020 Jun 12;3(1):1–15.

186. Hartmann FJ, Mrdjen D, McCaffrey E, Glass DR, Greenwald NF, Bharadwaj A, et al. Single-cell metabolic profiling of human cytotoxic T cells. *Nature Biotechnology*. 2020 Aug 31;1–12.
187. Salmon H, Idoyaga J, Rahman A, Leboeuf M, Remark R, Jordan S, et al. Expansion and activation of CD103+ dendritic cell progenitors at the tumor site enhances tumor responses to therapeutic PD-L1 and BRAF inhibition. *Immunity*. 2016 Apr 19;44(4):924–38.
188. Binnewies M, Mujal AM, Pollack JL, Combes AJ, Hardison EA, Barry KC, et al. Unleashing Type-2 Dendritic Cells to Drive Protective Antitumor CD4+ T cell Immunity. *Cell*. 2019 Apr 18;177(3):556-571.e16.
189. Böttcher JP, Bonavita E, Chakravarty P, Bles H, Cabeza-Cabrerizo M, Sammicheli S, et al. NK Cells Stimulate Recruitment of cDC1 into the Tumor Microenvironment Promoting Cancer Immune Control. *Cell*. 2018 Feb 22;172(5):1022-1037.e14.
190. Villablanca EJ, Raccosta L, Zhou D, Fontana R, Maggioni D, Negro A, et al. Tumor-mediated liver X receptor- α activation inhibits CC chemokine receptor-7 expression on dendritic cells and dampens antitumor responses. *Nature Medicine*. 2010 Jan;16(1):98–105.
191. Mastelic-Gavillet B, Balint K, Boudousquie C, Gannon PO, Kandalaft LE. Personalized Dendritic Cell Vaccines—Recent Breakthroughs and Encouraging Clinical Results. *Front Immunol*. 2019 Apr 11;10.
192. Gardner A, de Mingo Pulido Á, Ruffell B. Dendritic Cells and Their Role in Immunotherapy. *Front Immunol*. 2020 May 21;11.
193. Wculek SK, Khouili SC, Priego E, Heras-Murillo I, Sancho D. Metabolic Control of Dendritic Cell Functions: Digesting Information. *Front Immunol*. 2019;10.
194. Navarro-Barriuso J, Mansilla MJ, Naranjo-Gómez M, Sánchez-Pla A, Quirant-Sánchez B, Teniente-Serra A, et al. Comparative transcriptomic profile of tolerogenic dendritic cells differentiated with vitamin D3, dexamethasone and rapamycin. *Scientific Reports*. 2018 Oct 8;8(1):14985.
195. Ferreira GB, Kleijwegt FS, Waelkens E, Lage K, Nikolic T, Hansen DA, et al. Differential protein pathways in 1,25-dihydroxyvitamin d(3) and dexamethasone modulated tolerogenic human dendritic cells. *J Proteome Res*. 2012 Feb 3;11(2):941–71.
196. Ferreira GB, Vanherwegen A-S, Eelen G, Gutiérrez ACF, Van Lommel L, Marchal K, et al. Vitamin D3 Induces Tolerance in Human Dendritic Cells by Activation of Intracellular Metabolic Pathways. *Cell Reports*. 2015 Feb 10;10(5):711–25.
197. Vanherwegen A-S, Eelen G, Ferreira GB, Ghesquière B, Cook DP, Nikolic T, et al. Vitamin D controls the capacity of human dendritic cells to induce functional regulatory T

cells by regulation of glucose metabolism. *The Journal of Steroid Biochemistry and Molecular Biology*. 2019 Mar 1;187:134–45.

198. Malinarich F, Duan K, Hamid RA, Bijin A, Lin WX, Poidinger M, et al. High Mitochondrial Respiration and Glycolytic Capacity Represent a Metabolic Phenotype of Human Tolerogenic Dendritic Cells. *The Journal of Immunology*. 2015 Jun 1;194(11):5174–86.
199. Bell GM, Anderson AE, Diboll J, Reece R, Eltherington O, Harry RA, et al. Autologous tolerogenic dendritic cells for rheumatoid and inflammatory arthritis. *Ann Rheum Dis*. 2017 Jan;76(1):227–34.
200. Phillips BE, Garciafigueroa Y, Trucco M, Giannoukakis N. Clinical Tolerogenic Dendritic Cells: Exploring Therapeutic Impact on Human Autoimmune Disease. *Front Immunol*. 2017 Oct 12;8.

List of abbreviations

| | |
|--------|--|
| 2-DG | 2-deoxyglucose |
| ACC1 | acetyl-coA carboxylase |
| AMPK | 5' adenosine monophosphate-activated protein kinase |
| APC | antigen-presenting cell |
| ARG1 | arginase 1 |
| BMDC | bone marrow-derived dendritic cell |
| BNIP3 | BCL2/adenovirus E1B 19 kDa protein-interacting protein 3 |
| CCR7 | C-C chemokine receptor 7 |
| CDP | common dendritic cell precursor |
| CLL | chronic lymphocytic leukemia |
| CLR | C-type lectin receptors |
| CPT | carnitine palmitoyltransferase |
| CTL | cytotoxic T cell |
| CTLA-4 | cytotoxic T-lymphocyte-associated protein 4 |
| CXCL | C-X-C motif chemokine ligand |
| CXCR | C-X-C motif chemokine receptor |
| DAMP | danger-associated molecular pattern |
| DC | dendritic cell |
| DRP1 | dynamamin-related protein 1 |
| ECAR | extracellular acidification rate |
| ESAM | endothelial cell adhesion molecule |
| ETC | electron transport chain |
| eWAT | epididymal white adipose tissue |
| FACS | fluorescence-activated cell sorting |
| FAO | fatty acid oxidation |
| FLT3L | Fms related receptor tyrosine kinase 3 ligand |
| FRET | fluorescence resonance energy transfer |
| GAPDH | glyceraldehyde 3-phosphate dehydrogenase |
| GC-MS | gas chromatography-mass spectrometry |
| GM-CSF | granulocyte-macrophage colony-stimulating factor |
| HDM | house dust mite |

| | |
|----------------|---|
| HFD | high fat diet |
| HIF-1 α | hypoxia inducible factor 1a |
| HSC | hematopoietic stem cell |
| HSP70 | heat shock protein 70 |
| IDO | indoleamine 2,3-dioxygenase |
| IFN | interferon |
| IKK ϵ | inhibitor of kappa B kinase epsilon |
| ILC | innate lymphoid cell |
| iNOS | inducible nitric oxide synthase |
| IRF | interferon regulatory factor |
| LC-MS | liquid chromatography-mass spectrometry |
| LC3 | microtubule-associated protein 1A/1B-light chain 3 |
| LCMV | lymphocytic choriomeningitis |
| LDHA | lactate dehydrogenase A |
| LPS | lipopolysaccharide |
| MDP | monocyte-dendritic cell progenitors |
| MDSC | myeloid-derived suppressor cell |
| MHC | major histocompatibility complex |
| MIRO-1 | mitochondrial Rho GTPase 1 |
| mTOR | mammalian target of rapamycin |
| NF- κ B | nuclear factor kappa B |
| NLR | nucleotide-binding oligomerization domain-like receptor |
| NO | nitric oxide |
| NRF-1 | nuclear respiratory factor 1 |
| OCR | oxygen consumption rate |
| OXPPOS | oxidative phosphorylation |
| PAMP | pathogen-associated molecular pattern |
| PBMC | peripheral blood mononuclear cell |
| PD-1 | programmed cell death 1 |
| PD-L1 | programmed cell death ligand 1 |
| PDK1 | phosphoinositide-dependent kinase 1 |
| PFK1 | phosphofructokinase 1 |
| PFKFB4 | 6-phosphofructo-2-kinase/fructose-2,6-biphosphatase 4 |

| | |
|----------------|---|
| PGC-1 | peroxisome proliferator-activated receptor gamma, coactivator 1 |
| PGE2 | prostaglandin E2 |
| PI3K | Phosphoinositide 3-kinase |
| PKM2 | pyruvate kinase M2 |
| PPAR | peroxisome proliferator-activated receptor |
| PRC | PGC-related coactivator |
| PRR | pattern recognition receptor |
| PUFA | polyunsaturated fatty acid |
| RLR | retinoic acid-inducible gene-I-like receptor |
| ROR γ t | retinoic acid-related orphan receptor gamma t |
| ROS | reactive oxygen species |
| SFA | saturated fatty acid |
| SNP | single-nucleotide polymorphism |
| SIRT1 | sirtuin 1 |
| SQSTM1 | sequestosome 1 |
| SRC | spare respiratory capacity |
| SREBP | sterol regulatory-element binding protein |
| STAT6 | signal transducer and activator of transcription 6 |
| TBET | T-box expressed in T cells |
| TBK1 | TANK-binding kinase 1 |
| TCA cycle | tricarboxylic acid cycle |
| Teff cell | effector T cell |
| TFAM | transcription factor A, mitochondrial |
| TGF- β | transforming growth factor beta |
| TIL | tumor infiltrating lymphocytes |
| TLR | Toll-like receptor |
| TMRM | tetramethylrhodamine, methyl ester, perchlorate |
| TNF- α | tumor necrosis factor alpha |
| Treg cell | regulatory T cell |
| WNT5A | wingless-type family member 5A |
| XCR1 | X-C motif chemokine receptor 1 |
| ZBTB46 | zinc finger and BTB domain containing 46 |